THE FORMATION AND EVOLUTION OF MESOZOIC AGE OCEANIC LITHOSPHERE: RIFT MAGMATISM, SEAFLOOR SPREADING, AND SEDIMENT PROCESSES

A Dissertation

by

JOHN ANTHONY GREENE

Submitted to the Office of Graduate and Professional Studies of
Texas A&M University
in partial fulfillment of the requirements for the degree of

DOCTOR OF PHILOSOPHY

Chair of Committee,	Masako Tominaga
Co-Chair of Committee,	Robert Reece
Committee Members,	Mark Everett
	Wilford Gardner
Head of Department,	Julie Newman

August 2020

Major Subject: Geophysics

ABSTRACT

The formation and evolution of Mesozoic-age oceanic lithosphere documents the processes leading to the modern distribution of continents and ocean basins starting with the breakup of Pangaea, and plays an important role in global geochemical cycling. My dissertation research uses geophysical data to investigate two themes pertaining to the formation and evolution of Mesozoic-age oceanic lithosphere: (i) the Jurassic/Early Cretaceous continental breakup at the Eastern North American Margin (ENAM) and ensuing seafloor-spreading of the early Atlantic Ocean, and (ii) the construction of the deep-ocean sedimentary section in the Jurassic-age northwestern Pacific. To address the first theme, we analyzed and modeled magnetic anomaly data to understand both the mode of magmatism that facilitated continental breakup at the ENAM and the early seafloor spreading history of the Atlantic Ocean. Studying continental breakup and seafloor spreading provides insight into the initial formation of Mesozoic-age oceanic lithosphere, and the role this lithosphere plays in the progression of Wilson Cycles. Key findings from this research include: (1) both first- and second-order magmatic segmentation, representing variations in the amount and distribution of magmatism, were present to drive continental breakup at the ENAM; (2) variations in breakup magmatism could have been influenced by preexisting structure acquired during previous Wilson Cycles, and likely governed the segmentation and transform fault spacing of the ensuing Mid-Atlantic Ridge; (3) five newly identified magnetic anomalies can be correlated along the ENAM that may document the initial oceanic lithosphere

formation of the Atlantic Ocean; and (4) a reorientation of the early Mid-Atlantic Ridge, accommodated by asymmetric crustal accretion, can explain the difference in spreading center strike between the initial and modern Mid-Atlantic Ridge. To address the second theme, we interpreted multi-channel seismic reflection data from the northwestern Pacific to investigate the construction of the sedimentary section during the evolution of Mesozoic-age oceanic lithosphere, and the role of this sediment in global geochemical cycling. Results from this research suggest that a period of seafloor erosion impacted the sedimentary section, which would reduce the amount of chemical sequestration occurring in deep-ocean sediment during global geochemical cycles.

DEDICATION

To Pat, Julie, and Michael Greene for their continuous support.

ACKNOWLEDGEMENTS

First and foremost, I am immensely grateful for my advisor, Masako Tominaga. Thank you for years of support and guidance, and all the patience while I developed as a scientist. I am forever indebted to you for giving me my start as an undergraduate researcher, and for the incredible opportunities that took me all over the world (and oceans).

Thank you to my co-advisor Bobby Reece for always being available when I needed advice or help. I also appreciate the support that Mark Everett and Wilf Gardner provided as committee members, going above and beyond to support me during my time here.

I am grateful for the years of collaboration I had with Dan Lizarralde, Maurice Tivey, Nathan Miller, Debbie Hutchinson, and Matt Karl on my research projects. Without them, my research would not have been possible.

The Eastern North American Margin and GeoPRISMS research communities were instrumental in the development of my research and my growth as a scientist. In particular, I appreciate the discussions I had with Anne Bécel, Brandon Shuck, Bud Davis, Harm Van Avendonk, Collin Brandl, and Uri Ten Brink.

I thank the science parties and crewmembers from my research cruises aboard the R/V Sikuliaq, Falkor, Langseth, Armstrong, and Thompson for giving me the experience of a lifetime at sea.

It was a pleasure working with Tyler Ruchala, Estefania Ortiz, Paiden Pruett, and Noah Vento as part of the MAPLES (Multiscale Applied Physics Laboratory for Earth Science) research group. Thank you for years of productive and incredibly enjoyable research and camaraderie, and for putting up with ("appreciating") all my jokes.

I thank the students (and former students) of the Department of Geology & Geophysics who made my time at Texas A&M so enjoyable. Thank you to Justin Estep, Matt Couchman, Vicky Gao, Sebastian Smith, Chase Stanford, Pat Wagner, Eric Peavey, Dawid Szafrański, Kittipong Somchat, and Jingxuan Wei for always being there for me and making my Ph.D. so much fun.

Finally, I thank my parents, Pat and Julie, and my brother, Michael, for always supporting and encouraging me.

CONTRIBUTORS AND FUNDING SOURCES

Contributors

This work was supervised by a dissertation committee consisting of Professors Masako Tominaga (advisor), Robert Reece (co-advisor), and Mark Everett of the Department of Geology & Geophysics, and Professor Wilford Gardner of the Department of Oceanography.

Coauthors for the research presented in Section 2 were Masako Tominaga (current affiliation: Woods Hole Oceanographic Institution, Department of Geology & Geophysics), Nathaniel Miller (United States Geological Survey, Woods Hole Coastal and Marine Science Center), Deborah Hutchinson (United States Geological Survey, Woods Hole Coastal and Marine Science Center), and Matthew Karl (Michigan State University, Department of Earth & Environmental Sciences). The contents presented in subsections 2.5.3 and 2.6.2 of Section 2 were derived in part from the master's thesis by Matthew Karl[*] for contribution to the publication that this section produced. Coauthors for the research presented in Section 3 were Masako Tominaga and Nathaniel Miller. Coauthors for the research presented in Section 4 were Daniel Lizarralde (Woods Hole Oceanographic Institution, Department of Geology & Geophysics), Masako Tominaga, and Maurice Tivey (Woods Hole Oceanographic Institution, Department of Geology & Geophysics).

---

[*] Karl, M.R. (2016). The origin and implications of a high amplitude magnetic anomaly on the Eastern North American Margin, (master's thesis). Retrieved from MSU Libraries Digital Repository. (https://d.lib.msu.edu/etd/4205). East Lansing, MI: Michigan State University.

All other work conducted for the dissertation was completed by the student independently.

Funding Sources

Graduate study was supported by the Chevron Fellowship and Research Assistantships through the Department of Geology & Geophysics at Texas A&M University.

This work was also made possible in part by the National Science Foundation under Grant Numbers NSF-OCE-1029965, NSF-OCE-1543903, and NSF-EAR-1558188, and the NASA Astrobiology Institute under Grant Number NNA15BB02A. Its contents are solely the responsibility of the authors and do not necessarily represent the official views of the National Science Foundation or NASA Astrobiology Institute.

NOMENCLATURE

ABSMA	African Blake Spur Magnetic Anomaly
AFZ	Atlantis Fracture Zone
BMA	Brunswick Magnetic Anomaly
BSFZ	Blake Spur Fracture Zone
BSMA	Blake Spur Magnetic Anomaly
CAMP	Central Atlantic Magmatic Province
CDP	Common Depth Point
CFZ	Carolinas Fracture Zone
DBFZ	Delaware Bay Fracture Zone
DSDP	Deep-Sea Drilling Project
ECMA	East Coast Magnetic Anomaly
ENAM	Eastern North American Margin
HFMAH	Hudson Fan Magnetic Anomaly Highs
IMQZ	Inner Magnetic Quiet Zone
JQZ	Jurassic Quiet Zone
KFZ	Kane Fracture Zone
LIFZ	Long Island Fracture Zone
MCS	Multi-Channel Seismic
NAMAG	North American Magnetic Anomaly Group
NESC	New England Seamount Chain

NFZ	Norfolk Fracture Zone
NKFZ	Northern Kane Fracture Zone
NPSG	North Pacific Subtropical Gyre
NTFZ	Nantucket Fracture Zone
NYBFZ	New York Bight Fracture Zone
ODP	Ocean Drilling Program
OMQZ	Outer Magnetic Quiet Zone
SDRs	Seaward Dipping Reflectors

TABLE OF CONTENTS

Page

LIST OF FIGURES

Page

LIST OF TABLES

Page

1. INTRODUCTION

Mesozoic-age oceanic lithosphere represents the oldest oceanic lithosphere currently present on Earth, serving as a 180 Myr record of the geologic processes influencing Earths history (Müller et al., 2008). The formation of Mesozoic-age oceanic lithosphere records the breakup of the most recent supercontinent, Pangaea (Wilson, 1966; Peace et al., 2019), and the plate tectonic activity producing the modern distribution of continents and ocean basins (Müller et al., 2016). The evolution of oceanic lithosphere plays a key role in geochemical cycling (Elderfield et al., 1999; Tréguer & De La Rocha, 2013), with the sedimentary sections of oceanic lithosphere serving as a major sink in global geochemical cycles (DeMaster, 2001; Renaudie, 2016). Modern documentation of the formation and evolution of Mesozoic-age oceanic lithosphere is limited to rifted continental margins (Bradley, 2008; Buiter & Torsvik, 2014), the Mesozoic-age sections of the world's oceans (Larson & Chase, 1972; Boshchman & Van Hinsbergen, 2016), and accretionary orogens and ophiolites (Bortolotti & Principi, 2005; Kusky et al., 2013), providing a window into Earths history that is not available in the more widespread, younger oceanic lithosphere (Müller et al., 2008).

In my research, I use geophysical data from rifted continental margins and ocean basins to address two overarching themes regarding the formation and evolution of Mesozoic-age oceanic lithosphere. First, I investigate the continental breakup at the Eastern North American Margin (ENAM) and ensuing formation of Mesozoic-age

oceanic lithosphere in the early Atlantic Ocean at the start of the current Wilson Cycle. Second, I investigate the evolution of the deep-ocean sedimentary section of the Mesozoic-age oceanic lithosphere in the northwestern Pacific Ocean. The results of my research are discussed in Sections II-IV of this dissertation.

Section II investigates the Jurassic and Cretaceous seafloor-spreading regime of the early Atlantic Ocean following continental breakup at the ENAM using an integrated geophysical dataset. Results refine the history of crustal formation and the tectonics associated with the early Atlantic opening. This research has been published in the *Journal of Geophysical Research: Solid Earth* (J. A. Greene, M. Tominaga, N. C. Miller, D. R. Hutchinson, & M. R. Karl, 2017, Refining the Formation and Early Evolution of the Eastern North American Margin: New Insights From Multiscale Magnetic Anomaly Analyses, doi:10.1002/2017JB014308).

Section III investigates the magmatic activity that facilitated the Jurassic breakup of Pangaea and transition to seafloor spreading at the ENAM using three-dimensional magnetic anomaly modeling. Results indicate the presence of along-margin variations in the amount and distribution of the magmatism that were likely related to both the previous (continental collision) and subsequent (seafloor spreading) stages of the Wilson Cycle. This research has been submitted to the *Journal of Geophysical Research: Solid Earth* (J. A. Greene, M. Tominaga, & N. C. Miller, Along-Margin Variations in Breakup Volcanism at the Eastern North American Margin, manuscript #2020JB020040).

Section IV investigates the construction of the sedimentary section of the Jurassic-age oceanic lithosphere in the northwestern Pacific using multi-channel seismic

data. Results suggest a period of erosion on the paleo-seafloor that indicates a departure from the conventional pelagic sedimentation and diagenesis expected for this area, and a reduction in the amount of chemical sequestration during geochemical cycles. This research has been submitted to the *Marine Geology* (J. A. Greene, D. Lizarralde, M. Tominaga, & M. A. Tivey, Deep-ocean paleo-seafloor erosion in the northwestern Pacific identified by high-resolution seismic images, manuscript #MARGO-D-20-00142).

Section V summarizes and highlights the conclusions of the studies included within this dissertation.

2. REFINING THE FORMATION AND EARLY EVOLUTION OF THE EASTERN NORTH AMERICAN MARGIN: NEW INSIGHTS FROM MULTISCALE MAGNETIC ANOMALY ANALYSES*

2.1. Overview

To investigate the oceanic lithosphere formation and early seafloor spreading history of the North Atlantic Ocean, we examine multiscale magnetic anomaly data from the Jurassic/Early Cretaceous age Eastern North American Margin (ENAM) between 31-40°N. We integrate newly acquired sea surface magnetic anomaly and seismic reflection data with publicly available aeromagnetic and composite magnetic anomaly grids, satellite-derived gravity anomaly, and satellite-derived and shipboard bathymetry data. We evaluate these data sets to: (1) refine magnetic anomaly correlations throughout the ENAM and assign updated ages and chron numbers to M0-M25 and eight pre-M25 anomalies; (2) identify five correlatable magnetic anomalies between the East Coast Magnetic Anomaly (ECMA) and Blake Spur Magnetic Anomaly (BSMA), which may document the earliest Atlantic seafloor spreading or syn-rift magmatism; (3) suggest pre-existing margin structure and rifting segmentation may have influenced the seafloor spreading regimes in the Atlantic Jurassic Quiet Zone (JQZ); (4) suggest that, if the BSMA source is oceanic crust, the BSMA may be M-series magnetic anomaly M42

* Reprinted with permission from "Refining the formation and early evolution of the Eastern North American Margin: New insights from multiscale magnetic anomaly analyses" by John A. Greene, Masako Tominaga, Nathaniel C. Miller, Deborah R. Hutchinson, & Matthew R. Karl, 2017. Journal of Geophysical Research: Solid Earth, 122, 11, 8724-8748, Copyright 2017 by American Geophysical Union.

(~168.5 Ma); (5) examine the along and across margin variation in seafloor spreading rates and spreading center orientations from the BSMA to M25, suggesting asymmetric crustal accretion accommodated the straightening of the ridge from the bend in the ECMA to the more linear M25; and (6) observe anomalously high amplitude magnetic anomalies near the Hudson Fan, which may be related to a short-lived propagating rift segment that could have helped accommodate the crustal alignment during the early Atlantic opening.

2.2. Introduction

The Eastern North American Margin (ENAM) (Fig. 2.1) was formed by the opening of the North Atlantic Ocean following the rifting of the last supercontinent, Pangaea (Wilson, 1966). Advancing knowledge on the structure and development of the ENAM is critical for understanding not only the formation and evolution of passive margins (Sheridan, 1989; Withjack et al., 1998) but also the early opening history of the Atlantic Ocean (Vogt, 1973; Klitgord & Schouten, 1986; Bird et al., 2007; Schettino & Turco, 2009; Labails et al., 2010; Kneller et al., 2012; Biari et al., 2017). Furthermore, the rift-drift transition of the ENAM was coincident with and may have been triggered by the volcanism of the Central Atlantic Magmatic Province (CAMP) (Marzoli et al., 1999; Olsen et al., 2003; Schlische et al., 2003), which is also thought to be associated with a mass extinction event at the Triassic-Jurassic boundary (Nomade et al., 2007). Additionally, the architecture of the ENAM influences the prevalence and distribution of geohazards, including earthquakes and submarine landslides (Embley & Jacobi, 1986;

Folger, 1988; Chaytor et al., 2007; Chapman & Beale, 2010), and the origin and extent of natural resources (Dillon et al., 1986; Mattick & Libby-French, 1988; Riggs & Manheim, 1988).

M-series (Mesozoic) magnetic anomalies have been critical in characterizing the formation history of the ENAM. Many studies have identified M-series magnetic anomalies in the ENAM and western North Atlantic from M0 to M25, suggesting a slow spreading regime and an absence of ridge jumps (e.g. Klitgord & Schouten, 1986; Vogt, 1986; Sundvik & Larson, 1988; Müller et al., 1997; Bird et al., 2007; Schettino & Turco, 2009; Labails et al., 2010; Tominaga & Sager, 2010a, 2010b). For the earlier stage of the ENAM formation, however, only a few studies could extend magnetic anomaly identifications beyond anomaly M25 into the Atlantic Jurassic Quiet Zone (JQZ) (Barrett & Keen, 1976; Bird et al., 2007) due to the low amplitude magnetic anomalies that cause difficulty in identification (Fig. 2.1a) (Vogt et al., 1970; Larson & Pitman, 1972; Vogt, 1986; Bird et al., 2007). Furthermore, a notable change in magnetic anomaly strike is present from the significant bend in the East Coast Magnetic Anomaly (ECMA) offshore the New York Bight to the more linear M25 (Fig. 2.1a) (Klitgord & Schouten, 1986); however, the origin of the apparent straightening has yet to be explained. Additionally, early along and across margin seafloor spreading rates and patterns during the formation of the Atlantic JQZ have not been comprehensively examined, despite the seafloor formation between rifting and the more thoroughly studied M0-M25 region being a significant piece of the early Atlantic opening history.

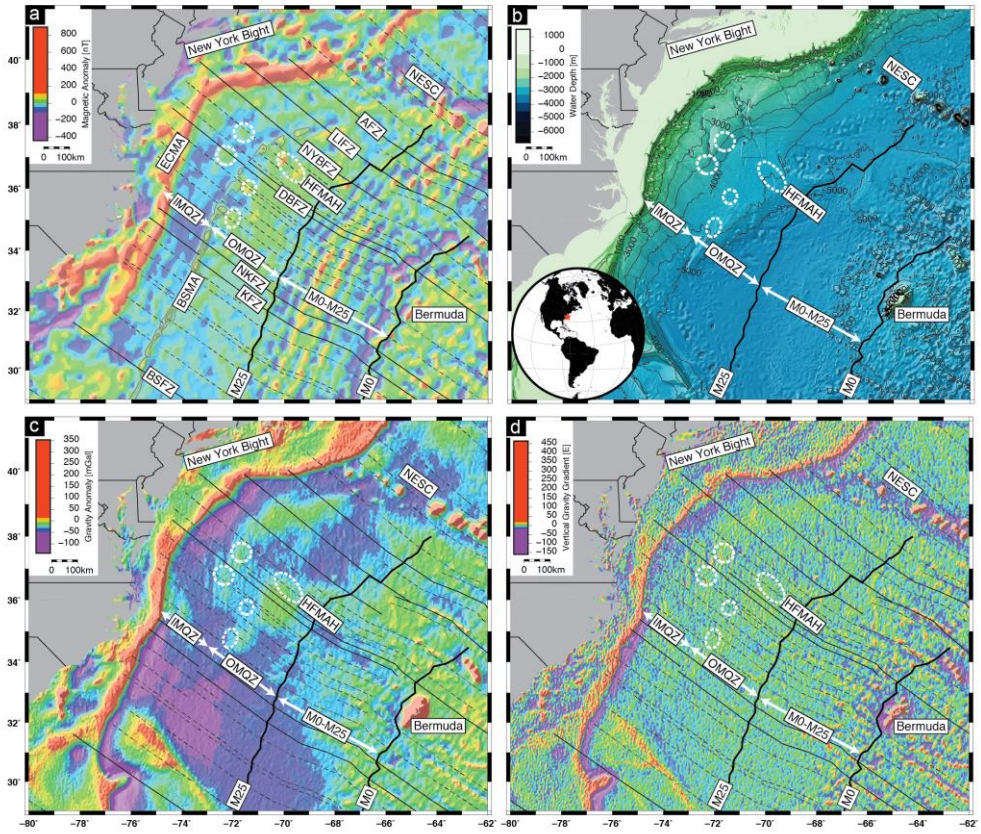

Figure 2.1 Geophysical data for the Eastern North American Margin: (a) EMAG2v3 composite magnetic anomaly grid (Meyer et al., 2016); (b) ETOPO1 satellite-derived bathymetry grid (Amante et al., 2009) contoured every 500 m; (c) Satellite-derived gravity anomaly grid (Sandwell et al., 2014); and (d) Satellite-derived vertical gravity gradient grid (Sandwell et al., 2014). Prominent features labeled: New York Bight, East Coast Magnetic Anomaly (ECMA), Blake Spur Magnetic Anomaly (BSMA), New England Seamount Chain (NESC), and island of Bermuda. White arrows show extent of the Inner Magnetic Quiet Zone (IMQZ) and Outer Magnetic Quiet Zone (OMQZ) subdivisions of the Atlantic JQZ, and M0-M25. White dashed circles indicate anomalous magnetic features, including the Hudson Fan Magnetic Anomaly High (HFMAH). Thick black lines indicate M-Series magnetic anomaly lineations M0 and M25. Dashed black lines are fracture zone picks of Klitgord and Schouten (1986). Solid black lines denote fracture zones referenced in this study: Blake Spur (BSFZ), Kane (KFZ), Northern Kane (NKFZ), Delaware Bay (DBFZ), New York Bight (NYBFZ), Long Island (LIFZ), and Atlantis (AFZ) (Klitgord & Schouten, 1986). Thin grey contours indicate BSMA (Klitgord & Schouten, 1986).

The prerift history of the eastern margin of the North American continent is likely to be an influence on the amount of volcanic activity experienced during continental breakup (Keen & Potter, 1995a) and the localization of rifting near the modern continental shelf (Manspeizer, 1988; Dunbar & Sawyer, 1989; Sheridan et al., 1993). The eastern edge of the North American Continent has experienced several cycles of tectonic collision and rifting throughout its formation history (e.g. Wilson, 1966; Manspeizer, 1988), resulting in a complex crustal structure from the accretion of terranes over time (Hatcher, 1989; Horton et al., 1989; Hatcher, 2010). However, the influence of preexisting structure on the subsequent seafloor spreading of the early Atlantic opening (e.g. Sawyer, 1985; Behn & Lin, 2000), particularly within the low amplitude magnetic anomaly region of the Atlantic JQZ, has not been extensively investigated.

In this study, we examine the magnetic anomalies of the ENAM and western Atlantic to refine our understanding of the early Atlantic seafloor spreading regimes and influence of preexisting margin structure. We use recently collected (Arsenault et al., 2017) and archived seasurface magnetic data from the National Centers for Environmental Information (NCEI) (www.ncei.noaa.gov), aeromagnetic (Zietz, 1982; Bankey et al., 2002), and the newly available high-quality EMAG2v3 (version 3) global magnetic anomaly grid compiling satellite, aeromagnetic, and shipboard magnetic data (Meyer et al., 2016). We integrate these data with newly acquired multichannel seismic (MCS) data (Arsenault et al., 2017), and satellite-derived gravity (Sandwell et al., 2014) and bathymetry grids (Butman et al., 2006; Amante et al., 2009; Andrews et al., 2016) (Figs. 2.1, 2.2). Based on magnetic anomaly analyses, we estimate seafloor spreading

rates and patterns in the Outer Magnetic Quiet Zone (OMQZ) of the Atlantic JQZ between the Blake Spur Magnetic Anomaly (BSMA) and M25 (Fig. 2.1a) (Klitgord & Grow, 1980) and from M0-M25, revealing, for the first time, a more comprehensive view on the pre-M25 stage of seafloor spreading. We also identify correlatable magnetic anomalies in the Inner Magnetic Quiet Zone (IMQZ) of the Atlantic JQZ between the ECMA and BSMA (Fig. 2.1a) (Klitgord & Grow, 1980) that have not previously been identified or discussed. We provide our georeferenced, digital magnetic anomaly data to the wider community for use in future studies.

2.3. Background

2.3.1. ENAM marine magnetic anomalies

Marine magnetic anomalies in the ENAM and western North Atlantic basin are one of the key observational datasets for understanding the formation and evolution of oceanic lithosphere during the Atlantic opening (Fig. 2.1a, 2.2). Deciphering magnetic anomaly character provides insight into the tectonic framework of the ENAM, including prominent features like the ECMA and BSMA, the low amplitude magnetic anomaly region of the Atlantic JQZ, and the M-series magnetic anomalies M0-M25 (Fig. 2.1a, 2.2).

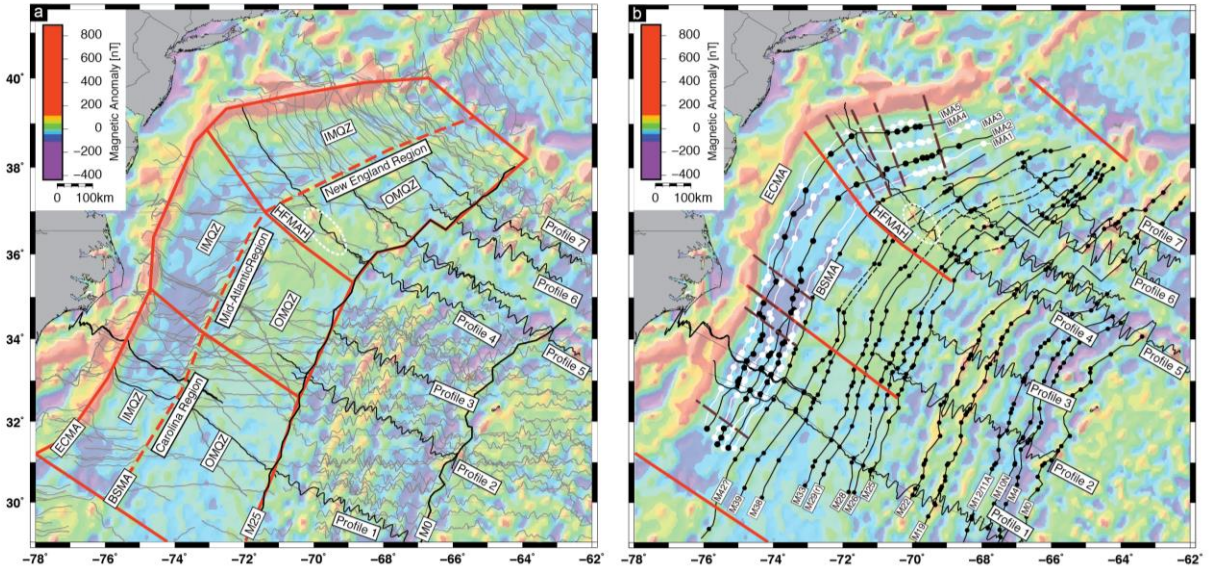

Figure 2.2 Magnetic anomaly data and correlations of Eastern North American Margin: (a) EMAG2v3 composite magnetic anomaly grid (Meyer et al., 2016) with recently collected (Arsenault et al., 2017) and archived shipboard magnetic anomaly profiles from the NCEI overlain in grey. Red lines outline IMQZ and OMQZ of the New England, Mid-Atlantic, and Carolina Regions. Black lines indicate M-Series magnetic anomaly lineations M0 and M25. Select profiles used in age/chron assignment and spreading rate calculations shown in black. Profiles 1, 2, 4, 5, and 7 consist of multiple segments concatenated together (see Fig. 2.4). (b) EMAG2v3 composite magnetic anomaly grid (Meyer et al., 2016) with magnetic anomaly correlations overlain. Solid black lines show select M-series magnetic anomaly lineations, with dashed sections denoting areas where there was difficulty tracing the lineations using the EMAG2v3 grid. Dots indicate location of corresponding magnetic anomalies on seasurface magnetic anomaly profiles. In IMQZ, solid lines indicate interpreted magnetic anomalies IMA1-5 (black- peaks; white- troughs). Red lines denote boundaries of the New England, Mid-Atlantic, and Carolina Regions. Dashed brown lines mark interpreted offsets in IMQZ magnetic anomalies IMA1-5.

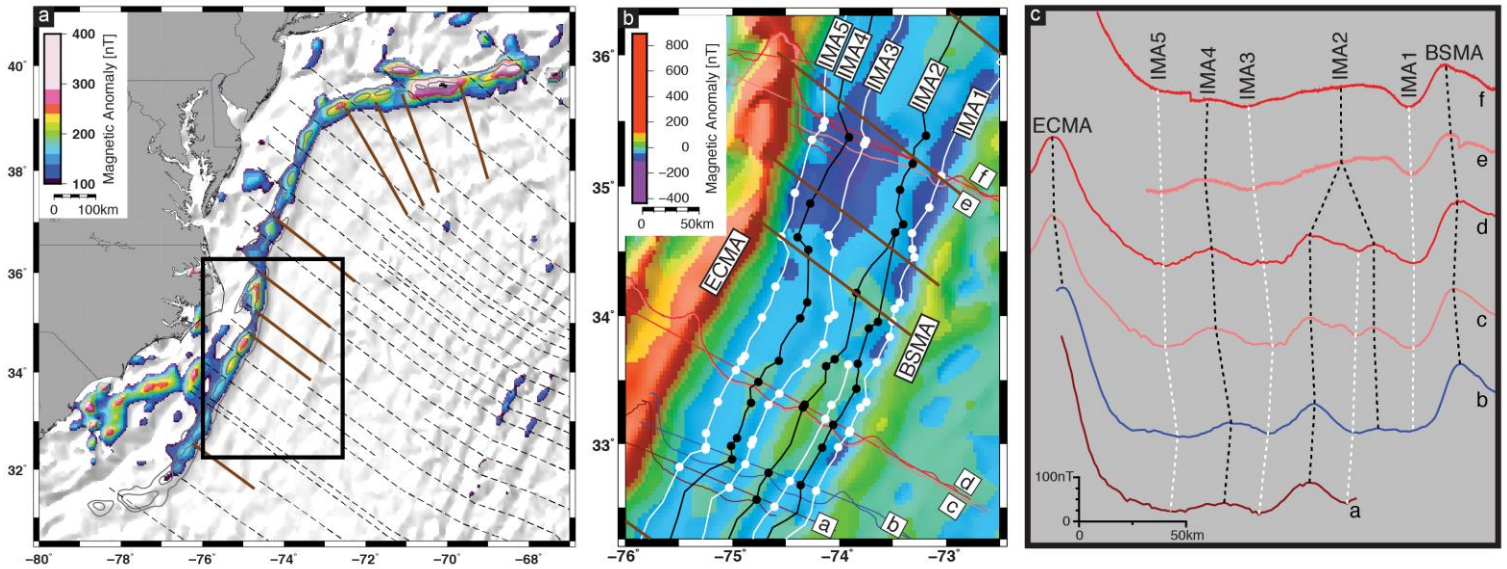

Figure 2.3 East Coast Magnetic Anomaly segmentation and Inner Magnetic Quiet Zone magnetic correlations: (a) EMAG2v3 composite magnetic anomaly grid (Meyer et al., 2016) with scale altered to highlight range of ECMA. ECMA contours in light gray showing segmentation (Klitgord & Schouten, 1986). Dashed black lines are fracture zone picks of Klitgord & Schouten (1986). Brown lines mark interpreted offsets in IMQZ magnetic anomalies IMA1-5. Black box shows location of panel 2.3b. (b) Close up of the IMQZ of the Carolina Region (see 2.3a for location). Overlays are recently collected (Arsenault et al., 2017) and archived shipboard magnetic anomaly profiles from the NCEI. Solid lines show interpreted magnetic anomalies IMA1-5 (black- peaks; white- troughs). Dots indicate location of corresponding magnetic anomalies on seasurface magnetic anomaly profiles (Fig. 2.2a). Brown lines mark interpreted offsets in IMQZ magnetic anomalies IMA1-5. Profiles b, c, and d make up Profile 1 (Fig. 2.2). (c) Correlation of magnetic anomalies IMA1-5 on select profiles within the IMQZ of the Carolina Region. Dashed lines show magnetic anomaly correlations (black- peaks; white- troughs). ECMA and BSMA labeled. Magnetic anomaly profiles a-f correspond to profiles in panel 2.3b.

The ECMA is a high amplitude, positive magnetic anomaly that follows the margin for 2,500 km, near the edge of the continental shelf, from offshore Georgia (at the Blake Spur Fracture Zone) to Nova Scotia (Fig. 2.1a) (Keller et al., 1954; Klitgord & Schouten, 1986; Keen & Potter, 1995b). The ECMA displays segmentation along its length, represented by a series of magnetic anomaly highs separated by zones of relatively lower amplitude (Fig. 2.3a) (Klitgord & Schouten, 1986; Behn & Lin, 2000; Wyer & Watts, 2006). The ECMA has been thought to represent the continent ocean transition (Klitgord & Behrendt, 1978; Klitgord et al., 1988; Tréhu et al., 1989; Austin et al., 1990), and has been attributed to a late Paleozoic Alleghanian suture (McBride & Nelson, 1988) or seaward dipping reflectors (SDRs) formed by the emplacement and subsidence of volcanic layers during continental breakup (Austin et al., 1990; Oh et al., 1995; Keen & Potter, 1995b; Talwani et al., 1995; Lizarralde & Holbrook, 1997; Talwani et al., 2000; Benson, 2003). Various ages have been proposed for the ECMA, with Klitgord & Schouten (1986) extrapolating an age of 175 Ma, while Benson (2003) suggested an updated age based on more recent geomagnetic timescales of 172 Ma to 179 Ma. A possible conjugate to the ECMA, the lower amplitude West African Coast Magnetic Anomaly, exists on the northwest African margin (Klitgord & Schouten, 1986; Sahabi et al., 2004; Labails et al., 2010).

The BSMA is another high amplitude, positive magnetic anomaly in the Atlantic JQZ located 150-250 km to the east and oriented parallel to the ECMA, diminishing around 39°N (Fig. 2.1a) (Taylor et al., 1968; Vogt et al., 1970; Klitgord & Schouten, 1986). The origin of this magnetic anomaly is unknown, but is thought to play a key role

in the early Atlantic opening (Vogt, 1973; Klitgord & Schouten, 1986; Bird et al., 2007; Schettino & Turco, 2009; Labails et al., 2010; Kneller et al., 2012). Like the ECMA, the BSMA is segmented along its length (Fig. 2.1a) (Klitgord et al., 1986). Klitgord & Schouten (1986) extrapolated an age of 170 Ma for the BSMA, while Benson (2003) suggested an updated age based on more recent geomagnetic timescales of 168 Ma to 171 Ma. A possible conjugate to the BSMA, the African Blake Spur Magnetic Anomaly, has been proposed for the northwest African margin (Sahabi et al., 2004; Labails et al., 2010).

The Atlantic JQZ is a zone of low amplitude magnetic anomalies between the ECMA and M25 (Fig. 2.1a) (Vogt et al., 1970; Larson & Pitman, 1972; Vogt, 1986). The low magnetic anomaly amplitudes of the Atlantic JQZ have been attributed to a low intensity geomagnetic field rapidly reversing polarity and/or a low paleomagnetic latitude for the plate at the time of crustal formation (Larson & Pitman, 1972; Tivey et al., 2006; Tominaga & Sager, 2010a). The Atlantic JQZ can further be subdivided into two zones of low amplitude magnetic anomalies: the IMQZ and OMQZ (Fig. 2.1a) (Klitgord & Grow, 1980). The IMQZ of the Atlantic JQZ is an approximately 100 km wide (west to east) zone between the ECMA and BSMA (Figs. 2.1a, 2.3b) (Vogt et al., 1971; Klitgord & Grow, 1980). Ages for the crust in the IMQZ are inferred to be older than 170 Ma, possibly as old as 190 Ma (Vogt, 1973; Barrett & Keen, 1976; Klitgord & Schouten, 1986; Vogt, 1986; Sheridan, 1987; Bird et al., 2007; Schettino & Turco, 2009; Labails et al., 2010). Furthermore, while the nature of the IMQZ crust is still unknown, Bird et al. (2007) proposed the IMQZ is composed with oceanic crust based on their

observation of subtle linear trends in the second vertical gradient of the total magnetic field intensity within the IMQZ oriented subparallel to the ECMA and BSMA, which could be the result of seafloor spreading.

The OMQZ of the Atlantic JQZ is an approximately 200-350 km wide (west to east) region between the BSMA to M25, becoming narrower from south to north (Fig. 2.1a) (Klitgord & Grow, 1980). Low amplitude pre-M25 M-series magnetic anomalies are not as easily identified in the OMQZ, compared to the M0-M25 anomalies to the east, with only a few studies proposing magnetic anomaly identifications in the OMQZ, such as Barrett and Keen (1976) (M26-M28; north of the New England Seamount Chain) and Bird et al. (2007) (M28, M29, M32, and M40).

M-series magnetic anomalies from M0 to M25 are widely accepted in the North Atlantic (Fig. 2.2) (e.g. Schouten & Klitgord, 1977; Klitgord & Schouten, 1986; Vogt, 1986; Sundvik & Larson, 1988; Müller et al., 1997; Bird et al., 2007; Schettino & Turco, 2009; Labails et al., 2010; Tominaga & Sager, 2010a, 2010b), with the magnetic anomaly correlations of most later studies based on the correlations of Klitgord and Schouten (1986). Magnetic anomalies M0-M25 are also widely identified on the conjugate northwest African margin (Rona et al., 1970; Klitgord & Schouten, 1986; Verhoef et al., 1990; Roest et al., 1992; Labails et al., 2010), and some pre-M25 anomalies have been identified (Roeser et al., 2002; Bird et al., 2007), suggesting the Atlantic JQZ does contain correlatable magnetic anomalies.

In addition to the prominent magnetic anomalies (ECMA, BSMA), low amplitude magnetic anomaly regions (Atlantic JQZ, IMQZ, and OMQZ), and M0-M25

magnetic anomalies, there are distinct, high amplitude, ellipsoidal magnetic anomalies within the Atlantic JQZ that have not yet been investigated, despite being present in older magnetic anomaly data (Fig. 2.1a, 2.2) (e.g. Klitgord & Behrendt, 1977; Zietz, 1982; Bankey et al., 2002; Meyer et al., 2016). Two distinct ellipsoidal magnetic anomaly highs, coinciding with the location of the Hudson Fan (hereafter called the Hudson Fan Magnetic Anomaly Highs (HFMAH)), are located ~620 km southeast of the New York Bight, with amplitudes much higher than the surrounding Atlantic JQZ and similar to the magnetic anomalies of Bermuda (Vogt, 1986) and the New England Seamount Chain (Duncan, 1984) (Figs. 2.1a, 2.2). However, no significant gravity anomaly highs has been identified in conjunction with the HFMAH (Figs. 2.1c, 2.1d), suggesting that a substantial igneous addition by late-stage magmatism, like Bermuda and the New England Seamount Chain, is unlikely to be the cause of the HFMAH.

2.3.2. Fracture zones and tectonic inheritance at the North Atlantic Margin

Fracture zones, recording approximate plate motion and spreading axis segmentation, are prevalent throughout the North Atlantic, and are identifiable by lateral offsets of magnetic anomaly lineations, as well as in gravity and bathymetry data (Fig. 2.1) (Vogt et al., 1971; Schouten & White, 1980; Müller & Roest, 1992; Klitgord & Schouten, 1986; Tucholke & Schouten, 1988; Bird et al., 2007; Schettino & Turco, 2009; Labails et al., 2010). Klitgord and Schouten (1986) determine the locations of fracture zones by offsets in their identified magnetic anomaly lineations from the Mid-Atlantic Ridge to M25, and extend the trend of these identified fracture zones landward

from M25 to the segmentation along the ECMA (Fig. 2.1a). Schettino and Turco (2009) find that the landward extension of these fracture zones in the OMQZ are consistent with the direction of seafloor spreading predicted by their plate reconstruction model, but not further landward to the ECMA through the IMQZ, possibly suggesting an unknown change in seafloor spreading rate and/or direction in the vicinity of the BSMA. Furthermore, Labails et al. (2010) do not find reliable indications of fracture zone directions in the IMQZ.

Many landward extensions of identified fracture zones intersect the margin between ECMA and isostatic gravity anomaly segments (Fig. 2.3a), which may indicate a relation to structural segmentation of the margin during rifting (Klitgord et al., 1988; Behn & Lin, 2000; Wyer & Watts, 2006). The amount of extension during rifting might have been reduced in some areas along the margin from preexisting structural zones of weakness arising from tectonic inheritance (e.g. Manspeizer, 1988; Sheridan et al., 1993). Along margin structural segmentation during continental rifting at the ENAM, represented by segmentation in the ECMA and margin wide isostatic gravity anomaly, is suggested to be the result of variations in both the strength of the continental lithosphere and igneous underplating (Behn & Lin, 2000; Wyer & Watts, 2006), and may be directly related to the formation of incipient fracture zones and the current Mid-Atlantic Ridge segmentation (e.g. Sawyer, 1985; Dunbar & Sawyer, 1989; Behn & Lin, 2000).

2.3.3. ENAM formation scenarios

Continental rifting and early Atlantic opening forming the ENAM was diachronous, with the rifting to seafloor spreading transition occurring earlier offshore the southeastern United States (~200 Ma) than offshore Canada (~185 Ma) (Klitgord & Schouten, 1986; Manspeizer, 1988; Withjack et al., 1998; Kneller et al., 2012). The southern ENAM (south of Nova Scotia) experienced voluminous magmatism during rifting, creating a volcanic margin, while to the north of Nova Scotia, the margin transitions from volcanic to nonvolcanic, marked by the termination of the ECMA and SDRs (Keen & Potter, 1995a, 1995b; Kelemen & Holbrook, 1995; McHone, 2000; Van Avendonk et al., 2006; Biari et al., 2017).

There have been two major scenarios proposed for the ENAM and early Atlantic formation: (1) a ridge jump (or two ridge jumps) (Vogt, 1973; Klitgord & Schouten, 1986; Vogt, 1986; Bird et al., 2007; Schettino & Turco, 2009; Kneller et al., 2012), or (2) a drastic change in spreading rate and direction (Sahabi et al., 2004; Labails et al., 2010). The origin of the BSMA differs in each of these scenarios. In the eastward ridge jump from within the IMQZ to the BSMA scenario, the BSMA would be formed by either the basement relief associated with the juxtaposition of crust the age of the ridge jump with comparatively older crust at the eastern edge of the IMQZ (Klitgord & Grow, 1980), or by a sliver of the African margin continental crust and igneous intrusives isolated by the ridge jump (Vogt, 1973). Alternatively, in the drastic change in seafloor spreading rate and direction scenario, the BSMA would be formed by the basement relief associated with this spreading change (Labails et al., 2010). In addition to the

suggested BSMA ridge jump, Bird et al. (2007) adds a second, westward ridge jump in the OMQZ between 164 and 159 Ma, possibly corresponding with the onset of seafloor spreading in the Gulf of Mexico (Van Avendonk et al., 2015).

Table 2.1 Proposed half spreading rates for the early Atlantic compiled from previous studies (Klitgord & Schouten, 1986; Bird et al., 2007; Schettino & Turco, 2009; Labails et al., 2010; Tominaga & Sager, 2010a, 2010b).

Publication	Chron/Age	Half Spreading Rate
Klitgord & Schouten [1986]	170Ma (BSMA ridge jump) to 150Ma (M21)	19 mm/yr
Klitgord & Schouten [1986]	150Ma (M21) to 141Ma (M16)	10 mm/yr
Klitgord & Schouten [1986]	141Ma (M16) to 132Ma (M10N)	7 mm/yr
Klitgord & Schouten [1986]	132Ma (M10N) to 126Ma (M4)	Variable
Klitgord & Schouten [1986]	126Ma (M4) to 118Ma (M0)	9 mm/yr
Bird et al. [2007]	~167.5Ma (M40) to ~154Ma (M25)	19.2 mm/yr
Bird et al. [2007]	~154Ma (M25) to ~120.6Ma (M0)	14.4 mm/yr
Schettino & Turco [2009]	200Ma to 185Ma (proposed ridge jump)	4.1 mm/yr
Schettino & Turco [2009]	185Ma to 147.7Ma (M21)	5.45 mm/yr
Schettino & Turco [2009]	147.7Ma (M21) and younger	22 mm/yr
Labails et al. [2010]	190Ma-170Ma (BSMA)	8 mm/yr
Labails et al. [2010]	170Ma (BSMA) to ~154Ma (M25)	17 mm/yr
Labails et al. [2010]	~154Ma (M25) to ~150Ma (M22)	27 mm/yr
Labails et al. [2010]	~150Ma (M22) to ~125Ma (M0)	13 mm/yr
Tominaga & Sager [2010a,b]	~154Ma (M25n) to ~148Ma (M21n)	32.6 mm/yr
Tominaga & Sager [2010a,b]	147.5Ma (M20r) to ~140Ma (M16n)	18.4 mm/yr
Tominaga & Sager [2010a,b]	~139Ma (M15) to ~131Ma (M6) [AMSZ]	9.5 mm/yr
Tominaga & Sager [2010a,b]	~131Ma (M6) and younger	22.9 mm/yr

Half spreading rates used in kinematic plate reconstructions of the early Atlantic vary based on the model, the magnetic anomalies identified, and/or the geomagnetic polarity timescale used (Table 2.1) (e.g. Klitgord & Schouten, 1986; Bird et al., 2007; Schettino & Turco, 2009; Labails et al., 2010; Tominaga & Sager, 2010a; 2010b). Seafloor spreading rates from M0 to M25 were found using the age assignments and distances between magnetic anomalies, while seafloor spreading rates in the Atlantic JQZ were estimated by either assuming the M21-M25 rate continues landward (Klitgord & Schouten, 1986), using stage pole rotations in plate-scale tectonic reconstructions to geometrically fit conjugate magnetic anomalies and the continents (Schettino & Turco, 2009; Labails et al., 2010), or using magnetic anomaly correlations where available in the OMQZ (Bird et al., 2007).

2.4. Methods

2.4.1. Magnetic data acquisition

In this study, we integrated both recently collected (Arsenault et al., 2017) and archived magnetic anomaly data from the NCEI (Fig. 2.2a). The archived magnetic data from the NCEI includes data from 39 cruises throughout the ENAM that we corrected for the international geomagnetic reference field (IGRF-11 model, Finlay et al. (2010)), providing extensive coverage of the study region. We also used the Decade of North American Geology (DNAG) (Zietz, 1982) and North American Magnetic Anomaly Group (NAMAG) (Bankey et al., 2002) aeromagnetic total magnetic field data, along with the high-quality EMAG2v3 (version 3) global magnetic anomaly grid composed of

a wide range of satellite, aeromagnetic, and shipboard magnetic data that has recently been made available (Meyer et al., 2016) (Figs. 2.1a, 2.2).

During MCS acquisition on the R/V Marcus G. Langseth cruises MGL1407, MGL1408, and MGL1506 along the ENAM, seasurface total magnetic field data was acquired using a Geometrics G882 cesium vapor marine magnetometer (Arsenault et al., 2017). The magnetometer was towed behind the ship navigation reference point at a distance of 253 m (MGL1407 and MGL1408) or 160 m (MGL1506). Seasurface total magnetic field data were also collected during the recent R/V Neil Armstrong cruise AR1-06 using a Seaspy Overhauser Magnetometer towed at a distance of 227 m. To obtain the seasurface crustal magnetic anomalies, the raw seasurface total magnetic field data collected during these cruises was corrected for (i) navigation offset from ship-to-magnetometer layback, (ii) outlying data points, (iii) the international geomagnetic reference field (IGRF-11 model, Finlay et al. (2010)), and (iv) diurnal field variations (NASA Stennis Space Center Magnetic Observatory, MS). Significant portions of the data collected during these cruises were on long, continuous, margin perpendicular segments that provide high-quality profiles ideal for studying magnetic anomalies produced by seafloor spreading.

2.4.2. Magnetic anomaly correlation

We organized straight-line profiles oriented approximately perpendicular to the margin from all of the available seasurface magnetic anomaly data (Fig. 2.2a) and integrated them with the aeromagnetic and EMAG2v3 magnetic anomaly data in

Quantum GIS (QGIS Development Team, 2015) to produce a comprehensive, georeferenced dataset of the region. Using this georeferenced dataset, we correlated magnetic anomalies on the ENAM by qualitatively matching the character (i.e. amplitude, spacing, and shape) of individual magnetic anomalies on adjacent seasurface magnetic anomaly profiles, using the aeromagnetic and EMAG2v3 magnetic grids to connect the correlated magnetic anomalies to produce lineations (Figs. 2.2, 2.3b, 2.3c, 2.4). An example of this process for the IMQZ near Cape Hatteras is shown in Figure 2.3b.

We further selected seven seasurface magnetic anomaly profiles from the dataset (Profiles 1-7), concatenating multiple segments, together to cover the latitudinal and longitudinal extent of the ENAM seafloor (see Profiles 1, 2, 4, 5, and 7 in Figures 2.2 and 2.4). The profiles were oriented as close to perpendicular to the margin as available to best display the character (i.e. amplitude, spacing, and shape) of magnetic anomalies that would be expected from seafloor spreading processes (Figs. 2.2, 2.4). We used Profiles 1-7 to assign chron numbers and corresponding ages to the magnetic anomalies using the 2012 Geomagnetic Polarity Time Scale (Ogg, 2012), and to calculate spreading rates for the ENAM.

2.4.3. Magnetic polarity block modeling

We created synthetic magnetic anomaly profiles using the Parker (1973) Fourier summation approach to determine ages for our identified magnetic anomalies. We used a magnetization distribution based on Pacific M-series magnetic polarity block models, a

basement depth of 8 km (Tucholke, 1986), various half spreading rates (7-30 mm/yr), and paleo-inclinations (34.2° to 44.5°) and declinations (-18.4° to -8.1°) estimated for the early Atlantic using the method of Schettino (2014) and the paleo-poles of Schettino and Scotese (2005). We correlated these synthetic magnetic anomaly profiles with Profiles 1-7 to assign chron numbers and ages to our identified magnetic anomalies using the 2012 Geomagnetic Polarity Time Scale (Ogg, 2012) (Fig. 2.4). With the spacing and assigned ages for the magnetic anomalies, we estimated spreading rates for Profiles 1-7 to evaluate the variation both along the margin and over time (Fig. 2.5). Using the estimated spreading rates, final synthetic profiles were created that best matched the observed magnetic anomalies of the region (Fig. 2.4).

2.4.4. Other geophysical data

To ensure our identified magnetic anomalies were produced by seafloor spreading processes, rather than secondary magmatic events that could significantly alter the observed magnetic anomaly signal (e.g. seamounts), we acquired and examined the latest satellite-derived gravity (Sandwell et al., 2014) and bathymetry (Butman et al., 2006; Amante et al., 2009; Andrews et al., 2016) data (Fig. 2.1). For Profiles 1, 2, and 4, MCS data were available (MGL1407 Lines 2, 3, 11A, 13, 14, and 15) to investigate whether any secondary magma additions and/or significant structural boundaries exist in the subsurface (Arsenault et al., 2017).

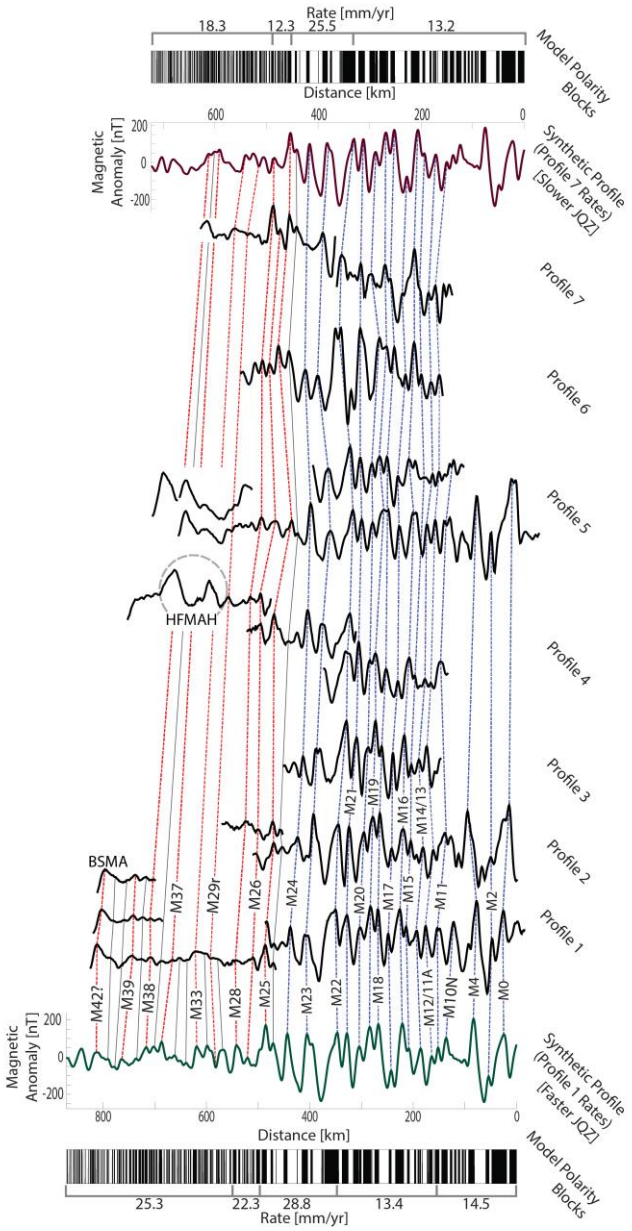

Figure 2.4 M-series magnetic anomaly correlations: Correlation of magnetic anomalies for Profiles 1-7 (Fig. 2.2a) with synthetic magnetic anomaly profile from Pacific M-series magnetic polarity block models and the 2012 Geomagnetic Polarity Time Scale (Ogg, 2012). Synthetic profile created using half spreading rates estimated for Profile 1 (bottom- green line) and Profile 7 (top- maroon line) (Table 2.2). Dashed lines show magnetic anomaly correlations (Red- OMQZ; Blue- M0-M25). Profiles 1, 2, 4, 5, and 7 consist of multiple profiles concatenated together (see Fig. 2.2). Chron numbers labeled.

2.5. Results

2.5.1. ENAM magnetic anomaly correlations

We assigned chron numbers and ages to 21 of the known anomalies between M0 and M25 (Figs. 2.2b, 2.4). Additionally, we assign chron numbers to eight previously unidentified magnetic anomalies in the OMQZ, where few previous studies have identified magnetic anomalies (e.g. Barrett & Keen, 1976; Bird et al., 2007), and identify five correlatable magnetic anomalies in the IMQZ (Fig. 2.4; Table 2.2).

In the IMQZ, we correlated five low amplitude magnetic anomalies approximately parallel to both the ECMA and BSMA from 31° to 40°N that have not previously been correlated or discussed, denoted as Inner Magnetic Anomalies (IMA) 1-5 from east to west (Figs. 2.2b, 2.3b, 2.3c). The correlations were made qualitatively by matching the character of IMA1-5 on margin perpendicular profiles crossing the IMQZ (Fig. 2.3c). From 31° to 33.5°N, the magnetic anomaly peak denoted as IMA2 splits into two peaks with an intervening trough (Figs. 2.2b, 2.3b, 2.3c). In the middle of the IMQZ, between 36° to 39°N, the linear magnetic anomalies are less coherent and there are low amplitude, circular magnetic anomaly highs seaward of the bend in the ECMA that partially obscure the linear magnetic anomalies and mark the location of a change in magnetic anomaly lineation strike and clarity, with more distinguishable lineations with a strike of ~30° to the south and less distinguishable lineations with a strike of ~70° to the north (Figs. 2.1a, 2.2b). Despite this less coherent middle section between 36° to 39°N where the linear anomalies are more difficult to follow, the consistent character of IMA1-5 and presence of five distinct magnetic anomalies throughout the IMQZ suggests

that these IMQZ magnetic anomalies continuously span the entire study area from 31° to 40°N.

Lateral offsets of IMA1-5, striking east/west in the southern IMQZ and northwest/southeast in the northern IMQZ, were interpreted throughout the IMQZ based on the combination of the seasurface magnetic anomaly data and the aeromagnetic and EMAG2v3 magnetic grids in our georeferenced dataset (Figs. 2.2b, 2.3b). These offsets were consistently oriented perpendicular to IMA1-5, striking east/west in the southern IMQZ and northwest/southeast in the northern IMQZ (Figs. 2.2b, 2.3a, 2.3b). Many of these IMQZ offsets documented in this study appear to intersect the ECMA at gaps between individual segments (Fig. 2.3a), and they often line up with previously identified traces of fracture zones extending through the OMQZ and M0-M25 (Figs. 2.2b, 2.3a, 2.3b) (Klitgord & Schouten, 1986).

Throughout the OMQZ, we correlated magnetic anomalies despite the low amplitude characteristic of the Atlantic JQZ (Fig. 2.2b). Similar to the ECMA, IMA1-IMA5, and the BSMA, there is a change in magnetic anomaly lineation strike on the west side of the OMQZ, but this change becomes less pronounced moving to the east. The magnetic anomaly lineations consistently have a strike of ~30° in the south, and in the north the strike varies from ~70° to ~55°, from west to east, in the north (Fig. 2.2b). Additionally, the OMQZ is wider in the south (~360 km at 31°N), becoming narrower moving northward (~220 km at 37°N), which corresponds to a wider magnetic anomaly lineation spacing in the south compared to the north (Fig. 2.2b). The middle portion of the OMQZ (approximately 34°-37°N) has multiple ellipsoidal magnetic anomaly highs

and lows, including the HFMAH, which created difficulty in correlating magnetic anomalies (Fig. 2.2).

We propose the existence of correlatable magnetic anomalies older than M25 in the OMQZ. Based on our synthetic profiles, we identified M-series magnetic anomalies M26, M28, M29r, M33, M37, M38 and M39 in the Atlantic JQZ (Figs. 2.2b, 2.4; Table 2.2). Additionally, the magnetic anomaly character of the BSMA on recently collected seasurface magnetic anomaly profiles (from MGL1407 and MGL1408) is similar to that of M42 (~168.5 Ma) in our synthetic profile, with a steep amplitude increase to the magnetic anomaly peak on the west, followed by a more gradual tapering off of amplitude moving to the east (see Profile 1 in Figs. 2.2, 2.4). In the MCS data, satellite-derived gravity anomaly, and satellite-derived bathymetry data available for our profiles, only one significant seamount was identified, on the west end of MGL1407 Line 11A (Profile 2 in Figures 2.2b and 2.4) (Arsenault et al., 2017), which does not appear to affect the magnetic anomaly signal given the excellent correlation with other profiles nearby along which the absence of seamounts is confirmed (e.g. MGL1407 Line 13; Profile 1 in Figures 2.2b and 2.4).

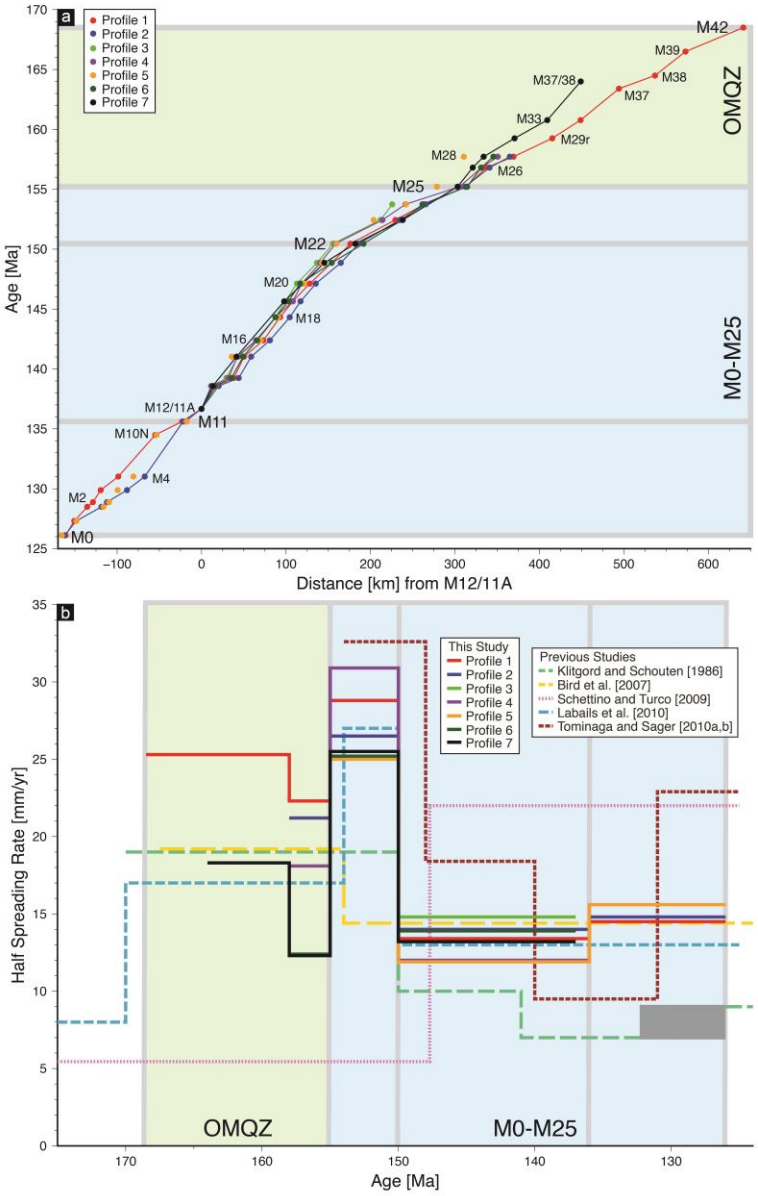

Figure 2.5 Seafloor spreading rates for the Early Atlantic: (a) Plot of age vs distance for magnetic anomalies. Blue and green backgrounds indicate M0-M25 and OMQZ regions, respectively. Distance expressed relative to M12/11A (youngest chron present on all seven profiles). (b) Comparison of half spreading rates for this study (solid lines) and previous studies (dashed lines) (Klitgord & Schouten, 1986; Bird et al., 2007; Schettino & Turco, 2009; Labails et al., 2010; Tominaga & Sager, 2010a, 2010b) (Tables 2.1, 2.2). Blue and green backgrounds indicate M0-M25 and OMQZ regions, respectively. Grey box denotes period of variable asymmetric spreading from M10N to M4 in Klitgord and Schouten (1986). (Modified from Labails et al. (2010))

We have identified coherent, correlatable magnetic anomalies from east of the OMQZ to Bermuda in the area where chrons M0-M25 have previously been identified (Fig. 2.2). Between M0 and M25, we identified M0-M4 and M10N-M25, with magnetic anomaly peaks corresponding to M11A and M12, M13 and M14, and M24A, M24B, M25 merging together due to the slow seafloor spreading (Fig. 2.4; Table 2.2). Magnetic anomalies M5-M10 were not distinguishable due to the close proximity of magnetic anomalies M4 and M10A (Fig. 2.2a, 2.4).

2.5.2. OMQZ and M0-M25 seafloor spreading rates

We documented the spatial and temporal variation in seafloor spreading rates, both in the OMQZ and from M0-M25, using the age assignments and magnetic anomaly spacing on Profiles 1-7 (oriented as close to perpendicular to the margin from the data available) (Fig. 2.5; Table 2.2). We divided the OMQZ into two age ranges (1) M28 to M25 (~158-155 Ma), and (2) pre-M28. M28 to M25 seafloor half spreading rates varied along the margin, with a value of ~20 mm/yr for Profiles 1, 2, and 4 in the south and middle of the OMQZ, decreasing to ~12.3 mm/yr for Profiles 6 and 7 in the north (Fig. 2.5; Table 2.2). Pre-M28 half spreading rates were 25.3 mm/yr from M42 to M28 (~168.5-158 Ma) on Profile 1 and 18.3 mm/yr from M37/38 to M28 (~164-158 Ma) for Profile 7 (Fig. 2.5; Table 2.2).

Table 2.2 Half spreading rates estimated in this study. Spreading rates calculated at seven profiles along the margin (see Fig. 2.2 for locations; Fig. 2.5b for comparison)

Chron Range	Age Range [Ma]	Half Spreading Rate [mm/yr]						
		Profile 1	Profile 2	Profile 3	Profile 4	Profile 5	Profile 6	Profile 7
M0-M11	126-136	14.5	14.8			15.6		
M11-M22	136-150	13.4	14.0	11.3 (M12-M22)	12.0	11.9	13.9 (M12-M22)	13.2 (M12-M22)
M22-M25	150-155	28.8	26.5		30.9	25.0	25.2	25.5
M25-M28	155-158	22.3	21.2		18.1		12.4	12.3
M28-M42*	158-168.5	25.3						
M28-M37/38**	158-164							18.3

* Chron range only available on Profile 1

** Chron range only available on Profile 7

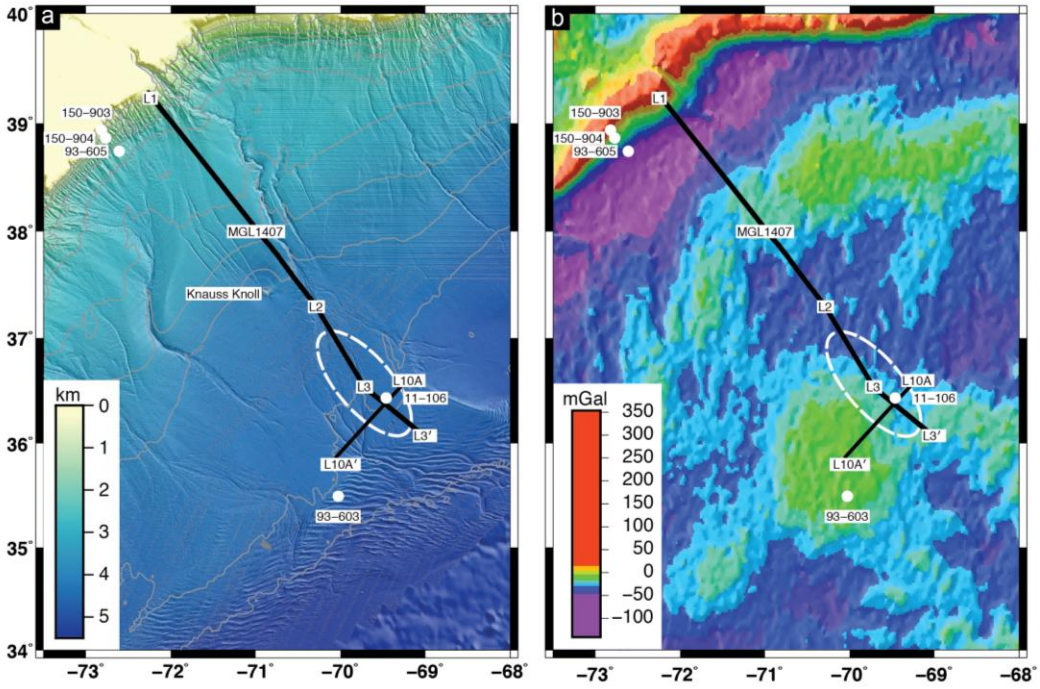

Figure 2.6 Hudson Fan Magnetic Anomaly High bathymetry and gravity: (a) Bathymetry in the vicinity of the HFMAH (Butman et al., 2006). White dashed line outlines HFMAH location (see Fig. 2.2). Grey contours every 500m. White circles denote locations of Deep Sea Drilling Program sites. Knauss Knoll location labeled (Lowrie & Heezen, 1967). (b) Gravity anomaly grid in the vicinity of the HFMAH (Sandwell et al., 2014). White dashed line outlines HFMAH location (see Fig. 2.2). White circles denote locations of Deep Sea Drilling Program sites.

To understand the temporal variation in seafloor spreading, we divided M0-M25 into three age ranges based on inflection points in the age-distance plot (Fig. 2.5a): (1) M25 to M22 (~155-150 Ma), (2) M22 to M11 (~150-136 Ma), and (3) M11 to M0 (~136-126 Ma). From M25 to M22, half spreading rates were estimated at ~25-31 mm/yr (Profiles 1, 2, 4-6) (Fig. 2.5; Table 2.2). At M22, the half spreading rate slowed, with estimated half spreading rates of ~12-14 mm/yr (Profiles 1-7) from M22 to M11 (or M12 when M11 was not identified) (Fig. 2.5; Table 2.2). The half spreading rate from M11 to M0 was estimated at ~15 mm/yr (Profiles 1, 2, and 5) (Fig. 2.5; Table 2.2).

During all three age range divisions from M0-M25, the seafloor spreading rates were similar on Profiles 1-7, not varying along the margin.

2.5.3. Anomalous magnetic features in the ENAM*

In addition to the well-known magnetic anomaly features such as the ECMA and BSMA, and the high amplitude magnetic anomalies associated with the New England Seamount chain and Bermuda, there are multiple distinct, high amplitude, ellipsoidal magnetic anomalies, including the HFMAH, which have not been previously investigated despite being of similar amplitude to the ECMA, New England Seamount Chain, and Bermuda (Fig. 2.1a). No major magmatic and/or structural disturbances were imaged by the MCS data in the crust, nor are there bathymetry or gravity anomaly highs present in conjunction with the HFMAH (Figs. 2.6a, 2.6b, 2.7b, 2.7c). MGL1407 MCS Lines 2, 3, and 10A over the HFMAH showed seafloor, basement, and Moho reflectors at approximately 4.4 km, 10.3 km, and 18.6 km, respectively (Figs. 2.7b, 2.7c). Two zones of rough basement topography, with variations up to ~400 m, were observed in the MCS data of MGL1407 MCS Lines 2 and 3 below the two peaks of HFMAH (Fig. 2.7b). In addition, MGL1407 MCS Line 10A, which crosses Line 3, shows that these zones of rough basement topography are three-dimensional in structure (Figs. 2.7b, 2.7c).

---

* Contents of this section derived in part from the master's thesis by study coauthor Matthew Karl for inclusion in publication. *Karl, M.R. (2016). The origin and implications of a high amplitude magnetic anomaly on the Eastern North American Margin, (master's thesis). Retrieved from MSU Libraries Digital Repository. (https://d.lib.msu.edu/etd/4205). East Lansing, MI: Michigan State University*.

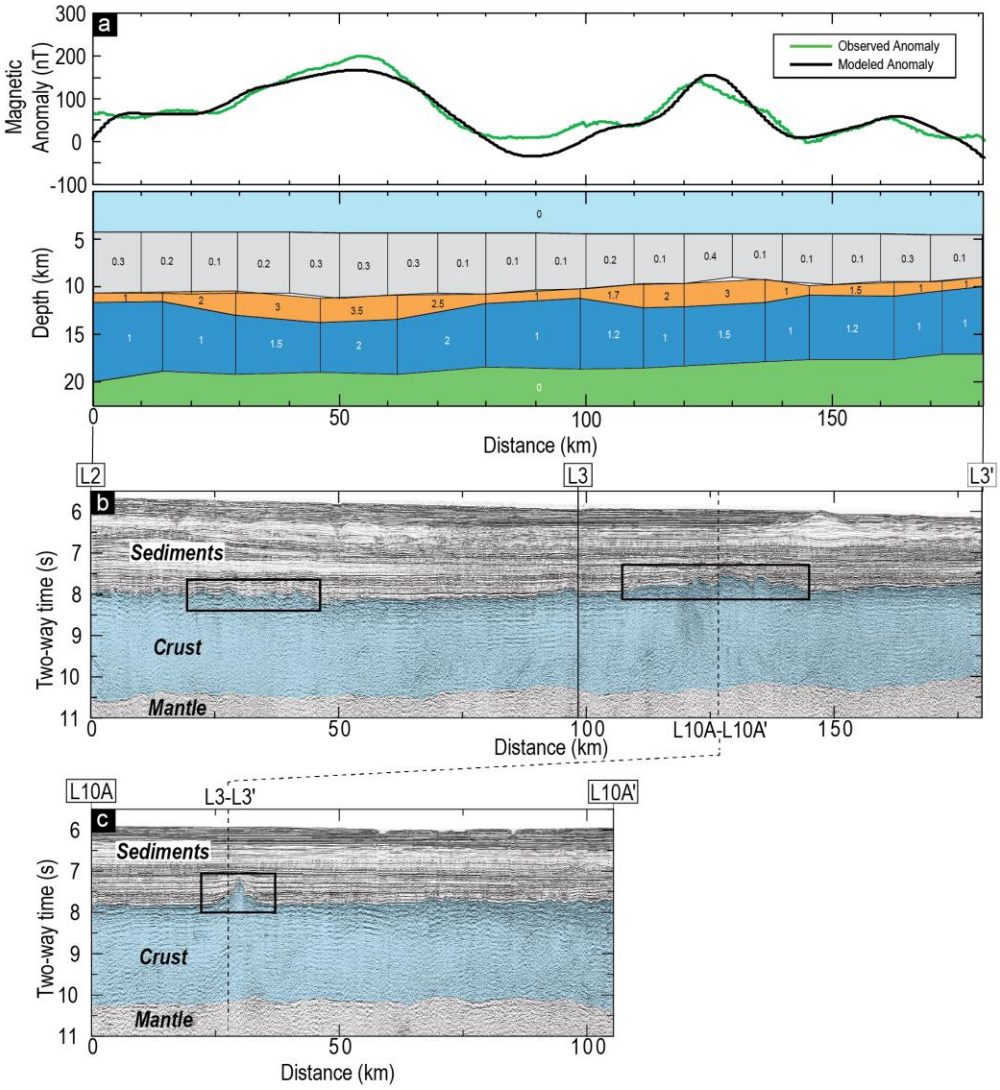

Figure 2.7 Hudson Fan Magnetic Anomaly High magnetic modeling and seismic: (a) Magnetic forward model varying both layer 2/3 thickness and magnetization for MGL1407 Lines 2 and 3 (see Fig. 2.6 for location). Upper panel: Green line is observed magnetic anomaly in MGL1407 seasurface data (Arsenault et al., 2017); black line is calculated magnetic anomaly from model. Lower panel: Prism geometry used in forward model showing water (light blue), sediment (gray), layer 2 (orange), layer 3 (blue), and mantle (green), with magnetizations (A/m) for each prism marked (~2:1 vertical exaggeration). (b) MCS data for MGL1407 Lines 2 and 3 (see Fig. 2.6 for location) (Arsenault et al., 2017) showing sediment, crust, and mantle. Dashed line shows Line 10A crossing. Black boxes mark areas of rough basement topography. (c) MCS data for MGL1407 Line 10A (see Fig. 2.6 for location) (Arsenault et al., 2017) showing sediment, crust, and mantle. Dashed line shows Line 3 crossing. Black box marks area of rough basement topography.

2.6. Discussion

The correlation of marine magnetic anomalies has played a prominent role in understanding the seafloor spreading history of the ENAM (e.g. Klitgord & Schouten, 1986; Bird et al., 2007; Schettino & Turco, 2009; Labails et al., 2010; Tominaga & Sager, 2010b). Our M0-M25 magnetic anomaly identifications reconfirm those from previous studies (e.g. Klitgord & Schouten, 1986; Labails et al., 2010), including the M25 location proposed by Labails et al. (2010) north of 35.5°N, which is at an anomaly ~50 km to the east of the M25 previously proposed by Klitgord and Schouten (1986) (Figs. 2.2b, 2.4). While we confirm the slow spreading regime from M0 to M25 (~126-155 Ma), found in previous studies (Fig. 2.5; Table 2.1) (Klitgord & Schouten, 1986; Bird et al., 2007; Schettino & Turco, 2009; Labails et al., 2010; Tominaga & Sager, 2010a, 2010b), our comprehensive magnetic anomaly and geophysical data analyses provided an unprecedented opportunity to closely investigate seafloor spreading rates and directions in the Atlantic JQZ. From these results, we are able to propose a scenario for the early Atlantic opening, including the possible influence of preexisting margin structure and rifting segmentation, and the subsequent seafloor spreading history forming the ENAM.

2.6.1. Early ENAM seafloor spreading regimes

We identify three regions within the Atlantic JQZ with different seafloor spreading regimes between the ECMA and M25 based on notable differences in magnetic anomaly coherency, magnetic anomaly lineation strike, and seafloor spreading

rates (Figs. 2.2b, 2.5; Table 2.2): (1) offshore New York and Massachusetts (New England Region); (2) offshore Virginia and New Jersey (Mid-Atlantic Region); and (3) offshore North and South Carolina (Carolina Region). In addition, the IMQZ, the previously identified area with low amplitude magnetic anomalies between the ECMA and BSMA (Vogt et al., 1971), extends south to north along the margin across these three Atlantic JQZ regions (Fig. 2.2a). We suggest these differences indicate that each region underwent different spreading regimes during the formation of the Atlantic JQZ, including accommodating the transitioning from the prominent bend characteristic of the ECMA offshore the New York Bight to the more linear strike at M25 (Fig. 2.2) that necessitates the emplacement of an additional ~28,000 km^2 of seafloor.

The New England Region extends ~470 km from east to west in its center at 38°N, with its northern boundary at the New England Seamount Chain and its southern boundary located offshore the New York Bight, near the prominent strike change in the ECMA and BSMA (Fig. 2.2a). Both the IMQZ and OMQZ sections of this region widen longitudinally from north to south (Fig. 2.2a). The magnetic anomalies in the New England Region are semi-coherent, and there is a change in magnetic anomaly lineation strike occurring from west to east across this region, being ~80° at the ECMA, ~70° at the BSMA, and ~55° at M25, suggesting a counterclockwise reorientation of the paleo-magmatic center during formation (Fig. 2.2b). Estimated half spreading rates in the New England Region in the OMQZ were 18.3 mm/yr from M37/38 to M28 and ~12.3-18.0 mm/yr from M28 and M25, being lower in north (Fig. 2.5b; Table 2.2).

The Mid-Atlantic Region extends ~620 km from east to west in its center at 36°N, with its northern boundary located offshore the New York Bight and its southern boundary located offshore Cape Hatteras, North Carolina (Fig. 2.2a). The magnetic anomalies in the Mid-Atlantic Region are the least coherent of the three regions, particularly in the OMQZ, and there is an approximately consistent magnetic anomaly lineation strike of 30° across this region, suggesting little region wide reorientation of the paleo-magmatic center during formation (Fig. 2b). The estimated half spreading rate in the Mid-Atlantic Region in the OMQZ was ~18.0 mm/yr from M28 to M25 (Fig. 2.5b; Table 2.2).

The Carolina Region extends ~575 km from east to west in its center at 32°N, with its northern boundary located offshore Cape Hatteras, North Carolina, and the southern boundary located offshore southern South Carolina and the southern termination of the ECMA (Fig. 2.2a). The IMQZ in the Carolina Region is approximately consistent in width, while the OMQZ widens slightly longitudinally from north to south (Fig. 2.2a). The magnetic anomalies in the Carolina Region are the most coherent of the three regions, and there is an approximately consistent magnetic anomaly lineation strike of 30° across this region (Fig. 2.2b). Estimated half spreading rates for the Carolina Region in the OMQZ were 25.3 mm/yr from M42 to M28 and 22.3 mm/yr from M28 to M25 (Fig. 2.5b; Table 2.2).

We further examine the along-margin differences in the Atlantic JQZ seafloor spreading regimes between the BSMA and M25 for the first time (Figs. 2.2a, 2.4). While we confirm that the spreading rates calculated from Profiles 1-7 are consistent with

previous estimates from M0 to M25 (Fig. 2.5b; Tables 2.1, 2.2) (e.g. Klitgord & Schouten, 1986; Bird et al., 2007; Schettino & Turco, 2009; Labails et al., 2010), we find that the seafloor spreading rates in the OMQZ of the ENAM are slower in the north (~12 mm/yr on Profiles 6 and 7) compared to the south and middle (~20 mm/yr on Profiles 1, 2, and 4) and are also slower than the rates calculated for the conjugate West African Margin (half spreading rates of 22.0 mm/yr and 24.6 mm/yr in Roeser et al. (2002) and Bird et al. (2007), respectively). Furthermore, our new identification of M-series anomalies in the Atlantic JQZ are in agreement with the M28 and M29 of Bird et al. (2007), while we confidently redefine M33 and M39 instead of the previously identified M32 and M40, respectively (Bird et al., 2007), based on our detailed investigation of the superposed anomalies produced by remnant magnetization in crust formed from slower spreading during a period of rapid polarity reversals and our use of an updated, more recent geomagnetic polarity timescale (2012 Geomagnetic Polarity Time Scale (Ogg, 2012)) (Figs. 2.4, A.1). Based on their interpreted duplicates of chrons M32-M38 on the West African Margin and absence on the ENAM, Bird et al. (2007) proposed a major westward ridge jump within the OMQZ. However, the presence of M33, M37, and M38 in this study (Figs. 2.2, 2.4) suggests that seafloor spreading between the BSMA and M25 occurred without this specific proposed ridge jump, consistent with previous studies (e.g. Klitgord & Schouten, 1986; Schettino & Turco, 2009; Labails et al., 2010), though we are unable to definitively rule out the presence of ridge jumps that could have occurred between our interpreted magnetic anomalies.

Along the margin in the IMQZ, throughout all three Atlantic JQZ regions, our systematic investigation of magnetic anomaly correlations enables us to discover five coherent, correlatable magnetic anomalies IMA1-5 extending along the margin in the IMQZ throughout all three Atlantic JQZ regions (Fig. 2.2b, 2.3b, 2.3c). We propose that the coherency of these linear magnetic anomalies is attributed to either: (1) syn-rift, extensional stage magmatism emplaced in stretched continental or transitional crust similar to what is seen in rift setting around the world (e.g. Gunn, 1997; Russel & Whitmarsh, 2003; Bronner et al., 2011; Bridges et al., 2012); or (2) steady state mid-ocean ridge magmatism forming the earliest oceanic crust of the Atlantic (e.g. Klitgord & Schouten, 1986; Bird et al., 2007; Schettino & Turco, 2009; Labails et al., 2010).

Although IMA1-5 are distinctive and correlatable along the entire margin, assigning ages/chron numbers to IMA1-5 and calculating seafloor spreading rates are currently challenging. In either the proposed ridge jump (Vogt, 1973; Klitgord & Schouten, 1986; Bird et al., 2007; Schettino & Turco, 2009; Kneller et al., 2012) or change in spreading rate and direction (Labails et al., 2010) early opening scenarios, the IMQZ formation predates the BSMA. The estimated age for the BSMA from previous studies is ~168-171 Ma (e.g. Klitgord & Schouten, 1986; Benson, 2003), and if the BSMA source is crust produced by seafloor spreading, it may be M42 (~168.5 Ma) based on the similarity in magnetic anomaly character (Fig. 2.4). These BSMA ages are near the age of the oldest chron in the M-series of the geomagnetic polarity timescale (~171 Ma) (Ogg, 2012). Consequently, the IMQZ formation prior to the BSMA predates the timescale, which currently precludes us from assigning ages/chon numbers to IMA1-

5. The lateral offsets of IMA1-5 in the Carolina and Mid-Atlantic Regions documented in this study coincide with predicted extensions of fracture zones made by Klitgord and Schouten (1986), while our interpreted offsets in the New England Region trend more towards the north, maintaining an orientation perpendicular to IMA1-5 (Figs. 2.1a, 2.3a), which is consistent with the findings of Schettino and Turco (2009). Regardless of the mode of IMQZ seafloor formation, the margin-wide presence of IMA1-5 indicates that the igneous activity forming the source of these magnetic anomalies extended along the entire margin during the formation of the IMQZ, recording the contemporaneous geomagnetic field at the time of emplacement.

2.6.2. Tectonic origin of anomalous magnetic features in the ENAM*

In the Atlantic JQZ, there are distinct, high amplitude, ellipsoidal magnetic anomalies, including the HFMAH at the south end of the New England Region and Mid-Atlantic Region (Fig. 2.1a), that have not been investigated, despite being historically present in magnetic anomaly data (e.g. Klitgord and Behrendt, 1977; Zietz, 1982; Bankey et al., 2002; Meyer et al., 2016). These magnetic anomalies do not exhibit the margin-wide, coherent anomaly character associated with syn-rift volcanism or seafloor spreading processes (e.g. Vogt, 1986; Gunn, 1997; Bridges et al., 2012), nor are they related to known volcanic features of the ENAM that produce high amplitude magnetic

* Contents of this section derived in part from the master's thesis by study coauthor Matthew Karl for inclusion in publication. *Karl, M.R. (2016). The origin and implications of a high amplitude magnetic anomaly on the Eastern North American Margin, (master's thesis). Retrieved from MSU Libraries Digital Repository. (https://d.lib.msu.edu/etd/4205). East Lansing, MI: Michigan State University.*

anomalies of similar dimensions, such as the New England Seamount Chain (Duncan, 1984), Bermuda (Vogt, 1986), the Great Stone Dome (Taylor et al., 1968; Grow et al., 1988), a buried seamount near the Hudson Canyon (Grow et al., 1988), or Knauss Knoll (Lowrie & Heezen, 1967; Sweeney et al., 2012) (Fig. 2.1, 2.2, 2.6b). Using recently collected high-resolution seasurface magnetic anomaly and MCS data from the HFMAH (Arsenault et al., 2017), we seek to identify the magnetic source creating the HFMAH and other distinct, high amplitude, ellipsoidal magnetic anomalies of the ENAM (Fig. 2.1a) based on observations, modeling, and the regional tectonic history of the Atlantic JQZ.

The most obvious marine magnetic anomaly sources are: (i) geomagnetic polarity boundaries, (ii) excess volcanic emplacement, and (iii) major lithological and structural boundaries. The HFMAH being sourced to a contrast from geomagnetic polarity reversals is unlikely since the frequent polarity reversals during a period of low geomagnetic field strength thought to occur during the formation of the Atlantic JQZ would produce low amplitude magnetic anomalies, as seen in the Atlantic JQZ surrounding the HFMAH (Fig. 2.1a) (Larson & Pitman, 1972; Tivey et al., 2006). Furthermore, late-stage magmatic events can emplace excess igneous material producing high amplitude magnetic anomalies, as seen at the New England Seamount Chain, Bermuda, and the ECMA (Duncan, 1984; Vogt, 1986; Talwani et al., 1995). However, neither the most recent satellite-derived bathymetry, gravity anomaly, and vertical gravity gradient grids nor the MCS data collected for MGL1407 Lines 2, 3, or 10A indicate any local additions of excess igneous material under the HFMAH (Figs. 2.6a,

2.6b, 2.7b, 2.7c); hence, excess volcanism as the predominant source of the HFMAH is also unlikely.

To investigate the possible magnetic source architecture producing the HFMAH, we conducted two-dimensional magnetic forward modeling (Fig. 2.7a) (Talwani & Heirtzler, 1964) with the source geometry identified beneath the HFMAH using the MCS data from MGL1407 MCS Lines 2 and 3 (Arsenault et al., 2017) and depths estimated with the velocity model of Lizarralde and Holbrook (1997), located ~550 km to the west of the HFMAH. MGL1407 MCS Lines 2 and 3 were selected for this modeling as they cross directly over both peaks of the HFMAH, and display the zones of rough basement topography (Fig. 2.7b). To match the calculated and observed magnetic anomaly signal in our forward modeling, we adjusted the magnetization values for layer 2 and 3 and the thickness of layer 2. The corresponding thickness of layer 3 is dependent on the layer 2 thickness since the total igneous crust is constrained by the basement and Moho reflector depths. After producing two end-member models varying only the layer 2 thickness and magnetization, respectively, we created a series of models to include variations in both the layer 2 and 3 thicknesses (1-2.5 km and 5-8 km for layers 2 and 3, respectively) and magnetizations (1 to 3.5 and 1 to 2 A/m for layers 2 and 3, respectively (e.g. Johnson & Pariso, 1993)) (final model shown in Figure 2.7a). In each model, the most distinctive magnetic source bodies (i.e. highest magnetization and/or thickest layer 2) were confined directly beneath the two peaks of the HFMAH, corresponding with the locations of rough basement topography in the MCS data, suggesting that processes

acting to increase the magnetization and/or layer 2 thickness could be responsible for producing the source of the HFMAH (Fig. 2.7).

Differences in the abundance and type of magnetic minerals in the neighboring rock formations create lithological contrasts (with different magnetic susceptibility of each rock formation) that could produce magnetic anomalies. While initial sediment deposition at the ENAM included evaporates and carbonates during the Jurassic, from the Cretaceous to the present, terrigeneous sediments have been deposited by river systems along the coast (Poag & Sevon, 1989). Numerous submarine canyon systems incise the ENAM continental slope, and some have been active over millions of years transporting the terrigeneous sediment from the continental shelf to the abyssal plain (Pilkey & Cleary, 1986; Gardner, 1989) (Fig. 2.1b). The Hudson Fan, coinciding with the location of the HFMAH, receives terrigenous sediments through the Hudson Canyon system forming a thick sedimentary package (Figs. 2.7b, 2.7c) (Poag & Ward, 1993; Butman et al., 2006). Nearby Deep Sea Drilling Program holes 11 and 106 penetrated the top 1,015 m of sediments on the shelf edge and slope (Fig. 2.6a), manifesting some discrete zones with up to 15 weight percent iron and sulfide bearing sediments (Hollister et al., 1972). Although this is a significant weight percentage of possible magnetic carriers, the contribution of the sedimentary magnetization to the total magnetic anomaly amplitude is only ~10% (~10-20 nT) in our forward modeling even if we distribute this concentration of iron-bearing minerals throughout the entire sediment package beneath the two HFMAH peaks. Therefore, the coincidence of the HFMAH and Hudson Canyon locations cannot explain the origin of HFMAH. Additionally, lithological contrasts with

a zone of higher magnetization could exist in the igneous basement from hydrothermal alteration processes. In the lower crust and upper mantle at the modern day Mid-Atlantic Ridge serpentinization processes have been known to produce strongly magnetized crust (e.g. Oufi et al., 2002; Tominaga et al., 2016); however, the MCS data clearly indicate that, beneath the two HFMAH peaks, there is no evidence of thin crust, exhumed lower crust and upper mantle, or deep penetrating faults that could promote alteration within the lower crust and upper mantle (Figs. 2.7b, 2.7c).

Structural boundaries can produce magnetic anomalies, including faults and basement offsets along long-lived fracture zones, some of which have been predicted to extend near the HFMAH (Fig. 2.1a) (e.g. Larson & Pitman, 1972; Klitgord & Schouten, 1986; Grauch et al., 2006). However, the directions of the predicted fracture zone extensions (Klitgord & Schouten, 1986) are perpendicular to the expected direction of a fault or basement offset that could produce the observed two-peak magnetic anomaly high, and there is no evidence in the MCS data of faults or basement structure that is indicative of a fracture zone (Figs. 2.1a, 2.7b, 2.7c) (Gudmundsson, 1993; Grauch et al., 2006).

To explain the origin of the HFMAH based on the combination of the basement morphology beneath the HFMAH and the regional tectonic history, we propose a hypothesis where the HFMAH is attributed to the emplacement of basalts enriched in iron and titanium produced by a short lived propagating rift, as seen at some modern day rifting and spreading centers (e.g. Hey, 1977; Hey et al., 1980; Sinton et al., 1983; Wanless et al., 2012). Magnetic anomalies in these areas are characterized by ellipsoidal

magnetic anomaly highs that are unrelated to the seafloor spreading magnetic anomalies (e.g. Hey et al., 1980; Hey & Wilson, 1982), suggesting ellipsoidal magnetic anomalies of the ENAM, such as the HFMAH, could be related to tectonic activity during the early Atlantic seafloor spreading. For a propagating rift, as the growing spreading center advances, the transform fault becomes inactive and it, along with a segment of the dying spreading center, is added to the adjacent oceanic lithosphere (see Figure 2.8b and 2.8c insets) (Hey, 1977). The wakes of propagating rifts have been associated with unusually high amplitude magnetic anomalies, which are correlated to basalts enriched in iron and titanium that create abundant single-domain magnetite from renewed crystal fractionation when the propagating rift breaks through older, thicker crust, or taps off-ridge, relatively differentiated magma chambers (Hey et al., 1980; Sinton et al., 1983; Horen & Fleutelot, 1998; Wanless et al., 2012). Additionally, it has been observed that there is thicker than average extrusive crust, represented by seismic layer 2A, at the propagating rift tip (Bazin et al., 2001; Wanless et al., 2012). The propagating rift also creates short-wavelength, rough basement topography as a result of the change in seafloor spreading rate at the area at the tip of the propagating rift, from zero to the rate present for the rest of the ridge (Hey et al., 1980). Furthermore, short-wavelength, rough basement topography is observed beneath the magnetic anomaly peaks of the HFMAH (Figs. 2.7b, 2.7c). We suggest that the thickened layer 2 with higher magnetization found in our modeling, confined beneath the two rough basement topography zones, could represent the magmatism emplacing a thicker extrusive layer of highly magnetized basalt, as has been observed at the tips of a propagating rift (Fig. 2.7) (Hey et al., 1980;

Wilson & Hey, 1995; Hey et al., 1986; Miller & Hey, 1986; Bazin et al., 2001; Wanless et al., 2012).

2.6.3. Effect of preexisting structure and rift segmentation on ENAM crustal formation

The juxtaposition of accreted terranes from past plate tectonic cycles are generally thought to play a key role in the localization of continental breakup, such as during the rifting of Pangea that led to the formation of the ENAM, with rifting occurring along a preexisting zone of weakness in the continental crust (Wilson, 1966; Sawyer, 1985; Manspeizer, 1988; Dunbar & Sawyer, 1989; Sheridan et al., 1993; Labails et al., 2010). Preexisting structure could also influenced the later crustal formation of the ENAM following the initial rifting, causing rifting segmentation and magmatic center offsets that may have led to the formation of early Atlantic fracture zones (e.g. Sawyer, 1985; Behn & Lin, 2000). Our newly identified patterns of correlated magnetic anomalies and interpreted offsets in the Atlantic JQZ and their apparent coincidence with possible indicators of rifting segmentation and terrane boundaries may support this hypothesized influence from preexisting structure, if the anomaly offsets are representative of incipient fracture zones (Williams & Hatcher, 1982; Higgins & Zietz, 1983; Sawyer, 1985; Behn & Lin, 2000; Boote & Knapp, 2016). One of the most prominent observations of this coincidence is that many of the lateral offsets of IMA1-5 within the IMQZ appear to intersect the ECMA at the gaps between major segments observed in the aeromagnetic and EMAG2v3 magnetic grids (Fig 2.2b,

2.3a). The ECMA segmentation is thought to represent along margin rifting segmentation from variations in magmatism and/or pre-existing lithospheric weaknesses, which may have led to incipient fracture zone formation (Dunbar & Sawyer, 1989; Behn & Lin, 2000; Wyer & Watts, 2006). The coincidence between the ECMA segmentation and IMA1-5 lineation offsets documented in this study, if they indicate fracture zones, could support the hypothesis that the early pattern of seafloor spreading or syn-rift magmatism forming the IMQZ seafloor could have been governed by the rifting architecture and pre-existing structure of the margin (Fig. 2.2b) (Dunbar & Sawyer, 1989; Behn & Lin, 2000; Wyer & Watts, 2006).

Furthermore, the New England, Mid-Atlantic, and Carolina Region boundaries, identified based on changes in magnetic anomaly character, are observed to coincide with the previously identified predicted extensions of major fracture zones and intersect the ECMA at major gaps between segments that are thought to be related to rifting segmentation and pre-existing zones of weakness (Klitgord & Schouten, 1986; Behn & Lin, 2000). The southernmost boundary coincides with the southern termination of the ECMA, as well as the Blake Spur Fracture Zone, which is thought to have formed from at an abrupt change in rheology associated with a suture (Figs. 2.2b, 2.3a) (Sawyer, 1985; Klitgord & Schouten, 1986; Boote & Knapp, 2016). Likewise, the boundary between the Carolina and Mid-Atlantic Regions coincides with the Northern Kane Fracture Zone (Tucholke & Schouten, 1988; Müller & Roest, 1992), which intersects a major gap between ECMA segments located offshore Cape Hatteras, North Carolina that also approximately coincides with the boundary between the Carolina and the Brunswick

(Charleston) terranes (Williams & Hatcher, 1982; Higgins & Zietz, 1983) and the revised location of an Alleghanian suture zone of Boote and Knapp (2016) (Figs. 2.2b, 2.3a). The boundary between the Mid-Atlantic and New England Regions coincides with the Delaware Bay Fracture Zone in the Atlantic JQZ (Klitgord & Schouten, 1986) before bending northward in the IMQZ to maintain a strike perpendicular to IMA1-5, where it aligns with a lateral offset of IMA1-5 documented in this study and intersects a major gap between ECMA segments offshore Delaware (Figs. 2.2b, 2.3a). The northern boundary of the New England Region is the New England Seamount Chain, which may have formed along a fracture zone, and also intersects a major gap between ECMA segments offshore Massachusetts (Figs. 2.2b, 2.3a) (de Boer et al., 1988). Based on our observed association of our newly interpreted offsets of IMA1-5 and the boundaries between the three Atlantic JQZ regions of distinct magnetic anomaly character with (i) evidence of rifting segmentation (e.g. Behn & Lin, 2000); and (ii) in some cases, hypothesized sutures at terrane boundaries (e.g. Williams & Hatcher, 1982; Higgins & Zietz, 1983; Sawyer, 1985; Boote & Knapp, 2016) (Fig. 2.2b, 2.3a), we suggest that the pre-existing margin structure and rifting segmentation of the ENAM have influenced the subsequent seafloor spreading regimes in the Atlantic JQZ.

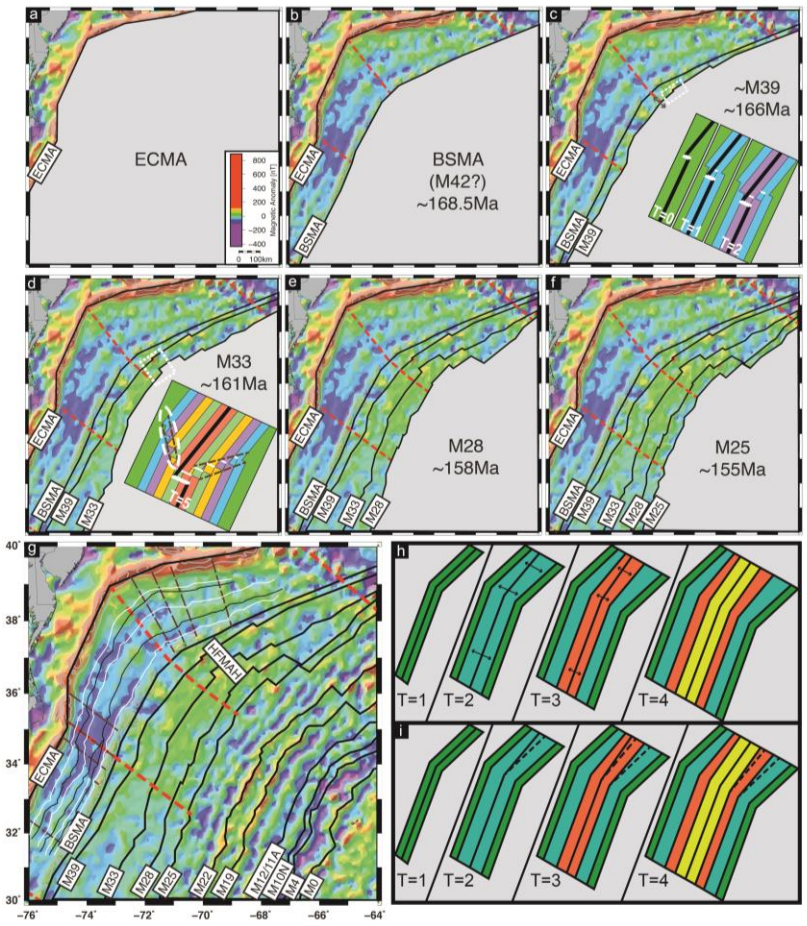

Figure 2.8 Schematic of early Atlantic formation history: (a-g) Schematic of Atlantic JQZ formation from the ECMA to M25. Magnetic anomaly name or chron number denote seafloor being formed at each time step, with solid black lines showing inferred ridge location. Arrows show inferred spreading direction for paleo-Mid-Atlantic Ridge. Red dashed lines mark New England, Mid-Atlantic, and Carolina Region boundaries (Fig. 2.1). White dashed box shows developing HFMAH (c, d). Brown dashed lines mark interpreted offsets in IMQZ magnetic anomalies IMA1-5. (h) Schematic showing ridge reorientation over four time steps by asymmetric spreading (indicated by arrow length in T=2 and T=3). (i) Schematic showing ridge reorientation over four time steps by westward ridge jumps in T=2 and T=3, with dashed line indicating ridge location prior to jump. Inset diagrams in panels (b) and (c) detail propagating rift evolution at time steps of 0, 1, 2, and 5: Like color bars represent crust of same age; thick black line is ridge axis; thick white line is active transform fault; thin white line is fossil transform fault; dashed brown lines in T=5 represent "pseudofault" trend, with the white dashed ellipse outlining the corresponding area of potentially high magnetic anomalies, such as those of the HFMAH (modified from Hey (1977), their Fig. 2).

2.6.4. Early ENAM formation history- from the ECMA to M25

Using our new Atlantic JQZ magnetic anomaly interpretations, we propose a crustal formation and evolution model from the ECMA to M25, specifically highlighting a missing piece of the ENAM history and early Atlantic opening (Figs. 2.1a, 2.8a-g). The IMQZ, bounded to the west by the ECMA, is the oldest crust of the Atlantic JQZ and was possibly formed by igneous activity associated with early seafloor spreading or late syn-rift magmatism, producing IMA1-5 (Figs. 2.2b, 2.3b). If the IMQZ is composed of oceanic crust, we suggest the initial seafloor spreading of the Atlantic following continental rifting was perpendicular to the margin using the consistent IMA1-5 strike parallel to the ECMA, along with the IMA1-5 offsets possibly representing fracture zones oriented approximately perpendicular to the ECMA, as indicators of seafloor spreading direction (Figs. 2.2b, 2.3). However, the lack of magnetic anomaly ages/chron numbers for IMA1-5 causes difficulty in determining a preferred scenario for the early Atlantic formation. A ridge jump at the BSMA (Vogt, 1973; Klitgord & Schouten, 1986; Vogt, 1986; Bird et al., 2007; Schettino & Turco, 2009; Kneller et al., 2012) would produce IMA1/IMA5 and IMA2/IMA4 as conjugate magnetic anomalies, with IMA3 in the center as the youngest, while a drastic change in spreading rate and direction at the BSMA (Labails et al., 2010) would produce independent magnetic anomalies younging from IMA5 to IMA1 (Figs. 2.2b, 2.3b). Likewise, if IMA1-5 are the result of syn-rift magmatism, we suggest that rifting occurred approximately perpendicular to the margin during the formation of the IMQZ, with igneous emplacement occurring along the rift

axis similar to observations along the nascent seafloor spreading near the Afar Depression (e.g. Bridges et al., 2012).

Following the formation of the IMQZ, the crust producing the BSMA was created (Figs. 2.2; 2.8b), which has been proposed to be related to either a ridge jump or a spreading rate/direction change (Vogt, 1973; Klitgord & Schouten, 1986; Bird et al., 2007; Schettino & Turco, 2009; Labails et al., 2010; Kneller et al., 2012). In this study, we are unable to determine whether the source of the BSMA is oceanic crust produced by seafloor spreading (e.g. Labail et al., 2010) or a sliver of continental crust and igneous intrusives isolated from the African margin by a ridge jump (e.g. Vogt, 1973). Nevertheless, if the BSMA source is crust emplaced by seafloor spreading (regardless of if a ridge jump occurred or not), the similarity in magnetic anomaly character between the BSMA and M42 in our synthetic profiles (see Profile 1 in Figure 2.4) could indicate that the BSMA may be M42, suggesting an age of ~168.5 Ma that is consistent with the BSMA ages of previous studies (168-171 Ma) (Klitgord & Schouten, 1986; Benson, 2003). Alternatively, if the BSMA is produced by an isolated sliver of continental crust and igneous intrusives (e.g. Vogt, 1973), the similarity of the magnetic anomaly character between the BSMA and M42 is merely coincidental, as the BSMA would not be sourced to crust produced by seafloor spreading.

Continuing after the formation of the BSMA, the OMQZ formed (Figs. 2.2; 2.8c-g). Our magnetic anomaly correlations in the New England, Mid-Atlantic, and Carolina Regions, along with anomalous ellipsoidal magnetic features such as the HFMAH, show that the seafloor spreading history from the BSMA to M25 was dictated by asymmetric

crustal accretion and ridge orientations, possibly accompanied by short lived propagating rifts. Across the New England Region, the strike of magnetic anomaly lineations rotate counterclockwise from ~70° to ~55° (west to east) between the BSMA and M25 (Figs. 2.2b, 2.8b-g), and the calculated seafloor spreading rates are slower in the northern part of the New England Region compared to those further south (~12 mm/yr on Profiles 6 and 7 versus ~20 mm/yr on Profiles 1, 2, and 4). The change in magnetic anomaly strike in the New England Region indicates a change in ridge orientation during the formation of the OMQZ.

The conjugate Northwest African Margin shows a similar change in magnetic anomaly orientation between the African Blake Spur Magnetic Anomaly (ABSMA), a possible conjugate to the BSMA (Labails et al., 2010), and M25. A plate reconstruction to 153Ma, using the GPlates software package (Boyden et al., 2011) and the rotation poles from the recent global plate reconstruction model of Müller et al. (2016), shows that the ABSMA, has a strike mirroring that of the BSMA (Fig. 2.9) (Labails et al., 2010). For the Mid-Atlantic and Carolina Regions and their conjugates, the BSMA/ABSMA are oriented parallel to M25, while for the New England Region and its conjugate, the BSMA and ABSMA parallel each other, but are oblique to M25 (Fig. 2.9). Additionally, the distance between the BSMA and M25 becomes narrower moving northward in the New England Region, while the corresponding distance between the ABSMA and M25 on the Northwestern African Margin becomes wider moving northward (Fig. 2.9). Regardless of if the ABMSA is the conjugate to the BSMA or not (e.g. Klitgord & Schouten, 1986; Schettino & Turco, 2009; Labails et al., 2010), the

orientation of these linear magnetic anomalies on the either side of the Atlantic are consistent.

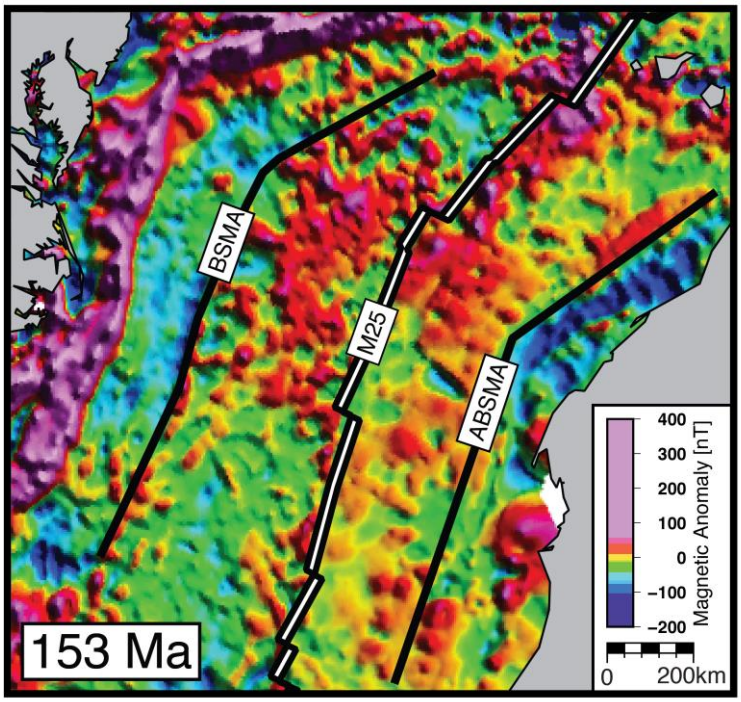

Figure 2.9 Early Atlantic plate reconstruction: Plate reconstruction at 153 Ma, just following the creation of M25, the oldest generally accepted chron in the Atlantic, at ~155 Ma showing the ENAM and Northwestern African Margin and the EMAG2v3 composite magnetic anomaly grid (Meyer et al., 2016). Compares the orientation of the BSMA/Atlantic Blake Spur Magnetic Anomaly (ABSMA) orientation and the paleo-Mid-Atlantic Ridge at M25. Note that south of the bend in the BSMA/ABSMA, the BSMA/ABSMA are oriented parallel to M25, while to the north, the BSMA and ABSMA parallel each other, but are oblique to M25. ABSMA interpretation is based on Labails et al. (2010).

2.6.5. Crustal accretion style during the early formation of the ENAM

To account for both the slower spreading rates and magnetic anomaly lineation strike change in the New England Region (and its conjugate on the Northwest African

margin), we suggest asymmetric crustal accretion occurred during the formation of the OMQZ crust of the western North Atlantic, causing a reorientation of the ridge during the formation of the OMQZ from the bend of the ECMA, IMA1-5, and BSMA to the more linear strike of the M25 lineations and contemporaneous Mid-Atlantic Ridge (Figs. 2.8, 2.9). Spreading center reorientations have globally been identified based on rotations of magnetic anomaly lineation trends, caused by the asymmetric accretion of crust on either side of a spreading center. Ramberg et al. (1977) documented a spreading axis reorientation of the Mid-Atlantic Ridge southwest of the Azores, which they propose was facilitated by a combination of asymmetric spreading and small (5-10 km) ridge jumps of individual ridge segments. Likewise, Rona and Gray (1980) identified reorientations of the Mid-Atlantic Ridge in the young seafloor between the Kane and Atlantis Fracture Zones, which they attribute to asymmetric seafloor spreading. At the Juan de Fuca Ridge, Menard and Atwater (1968) and Wilson et al. (1984) suggest the ridge reorientation could be facilitated by either asymmetric spreading or ridge jumps (with which they find associated propagating rifts), respectively. Altogether, asymmetric crustal accretion mechanisms could account for the ridge reorientation observed between the BSMA/ABSMA and M25 (Fig. 2.8b-g), with the asymmetric accretion caused by: (1) asymmetric seafloor spreading, with slower spreading in the northern New England Region on the North American side and faster spreading on the African side (Fig. 2.8h); and/or (2) small, successive westward ridge jumps during the formation of the New England Region that adjusted the orientation of the ridge (Fig. 2.8i). With either mechanism (or a combination of both), the change in orientation observed on the

Northwest African Margin and asymmetric crustal accretion balances that on the ENAM in the New England Region (Fig. 2.9).

We do not directly interpret any missing chrons indicative of ridge jumps in the New England region, but the presence of ridge jumps could not entirely be omitted as a mechanism responsible for the reorientation since ridge jumps could have occurred between the identified chrons in the OMQZ (Fig. 2.2b). Additionally, if ridge jumps occurred, the entirety of the ridge in the New England Region did not necessarily jump simultaneously; rather, individual spreading segments may have jumped independently, with the combined overall effect of changing the ridge orientation (e.g. Ramberg et al., 1977). Either mechanism of asymmetric accretion, or a combination of both, would create the comparatively lower seafloor spreading rates calculated in the New England Region while changing the ridge orientation (Fig. 2.8b-g). If asymmetric seafloor spreading occurred, a slower spreading on the North American side of the ridge in the New England Region would produce the lower rates (Fig. 2.8h). If westward ridge jumps occurred in the New England Region, the crust formed on the North American side of the ridge would be transferred to the African side, causing an apparently slower spreading rate due to the reduced amount of seafloor remaining (Fig. 2.8i).

Changes in plate motion are a potential cause of asymmetric accretion and changes in spreading axis orientations (e.g. Menard and Atwater, 1968; Wilson et al., 1984). At the ENAM, Labails et al. (2010) suggested a change in plate motion, from NNW–SSE to NW–SE, occurred at the BSMA. If this change in plate motion occurred, coinciding with the beginning of the OMQZ formation (Fig. 2.8b), it may have triggered

the spreading axis reorientation observed in the New England Region (Fig. 2.8c-g), as the BSMA in this region is oriented more oblique to the new spreading direction compared to the BSMA of the Mid-Atlantic/Carolina Regions and M25 (Figs. 2.8b-g, 2.9).

Short-lived propagating rift segments, such as those hypothesized to be represented by the HFMAH, could have further contributed to the change in spreading center orientation (Figs. 2.2, 2.8a-g). We suggest that these propagating rifts lined up seaward of the bend observed in the ECMA and the coastline at the New York Bight, near the boundary between the Mid-Atlantic and New England Regions, where it may have helped accommodate the spreading center straightening to that observed at M25 (Figs. 2.8c, 2.8d), as propagating rifts have been found to be accompanied by changes in spreading center strike (Hey et al., 1980, 1986, 1988).

South of the New England Region, in the Mid-Atlantic and Carolina Regions, the identified magnetic anomaly lineations are all approximately parallel to both the BSMA and M25, and the calculated spreading rates are consistent (~20 mm/yr) (Figs. 2.2b, 2.8b-g; Table 2.2). This suggests that the seafloor spreading forming the OMQZ in the Mid-Atlantic and Carolina Regions proceeded without any ridge reorientation (Fig. 2.8b-g). Overall, seafloor spreading from M25 to the present-day Mid-Atlantic Ridge has taken place without the notable along strike variation in spreading rates and spreading axis reorientation observed in the OMQZ (Figs. 2.2b, 2.5, 2.8g; Table 2.2) (Klitgord & Schouten, 1986; Bird et al., 2007; Müller et al., 2008; Schettino & Turco, 2009; Labails et al., 2010; Tominaga & Sager, 2010a, 2010b).

2.7. Conclusions

From this study we draw the following conclusions:

(1) Five newly identified coherent, correlatable magnetic anomalies exist along the entire margin in the IMQZ, which could be related to the earliest seafloor spreading of the Atlantic or igneous emplacement during the final stages of continental rifting.

(2) If the source of the BSMA is oceanic crust, the BSMA may be M-series anomaly M42 (~168.5 Ma) based on the similarity of magnetic anomaly character between the BSMA and M42.

(3) Seafloor spreading rates during the formation of the OMQZ in the northwestern Atlantic were slower in the north compared to the south, and a 15° counterclockwise reorientation of the spreading axis occurred and straightened the prominent bend in the ECMA to the more linear strike of M25 and the contemporaneous Mid-Atlantic Ridge, possibly caused by asymmetric spreading and/or westward ridge jumps.

(4) The HFMAH may be sourced from magma emplaced during a short-lived propagating rift that may have helped accommodate the straightening of the ridge during the formation of the OMQZ.

(5) The newly identified magnetic anomalies and lineations offsets documented in this study possibly refine fracture zone locations in the IMQZ and OMQZ. These interpreted offsets that could indicate fracture zones project into segmentation in ECMA, which may support earlier hypotheses that pre-existing

margin structure controlled rift segments, which in turn influenced segmentation in the ECMA and the subsequent seafloor spreading regimes in the Atlantic JQZ.

3. ALONG-MARGIN VARIATIONS IN BREAKUP VOLCANISM AT THE EASTERN NORTH AMERICAN MARGIN

3.1. Overview

To understand the distribution and amount of magmatic activity that facilitated the breakup of Pangaea and early Atlantic opening at the Eastern North American Margin (ENAM), we conduct magnetic modeling of the volcanics that represent the surficial expression of breakup magmatism. Along-strike variations in the amplitude and character of the prominent East Coast Magnetic Anomaly (ECMA) suggest that the emplacement of the volcanic layers producing this anomaly similarly varied along the margin. We conduct three-dimensional magnetic forward modeling, constrained by seismic interpretations, to identify the along-margin variations in volcanic thickness and width that can explain the observed ECMA amplitude and character. Our model results suggest that the margin-scale magmatism that drove continental breakup at the ENAM was similar in scale to the other magma-rich margins bounding the Atlantic Ocean, and that a combination of both first-order (~600-1000 km) and second-order (~50-100 km) magmatic segmentation was present. The first-order magmatic segmentation was likely separated by a rift transfer zone, and could be the result of parameters governed by preexisting structure acquired during previous Wilson Cycles. The second-order magmatic segmentation during breakup likely influenced the segmentation and transform fault spacing of the initial, and modern, Mid-Atlantic Ridge. These variations in magmatism indicate how extension accommodation and thermal weakening was

distributed at the ENAM to drive continental breakup, and how this breakup magmatism was related to both previous and subsequent stages of the Wilson Cycle.

3.2. Introduction

The cyclic amalgamation and breakup of (super-)continents during Wilson Cycles are responsible for the configuration and evolution of Earth's surface through time (Wilson, 1966). The continental rifting stage of the Wilson Cycle can be accompanied by extensive magmatism, which allows for continental breakup to occur at considerably lower stress by accommodating extension and thermally weakening the plate (Ebinger & Casey, 2001; Kendall et al., 2005; Buck, 2004; Bialas et al., 2010; Daniels et al., 2014). This breakup magmatism emplaces a thick wedge of volcanic layers that is a characteristic feature observed at magma-rich rifted continental margins worldwide (e.g. Hinz, 1981; Mutter, 1985; Morgan & Watts, 2018). Understanding continental breakup is significant due to its impact on Earth's climate and mass extinction events (Simms & Ruffell, 1989; Donnadieu et al., 2006; Nomade et al., 2007). The architecture of the ensuing rifted continental margin is governed by the rifting and breakup history, and influences the prevalence of both natural resources (Nelson et al., 1992; Mann et al., 2003) and geohazards (Chaytor et al., 2009; Brune, 2016).

The Eastern North American Margin (ENAM) (Figs. 3.1, 3.2) represents a showcase of the beginning of the current Wilson Cycle, which initiated with the breakup of the supercontinent Pangaea and continues with the ongoing formation of the Atlantic Ocean (Wilson, 1966; Thomas, 2019). The ENAM is a prime location for understanding

the processes involved in the formation and evolution of rifted margins (Sheridan, 1989; Withjack et al., 1998). The prominent East Coast Magnetic Anomaly (ECMA) extending along the ENAM (Fig. 3.1a) is commonly attributed to the volcanics associated with the magmatism facilitating continental breakup (Austin et al., 1990; Talwani et al., 1995; Davis et al., 2018). Along-strike variation in the ECMA amplitude and character (Fig. 3.1b) suggests that the amount and distribution of breakup magmatism at the ENAM likewise varied along the margin (e.g. Behn & Lin, 2000). As rifting is a three-dimensional process, identifying how the amount and distribution of magmatism changes along the margin, along with the associated extension accommodation and thermal weakening (e.g. Kendall et al., 2005), is critical for understanding the wholesale breakup process at both the ENAM and other magma-rich rifted continental margins worldwide. However, the amount and distribution of this breakup magmatism at the ENAM has not been extensively investigated in an along margin framework.

Magmatic segmentation and transform fault locations along seafloor spreading centers may be inherited from preexisting structure in the continental lithosphere and the continental breakup process (e.g. Hayward & Ebinger, 1996; Behn & Lin, 2000; Keranen et al., 2004; Beutel et al., 2010; Bellahsen et al., 2013; Hammond et al., 2013; Collier et al., 2017). Structural elements developed during previous Wilson Cycles can be transferred to the mid-ocean ridge during rifting and breakup, and further mid-ocean ridge segmentation may develop out of the breakup magmatic segmentation (Hayward & Ebinger, 1996; Keranen et al., 2004; Franke et al., 2007; Beutel et al., 2010; Bellahsen et al., 2013). This scenario suggests that the successive stages of a Wilson Cycle, and of

consecutive Wilson Cycles, influence each other and have consistent elements that persist through time (Hayward & Ebinger, 1996; Bellahsen et al., 2013). A relationship between breakup and seafloor spreading segmentation has been suggested for the ENAM based on the similarity of the potential fields anomaly wavelengths along the margin and modern Mid-Atlantic Ridge (e.g. Behn & Lin, 2000). However, how the three-dimensional distribution of breakup magmatism at the ENAM corresponds with the Mid-Atlantic Ridge magmatic segmentation following breakup has not been comprehensibly examined to understand their possible genetic relationship and connection with preexisting structure.

In this study, we investigate along-margin variations in the thickness and width of the breakup volcanism at the ENAM, which serves as the surficial indicator of the amount and distribution of magmatism facilitating breakup and the transition to seafloor spreading (Holbrook & Kelemen, 1993). We use magnetic modeling with the extensive, and continuous, coverage of magnetic anomaly data available at the ENAM (Fig. 3.1) (Bankey et al., 2002). Other geophysical data, such as seismic, are limited by the distribution of data and difficulty imaging deep structure at this margin, but provide valuable constraints for our magnetic modeling where they are available (Fig. 3.2) (Hinz, 1981; LASE Study Group, 1986; Trehú et al., 1989; Austin et al., 1990; Sheridan et al., 1993; Holbrook et al., 1994; Talwani et al., 1995; Bécel, 2016). Based on our magnetic modeling, we identify first- and second-order along-strike variations in the thickness and width of breakup volcanism at the ENAM that have not previously been investigated. Our magnetic modeling results provide insight into the distribution and amount of

magmatism at the ENAM. The along-margin variations in magmatism facilitated continental breakup by accommodating extension and providing thermal weakening (similar to processes interpreted in Ethiopia; e.g. Kendall et al., 2005), and may have an intrinsic relationship with the magmatic segmentation of the ensuing Mid-Atlantic Ridge.

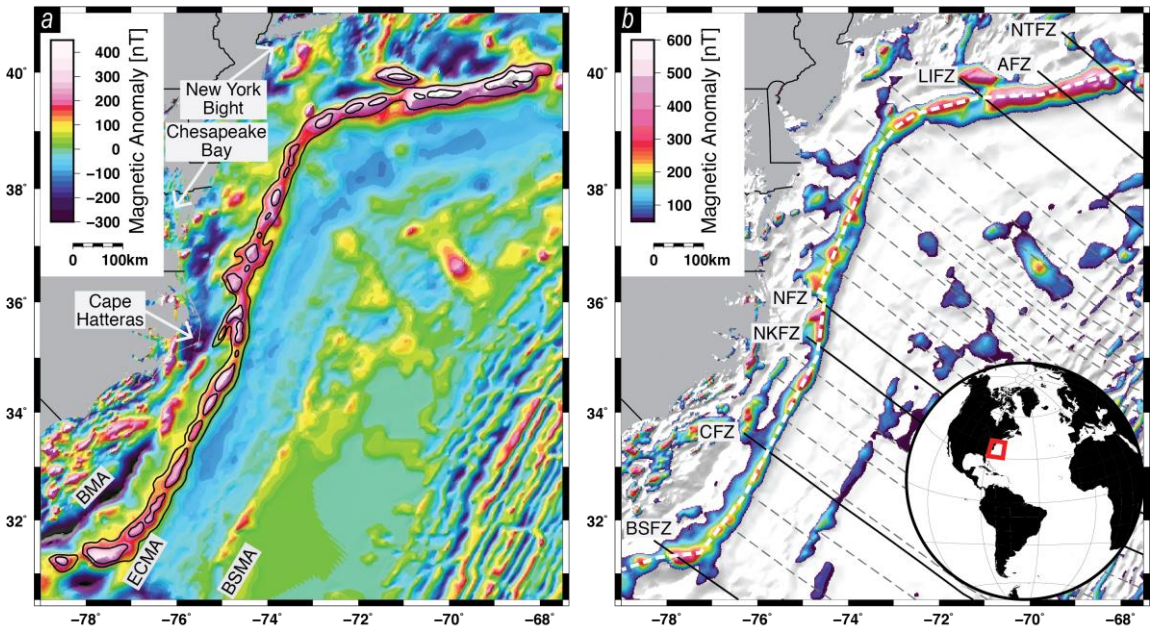

Figure 3.1 Magnetic data for the East Coast Magnetic Anomaly: (a) NAmag compilation magnetic anomaly grid (Bankey et al., 2002). Extent of ECMA shown with dark contours (Klitgord et al., 1988). (b) Magnetic anomaly grid with scale adjusted to highlight ECMA amplitude variation. Black lines show landward extrapolations of major (solid) and minor (dashed) fracture zones for the Atlantic, with Blake Spur (BSFZ), Carolinas (CFZ), Northern Kane (NKFZ), Norfolk (NFZ), Long Island (LIFZ), Atlantis (AFZ), and Nantucket (NTFZ) Fracture Zones labeled (Klitgord et al., 1988). White dashed line shows profile for along-margin extractions of data and model results (Fig. 3.4).

3.3. Background

3.3.1. Continental rifting and breakup

The continental rifting and breakup stage of Wilson Cycles (Wilson, 1966) results in the formation of rifted continental margins and the initiation of seafloor spreading producing ocean basins (Ebinger, 2005; Brune, 2016). Rifted continental margins total ~105,000 km in length globally, and record the history of continental rifting/breakup and the post-rift evolution of these settings (Bradley, 2008; Brune, 2016). Continental rifting is active in the East African Rift (Markis & Ginzburg, 1987; Ebinger & Casey, 2001), and the transition to seafloor spreading is ongoing or has recently occurred in the Red Sea (Almalki et al., 2015), the Eastern Black Sea (Monteleone et al., 2019), and the Gulf of California (Lizarralde et al., 2007). These modern rift sites provide valuable analogues to understand the mechanical processes and architecture of the fossilized continental breakups preserved in rifted continental margins around the world (Bradley, 2008).

Rifted margins fall on a spectrum between two end-member types, magma-rich and magma-poor, based on the amount of magma present during breakup (Franke, 2013; Tugend et al., 2018). At magma-rich rifted margins, voluminous intrusive and extrusive magmatic activity facilitates continental rifting and breakup at a lower stress by thermally weakening the plate, localizing strain, and accommodating extension (Ebinger & Casey, 2001; Buck, 2004; Bialas et al., 2010; Bastow & Keir, 2011; Daniels et al., 2014). Flood basalts are generally emplaced during the pre- and/or syn-rift stages of rifting (Menzies et al., 2002; Marzoli et al., 2018). Additionally, magmatism expressed

as volcanic flows, mafic intrusions, and/or igneous underplating occurs during continental breakup, facilitating the transition to seafloor spreading (White et al., 1987; Bastow & Keir, 2011; Geoffroy et al., 2015). In contrast, magma-poor rifted margins exhibit extreme crustal thinning, detachment faulting, and/or mantle exhumation during rifting and breakup (Franke, 2013).

A wedge-shaped accumulation of volcanics is emplaced along magma-rich margins as the extrusive portion of breakup magmatism (Mutter, 1985; White et al., 1987). This volcanic wedge is imaged as seaward dipping reflectors (SDRs) interpreted in seismic data at magma-rich rifted margins around the world (e.g. Hinz, 1981; Mutter et al., 1982; Mutter, 1985; Eldholm et al., 2000; Morgan & Watts, 2018). Horizontal volcanic flows are erupted subaerially before acquiring a seaward dip from either magmatic loading of the lithosphere or slip along bounding normal faults (Buck, 2017; Morgan & Watts, 2018). The volcanic wedge is associated with and likely responsible for a high-amplitude, margin parallel magnetic anomaly (e.g. Keen & Potter, 1995; Berndt et al., 2001; Corner et al., 2002; Collier et al., 2017; Davis et al., 2018; Franke et al., 2019). The presence of breakup volcanic wedges has been confirmed by drilling at the Greenland and Norwegian margins (e.g. Eldholm et al., 1989; Vandamme & Ali, 1998), and analogous volcanic flows exist at modern rift sites, such as the Afar region of Ethiopia (e.g. Bastow & Keir, 2011; Beutel et al., 2010; Keir et al., 2013). Beneath the SDRs, high-velocity lower crust is often observed in seismic data, interpreted to represent mafic intrusives and/or underplating during breakup (White et al., 1987, 2008; Kelemen & Holbrook, 1995; Talwani & Abreu, 2000; Mjelde et al., 2016).

Magma-rich rifted continental margins are prevalent worldwide (Hinz, 1981; Menzies et al., 2002). Rifted margins that are thought to be closer to the magma-rich end-member of the spectrum include the ENAM in the Central Atlantic (e.g. Austin et al., 1990; Holbrook & Kelemen, 1993), portions of the conjugate margins of the South Atlantic (e.g. Franke et al., 2007; Koopmann et al., 2014) and North Atlantic (e.g. Mutter et al., 1982; Eldholm & Grue, 1994), the margin of the Canadian Arctic (Funck et al., 2011), the margin of East Antarctica (Gupta et al., 2017), the Northwestern Australian Margin (e.g. Hopper et al., 1992), and the Southwest Indian Margin (e.g. Ajay et al., 2010). Magma-poor margins include the conjugate Newfoundland, Canada, and Iberia Peninsula margins (e.g. Whitmarsh et al., 2001; Shillington et al., 2006). Intermediate examples, with elements of both end-members, include the South China Sea (e.g. Weiwei et al., 2012; Franke, 2013) and the Gulf of California (Lizarralde et al., 2007).

Both presently active rifts and magma-rich rifted continental margins display along-axis magmatic segmentation (e.g. Hayward & Ebinger, 1996; Ebinger & Casey, 2001; Beutel et al 2010; Hammond et al., 2013; Keir et al., 2013; Koopmann et al., 2014; Collier et al., 2017; Franke et al., 2019). The greater amount of magma in the center of these segments creates along-margin variations in extension accommodation during breakup (Ebinger & Casey, 2001; Geoffroy, 2001). Following successful continental breakup, a segmented mid-ocean ridge develops as the tectonic regime enters the seafloor spreading stage of the Wilson Cycle (Ebinger, 2005; Bellahsen et al., 2013). The magmatic segmentation currently observed in both rifts and mid-ocean ridges are

thought to be caused by either along-strike variations in magma production, from focused upwelling of warmer asthenospheric mantle initiated by Rayleigh-Taylor gravitational instability (Whitehead et al., 1984; Lin et al., 1990; Sempéré et al., 1993; Schouten et al., 1985; Geoffroy, 2001), or magma focusing, from melt transport at the base of the lithosphere (e.g. Magde & Sparks, 1997; Shillington et al., 2009; Keir et al., 2015). The length scale of magmatic segmentation is similar in both rifts and the ensuing mid-ocean ridges, which suggests that mid-ocean ridge segmentation is inherited from the magmatic segmentation present during the continental breakup process (e.g. Hayward & Ebinger, 1996; Behn & Lin, 2000; Keranen et al., 2004; Beutel et al., 2010; Bellahsen et al., 2013; Hammond et al., 2013; Collier et al., 2017).

3.3.2. Eastern North American Margin formation

Eastern North America has been the site of repeated continental amalgamation and breakup through time (Rankin, 1994; Thomas, 2019). The ENAM (Fig. 3.1) formed from the diachronous breakup of Pangaea, which occurred earlier (earliest Jurassic) off the southeastern United States and later (early Cretaceous) off Canada (Withjack et al., 2012). The southern ENAM (south of Nova Scotia) is thought to be a magma-rich continental margin, whereas the northern ENAM is magma-poor (Keen & Potter, 1995; Kelemen & Holbrook, 1995; Shillington et al., 2006).

Continental rifting of Pangaea in modern eastern North America initiated in the Late Triassic (Withjack et al., 2012). Northwest-southeast crustal extension was initially accommodated over a broad zone by faults bounding long-lived rift basins (Manspeizer

& Cousminer, 1988; Schlische, 1993). Many of these extensional faults were reactivated preexisting Paleozoic structures (Schlische, 1993). During rifting, widespread magmatism associated with the Central Atlantic Magmatic Province (CAMP) was emplaced at ~200 Ma (Blackburn et al., 2013; Marzoli et al., 2018). As rifting progressed, extension was localized at the site of eventual continental breakup and rift basin activity ceased (Withjack et al., 1998, 2012).

At the southern ENAM, continental breakup and the transition to seafloor spreading was accommodated by magmatic activity (Withjack et al., 1998; Schlische et al., 2003). The breakup magmatism included the subaerial emplacement of a volcanic wedge, interpreted as SDRs in ENAM seismic reflection data (Fig. 3.2b) (e.g. Hinz, 1981; LASE Study Group, 1986; Trehú et al., 1989; Austin et al., 1990; Sheridan et al., 1993; Holbrook et al., 1994; Bécel, 2016). These SDRs are overlaid by the thick sediment of the Carolina Trough, Baltimore Canyon Trough, and Georges Bank sedimentary basins (Fig. 3.2c) (Klitgord et al., 1988). In the Carolina and Baltimore Canyon troughs, crustal seismic refraction measurements also exist, which are not available in the Georges Bank Basin to the north (e.g. LASE Study Group, 1986; Trehú et al., 1989; Holbrook et al., 1994; Kelemen & Holbrook, 1995). These refraction measurements show that the SDRs are underlain by high-velocity lower crust, interpreted to represent mafic intrusions and/or igneous underplating during breakup (e.g. LASE Study Group, 1986; Trehú et al., 1989; Holbrook et al., 1994; Kelemen & Holbrook, 1995).

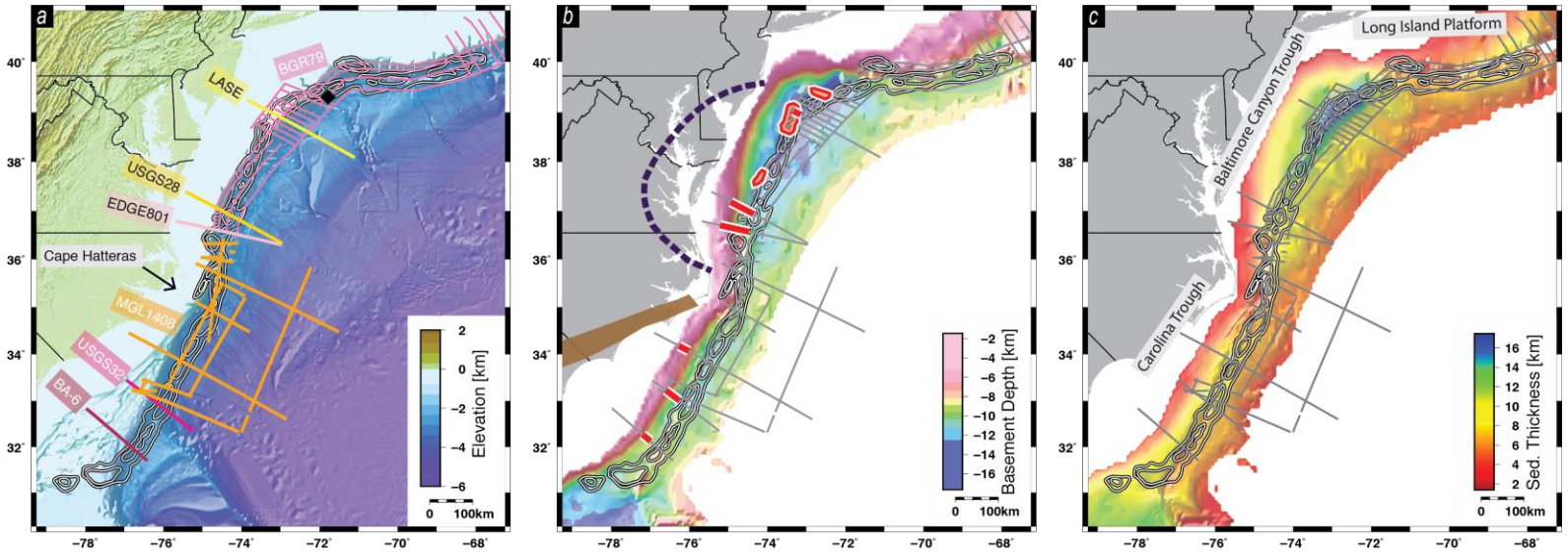

Figure 3.2 Eastern North American Margin bathymetry, basement, and sediment thickness: (a) ETOPO1 bathymetry (Amante & Eakins, 2009), (b) seismically-derived basement depth (Klitgord et al., 1994; Hutchinson et el., 1995), and (c) sediment thickness. ECMA extent indicated by black/white contours (Fig. 3.1a) (Klitgord et al., 1988). Key seismic lines/surveys labeled; red lines/polygons indicate extent of SDR interpretations from previous studies (Hinz, 1981; LASE Study Group, 1986; Trehú et al., 1989; Austin et al., 1990; Sheridan et al., 1993; Holbrook et al., 1994; Bécel, 2016). Purple dashed line indicates the inferred suture zone surrounding an isolated piece of West African Craton under Chesapeake Bay (Lefort & Max, 1991; their figure 7). Brown polygon indicates the inferred location of the Alleghanian suture zone separating pre-Alleghanian Laurentian terranes (to the north) from the Gondwanan terranes (to the south) (Higgins & Zietz, 1983; Boote & Knapp, 2016). Black diamond indicates location of heat flow Site V20-232 (Pollack et al., 1993).

The East Coast Magnetic Anomaly (ECMA) is a 2,500-km long, high-amplitude, positive magnetic anomaly extending along the ENAM from offshore Georgia to Nova Scotia (Fig. 3.1) (Keller et al., 1954; Klitgord & Schouten, 1986). The ECMA is attributed to the volcanic wedge emplaced during breakup based on 2D magnetic forward modeling and SDR interpretations (e.g. Austin et al., 1990; Talwani et al., 1995; Davis et al., 2018). Talwani et al. (1995) suggests that the ECMA is a remanent anomaly from a rapidly emplaced volcanic wedge. Alternatively, Davis et al. (2018) suggest that the ECMA is an induced anomaly, with a longer-duration (6-31 Myr) of emplacement over multiple polarity periods causing the remanent magnetization of the volcanic wedge layers to cancel out. To the north, offshore Nova Scotia, the ECMA diminishes and SDRs are not found as the margin becomes magma-poor (Keen & Potter, 1995; Van Avendonk et al., 2006).

The ECMA displays notable along-strike variations in amplitude and character at multiple scales (Fig. 3.1b) (Klitgord et al., 1988; Behn & Lin, 2000). A regional change in the ECMA character occurs near Cape Hatteras, North Carolina, with the single peak ECMA to the north of Cape Hatteras and a comparatively lower amplitude, broader ECMA with two peaks to the south (Fig. 3.1) (Klitgord et al., 1988). A change in ECMA amplitude is present offshore the New York Bight, being higher to the northeast in the Long Island Platform, and comparatively lower to the south in the Baltimore Canyon and Carolina troughs (Fig. 3.1). The ECMA also displays amplitude variation at a 100-150 km wavelength, with magnetic anomaly highs separated by zones of relatively lower amplitude (Fig. 3.1b) (Behn & Lin, 2000).

A second prominent magnetic anomaly at the ENAM, the Brunswick Magnetic Anomaly (BMA), is located inboard and parallel to the ECMA in the Carolina Trough before curving westward and proceeding onshore Georgia and Alabama (Klitgord et al., 1988) (Fig. 3.1). The source of the BMA is debated, but is thought to play a role in the ENAM rift history (Duff & Kellogg, 2019). Proposed sources for the BMA include an Alleghanian Suture Zone (McBride & Nelson, 1988; Parker, 2014), rift-related mafic intrusions (Lizarralde et al., 1994; Duff & Kellogg, 2019), the negative anomaly component of a low-high pair with the ECMA from the breakup volcanic wedge (Austin et al., 1990), or a rift basin (the Brunswick Graben; Hutchinson et al., 1983).

The formation of the Atlantic Ocean followed continental breakup at the ENAM (Vogt, 1973). Various tectonic scenarios have been proposed for the early Atlantic opening. Scenarios such as a ridge jump (or two ridge jumps) (Vogt, 1973; Klitgord & Schouten, 1986; Bird et al., 2007; Schettino & Turco, 2009), asymmetric spreading that underwent a drastic change in rate and direction (Labails et al., 2010), or a period of proto-oceanic crust prior lithospheric rupture (Shuck et al., 2019) between the ECMA and the Blake Spur Magnetic Anomaly (Fig. 3.1) have been proposed to explain the wider domain of early ocean crust that is present offshore the ENAM compared to the conjugate margin offshore northwest Africa. Additionally, a spreading axis reorientation may have been present to accommodate the difference in strike between the initial seafloor spreading outboard of the ECMA and the modern Mid-Atlantic Ridge (Greene et al., 2017). Under all of the proposed scenarios, seafloor spreading rates for the early Atlantic indicate a slow-spreading regime (e.g. Klitgord & Schouten, 1986; Schettino &

Turco, 2009; Labails et al., 2010; Bird et al., 2007; Greene et al., 2017), which continues in the present day (Müller et al., 2008).

The modern Mid-Atlantic Ridge displays along-strike segmentation at a similar spatial scale as the 100-150 km wavelength variation in ECMA amplitude (Fig. 3.1b), suggesting that the segmentation of the Mid-Atlantic Ridge was inherited from rifting and breakup at the ENAM (Behn & Lin, 2000). Fracture zone traces for the Atlantic indicate that this spreading center segmentation has persisted through time, and the landward extrapolations of many Atlantic fracture zones intersecting the ECMA between amplitude segments (Fig. 3.1) (Klitgord et al., 1988; Behn & Lin, 2000; Greene et al., 2017).

3.4. Methods

3.4.1. Data and model constraints

In this study, we use the North American Magnetic Anomaly Group (NAMAG) magnetic anomaly grid, composed of merged aeromagnetic and shipboard magnetic data, to model the volcanic wedge producing the ECMA (Fig. 3.1) (Bankey et al., 2002). We created a depth to basement grid to constrain the top of the volcanic wedge by merging seismically-derived basement depth grids from the Carolina Trough (Hutchinson et al., 1995) and Baltimore Canyon Trough/Georges Bank Basin (Klitgord et al., 1994) (Fig. 3.2b). We also compiled available constraints on the extent of the volcanic wedge from previous seismic interpretations of SDRs at the ENAM (Fig. 3.2b)

(Hinz, 1981; LASE Study Group, 1986; Trehú et al., 1989; Austin et al., 1990; Sheridan et al., 1993; Holbrook et al., 1994; Bécel, 2016).

3.4.2. Magnetic anomaly modeling

We conducted 2D and 3D magnetic modeling of the volcanic wedge producing the ECMA using the Fourier summation approach (Parker, 1973). We first created a series of 2D magnetic forward models using profiles perpendicular to the ECMA (Fig. B.1, B.2). The volcanic wedge geometry we use in our modeling increases in thickness from the inboard pinchout towards a maximum thickness then thins to zero thickness as the volcanic wedge transitions into ocean crust on the outboard end (Fig. B.1). The volcanic wedge geometries derived from these 2D models were interpolated along the margin to create an initial 3D volcanic wedge for our 3D magnetic modeling. The top of the 3D modeled volcanic wedge was constrained by the seismically-derived basement depth grid (Fig. 3.2b). We then iteratively adjusted the lateral extent (perpendicular to the ECMA) and thickness of the 3D modeled volcanic wedge along the margin to achieve a calculated magnetic anomaly consistent with the observed ECMA amplitude and character (Fig. 3.1a). Both previous studies and our 2D magnetic modeling suggest that the volcanic wedge extends landward and seaward of where SDRs are interpreted (Eldholm et al., 1995; Talwani et al., 1995; Davis et al., 2018) (Fig. B.1), so we incorporated SDRs interpretations (Fig. 3.2b) as a minimum constraint on our modeled volcanic wedge extent.

Our 3D magnetic model assumed a constant magnetization of 5 A/m, with an inclination of 45° and a declination of -2° based on the estimates of the Jurassic geomagnetic pole (Austin et al., 1990; Talwani et al., 1995). This magnetization is consistent with drilling results that penetrated SDRs at other margins (see Davis et al., 2018, their figure 3), and is similar to the magnetization used in 2D magnetic modeling of volcanic wedges at both the ENAM (Fig. B.1) (Austin et al., 1990; Talwani et al., 1995) and other volcanic rifted margins (e.g. Bauer et al., 2000; Franke et al., 2019). We also validated this magnetization with a 2D magnetization inversion (Fig. B3) (Parker & Huestis, 1974). Davis et al. (2018) alternatively suggest that the ECMA is an induced, rather than remanent, magnetic anomaly produced by a 0.05 SI susceptibility volcanic wedge (present-day field inclination of 60°, declination of -10°, and strength of ~50,000 nT). A 5 A/m remanent volcanic wedge with Jurassic geomagnetic field directions produces a similar magnetic anomaly to a 0.05 SI induced volcanic wedge with the steeper inclination of the present day field (Behn & Lin, 2000; Davis et al., 2018). Therefore, we used a 5 A/m magnetization in our ECMA modeling, recognizing that an induced anomaly, or a combination of remanent and induced components, would result in a similar modeled volcanic wedge with comparable along-strike variations in thickness and width.

A maximum depth constraint for our modeled volcanic wedge is the depth to the Curie temperature, as material below this depth would lose remanent magnetization and not contribute to the magnetic anomaly (Blakely, 1995; Rajam, 2007). A global estimation based on magnetic anomaly inversion suggests that the Curie depth at the

ENAM is greater than 27 km (Li et al., 2017) (Fig. B.4). We independently estimate the Curie depth to be ~23-25 km based on heat flow data collected at Site V20-232 (Pollack et al., 1993) (Figs. 3.2a, B.4).

3.5. Results

3.5.1. Volcanic wedge distribution and variations

Our magnetic modeling (Fig. 3.3) shows that the volcanic wedge emplaced as part of the breakup magmatism can explain the ECMA (Fig. 3.3) (Holbrook & Kelemen, 1993). Our modeled volcanic wedge mimics the strike of the ECMA and the modern-day shelf break along the margin. The top of the modeled volcanic wedge ranges from ~2-17 km in depth, with the greatest depths in the northern Baltimore Canyon Trough (Fig. 3.3). The base of our modeled volcanic wedge at its thickest points along the margin ranges from ~14-23 km (Fig. B.5). The base of our modeled volcanic wedge is shallower than the Curie depths estimates for this area (~23-27 km; Fig. B.4), suggesting that the entire modeled volcanic wedge contributes to the magnetic anomaly signal.

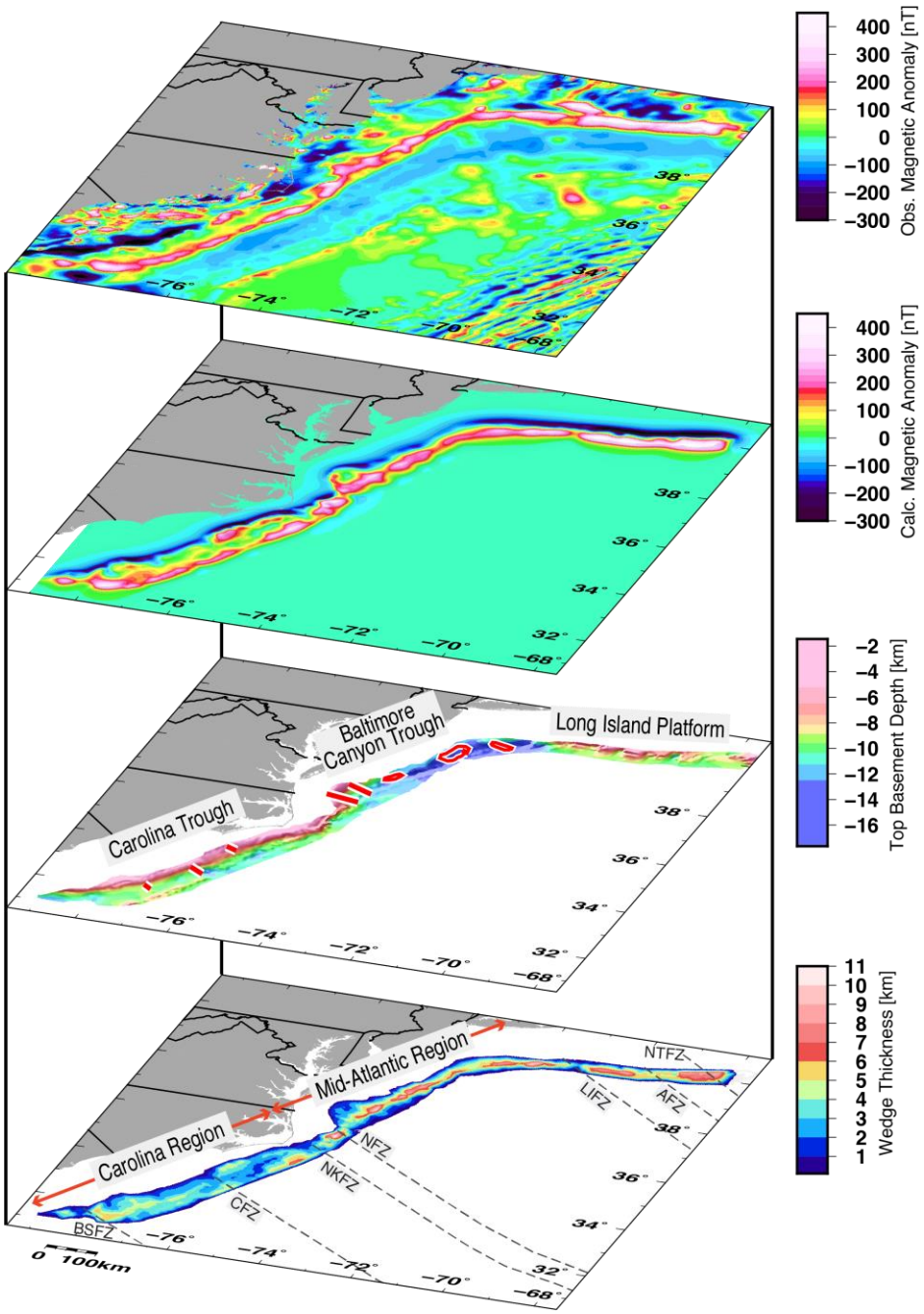

Figure 3.3 Results of 3D magnetic forward modeling of the East Coast Magnetic Anomaly: From top to bottom: Observed magnetic anomaly (Fig. 3.1a), model calculated magnetic anomaly, top of modeled volcanic wedge from basement depth grid (Fig. 3.2b), and modeled volcanic wedge thickness. Locations of SDR interpretations from previous studies indicated by red/white lines (Fig. 3.2b). Grey dashed lines show landward extrapolations of major Atlantic fracture zones (Fig. 3.1b) (Klitgord et al., 1988).

Our modeled volcanic wedge exhibits both first-order (~600-1000 km) and second-order (~50-100 km) variations in thickness and width along the ENAM (Figs. 3.3, 3.4). The first-order volcanic wedge variation can be separated into two regions. The boundary separating the first-order variation in modeled volcanic wedge thickness and width is located near Cape Hatteras, North Carolina. South of this boundary (hereafter referred to as the Carolina Region), the modeled volcanic wedge has a more widely distributed thickness, corresponding to the broader, two-peak ECMA (Fig. 3.3). The maximum thicknesses of the modeled volcanic wedge in the Carolina Region is ~4-7 km. To the north of this boundary (hereafter referred to as the Mid-Atlantic Regions), the modeled volcanic wedge is thicker and has a narrower distribution of thickness compared to the Carolina Region (Fig. 3.3), corresponding with the higher-amplitude, single peak ECMA. The steeper thickening gradient reflects the overall narrower distribution of the modeled volcanic wedge thickness in the Mid-Atlantic Region. The maximum thickness of the modeled volcanic wedge in the Mid-Atlantic Region is ~7-10 km.

In the Carolina Region, the modeled volcanic wedge is able to replicate the positive, high-amplitude ECMA character, and produces a thin, paired negative anomaly inboard of the ECMA (Fig. 3.3). However, the strong negative amplitude and width of the BMA are not produced by the modeled volcanic wedge (Fig. 3.3). This suggests that the BMA does not represent a low-high anomaly pair with the ECMA produced by the breakup volcanic wedge (e.g. Austin et al., 1990).

The overall modeled volcanic wedge thickness (Fig. 3.3) is similar throughout the entire Mid-Atlantic Region. However, there is a difference in both the modeled volcanic wedge depth and orientation within the Mid-Atlantic Region between the Baltimore Canyon Trough and Long Island Platform (Fig. 3.3). The strike of the volcanic wedge, and the ECMA, is north-south in the Baltimore Canyon Trough, and more east-west on the Long Island Platform (Fig. 3.3). The basement depth (representing the top of the modeled volcanic wedge) is shallower on the Long Island Platform compared to the deep basement of the Baltimore Canyon Trough (Figs. 3.2, 3.3, 3.4). A change in ECMA amplitude is coincident with these changes in depth and strike, being ~100-200 nT higher on the Long Island Platform compared to in the Baltimore Canyon Trough (Figs. 3.1, 3.3, 3.4). Both the strike and depth of the magnetic source body can influence magnetic anomaly amplitudes, which suggests that the higher ECMA amplitude on the Long Island Platform is not indicative of a thicker volcanic wedge; rather, it corresponds to a decrease in volcanic wedge depth and change in volcanic wedge strike within the Mid-Atlantic Region (e.g. Behn & Lin, 2000) (Figs. 3.2, 3.3, 3.4).

The second-order variation in the thickness and width of our modeled volcanic wedge mimic the ~100-150 km wavelength amplitude variation along the ECMA (Behn & Lin, 2000) (Fig. 3.3, 3.4). Depth variation in the top of the basement has no apparent relationship with the 100-150 km wavelength ECMA amplitude variation, suggesting that this ECMA variation can be attributed to second-order segmentation of the volcanic wedge (Figs. 3.3, 3.4).

Magnetic anomalies can also be produced by variations in the distribution of magnetization. In addition to the along-strike variations in the thickness and width of our modeled volcanic wedge at the ENAM, along-strike variations in the magnetization could conceivably arise from processes such as hydrothermal alteration (Pariso & Johnson, 1991) or partial cancellation of magnetization due to volcanic emplacement over alternating polarity periods (Davis et al., 2018). We test if along-strike variations in magnetization alone could explain the observed ECMA amplitude and character variation using a 3D magnetic forward model with a constant volcanic wedge geometry. The variable-magnetization model has considerable difficulty recreating both the amplitude and character of the ECMA simultaneously by just adjusting this parameter (Fig. B.6). It is difficult to adjust the magnetization value alone to account for the ECMA amplitude without also causing a poor fit for the ECMA width, indicating that a spatial variation in the geometry of volcanics is likely needed to fully capture both the width and amplitude of the ECMA. This suggests that the ECMA cannot be explained solely by systematic, along-strike variation in magnetization, and supports the variable volcanic wedge thickness and width used in our 3D magnetic modeling (Fig. 3.3). However, we cannot rule out some secondary contribution of magnetization variations, though these cannot be uniquely separated from modeled volcanic wedge thickness and width variations.

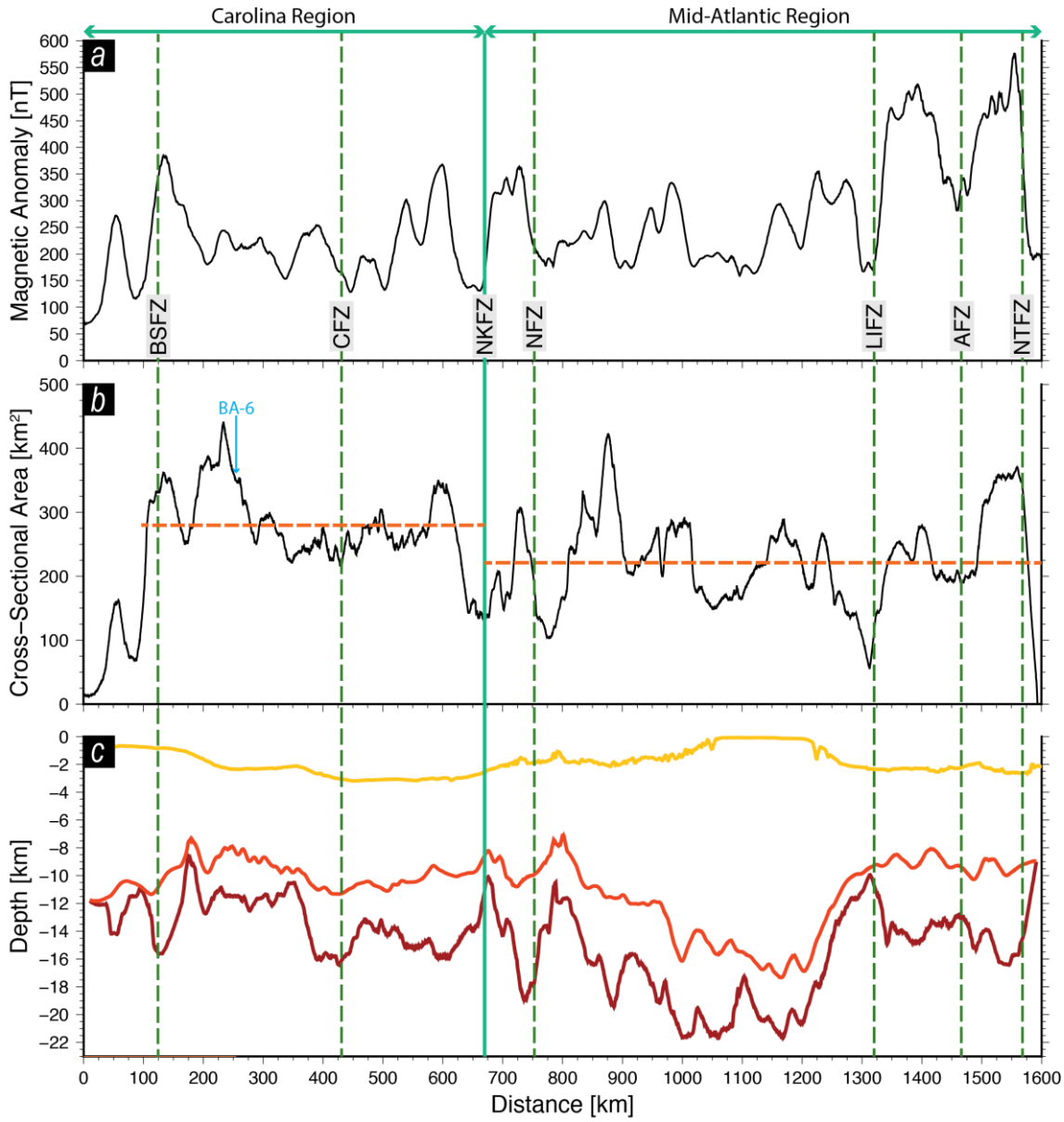

Figure 3.4 Along-margin extractions along the East Coast Magnetic Anomaly axis (see Fig. 3.1b): (a) Observed magnetic anomaly along-strike. (b) Modeled volcanic wedge cross-sectional area along-strike. (c) Seafloor (orange), top of modeled volcanic wedge (red), and base of modeled volcanic wedge (dark red) beneath the ECMA axis. Extent of Carolina and Mid-Atlantic Regions marked. Red dashed lines show average cross-sectional areas for regions. Margin intersections of major Atlantic fracture zones indicated by green dashed lines (see Fig. 3.1b) (Klitgord et al., 1988). Location of BA-6 (Austin et al., 1990) labeled.

3.5.2. Volcanic wedge volume estimates

Based on our interpretation of the magnetic forward modeling results, we estimate that the volcanic wedge emplaced as part of the ENAM breakup magmatism has a volume of ~373,000 km^3 from just south of the Blake Spur Fracture Zone to just north of the Nantucket Fracture Zone. Of this total volume, we estimate ~167,000 km^3 in the Carolina Region, with the remaining ~206,000 km^3 in the larger Mid-Atlantic Region.

We examined along-strike variations in the volume of the modeled volcanic wedge using changes in cross-sectional area (area perpendicular to the ECMA strike) as a proxy (Fig. 3.4). The average cross sectional area of the modeled volcanic wedge in the Carolina Region is ~280 km^2 (omitting the minor segment south of the Blake Spur Fracture Zone), and ranges between 220-450 km^2 between the centers and edges of the second-order geometry variations within this region (Fig. 3.4). The average cross sectional area of the modeled volcanic wedge in the Mid-Atlantic Region is ~225 km^2, and ranges between 75-450 km^2 between the centers and edges of the second-order geometry variations within this region (Fig. 3.4). The average cross sectional area of the Mid-Atlantic Region is comparatively smaller despite having a greater modeled volcanic wedge thickness, and this is due to the broader distribution of modeled volcanic wedge thickness in the Carolina Region (Fig. 3.3).

Previous studies have estimated the volume of breakup volcanism at the ENAM (Austin et al., 1990; Talwani et al., 1995). Austin et al. (1990) estimate a cross-sectional area of 370 km^2 for the volcanic wedge on BA-6 (Fig. 3.2), which consistent with the

~350 km^2 in our model (Fig. 3.4). Extrapolating on this estimate, Austin et al. (1990) evaluate a total volcanic wedge volume of ~166,500 km^3 in the Carolina Trough, which is similar to the volume we estimate for our Carolina Region. Talwani et al. (1995) suggest a rough estimate of ~1 million km^3 for the volcanic wedge by assuming that a 100 km wide and 10 km thick volcanic wedge extends 1000 km along the margin. The estimate by Talwani et al. (1995) is larger than what we estimate due to their 10 km thick volcanic wedge assumption, which is greater than what our modeling suggests is typical along the ENAM (Fig. 3.3). Additionally, our modeling shows that a volcanic wedge with a constant along-strike geometry is not consistent with the observed variations in ECMA amplitude and character (Fig. 3.3). This discrepancy indicates that it is important to account for along-strike variations in volcanic wedge thickness and width when estimating the volume of breakup volcanism at rifted margins.

3.6. Discussion

Continental breakup marks the final stage of successful rifting during the Wilson Cycle as the rift transitions to seafloor spreading and the formation of ocean basins (Wilson, 1966; Bradley, 2008; Stein et al., 2018). The ENAM is an archetypical magma-rich rifted margin that captures the wholesale process of continental rifting and breakup to the initiation of seafloor spreading in a margin-to-basin framework (Fig. 3.5) (Klitgord et al., 1988; Sheridan, 1989; Holbrook and Kelemen, 1993; Withjack et al., 1998, 2012; Lynner et al., 2020). The ECMA marks the volcanic component of the magmatism present during continental breakup at the ENAM (e.g. Holbrook and

Keleman, 1993; Talwani et al., 1995). Our modeled volcanic wedge can be used to show how the margin-scale breakup magmatism at the ENAM compares to both other magma-rich margins around the Atlantic and other magmatic settings (Crisp, 1984; Eldholm et al., 2000; White et al., 2006). Our modeling results also reveal variations in the volcanic wedge width and thickness (Figs. 3.3, 3.4) that suggest that both first- and second-order magmatic segmentation, represented by along-margin variations in the distribution/amount of magmatism, was present at the ENAM during breakup. These variations in breakup magmatism impact the extension accommodation and thermal weakening that this magmatism provides to facilitate continental breakup (e.g. White & McKenzie, 1989; Buck, 2004; Kendall et al., 2005; Bialas et al., 2010; Daniels et al., 2014). The first-order magmatic segmentation may be related to differences in mantle temperature and/or the timing and amount of crustal extension/thinning caused by preexisting (inherited) structure acquired during the previous Wilson Cycle (e.g. Withjack et al., 2012; Shuck et al., 2019). The second-order magmatic segmentation suggests variations in melt production and/or transport during breakup (e.g. Magde & Sparks, 1997; Geoffroy, 2001), and may have ultimately governed the segmentation of the initial and modern Mid-Atlantic Ridge (e.g. Hayward & Ebinger, 1996; Behn & Lin, 2000; Bellahsen et al., 2013).

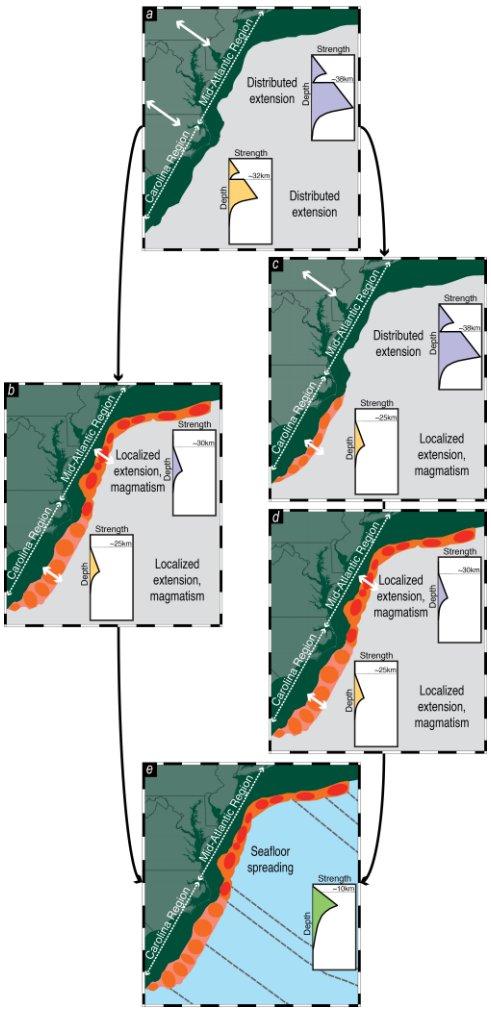

Figure 3.5 Schematic of rifting history and breakup magmatism at the Eastern North American Margin. White arrows show approximate direction of extension. Volcanic wedge shown in orange; second-order segmentation shown with ovals; darker colors correspond to areas of a thicker volcanic wedge. Present day coast and state boundaries shown for spatial reference. (a) Distributed extension onshore prior to breakup magmatism. (b) Volcanic wedge emplacement scenario with a synchronous localization of extension between the Carolina and Mid-Atlantic Regions. (c/d) Volcanic wedge emplacement scenario with an earlier localization of extension in the Carolina Region (panel c) and a later localization in the Mid-Atlantic Region (panel d). (e) Seafloor spreading following continental breakup; dashed lines indicate major Atlantic fracture zones (Fig. 3.1a). Inset plots illustrate hypothetical lithosphere strength envelopes with possible effects of crustal thickness, rheological differences, and presence of magmatism on extension in the Carolina and Mid-Atlantic Regions (Buck, 2004, their figure 1.1; Lowrie, 2007, their figure 2.69; Marzen et al., 2019). Horizontal grey lines indicate crustal thickness (Talwani et al., 1995; Marzen et al., 2019).

3.6.1. Margin-scale magmatism that drove the Atlantic opening

Magma-rich rifted continental margins, including the ENAM, bound 75% of the Atlantic Ocean and facilitated the breakup of Pangaea and the opening of the Atlantic Ocean (Eldholm et al., 2000; Menzies et al., 2002). The volcanic wedges emplaced at these margins serve as the surficial indicator of the margin-scale breakup magmatism (Holbrook & Kelemen, 1993; Keen & Potter, 1995), and how these rift settings compare with other magmatic settings worldwide (Crisp, 1984; White et al., 2006). Understanding the amount and intensity of this margin-scale magmatism provides insight into a key component driving continental breakup and the opening of ocean basins like the Atlantic Ocean (Buck, 2004; Bialas et al., 2010; Daniels et al., 2014; Kendall & Lithgow-Bertelloni, 2016).

The dimensions of our modeled breakup volcanic wedge at the ENAM are consistent with the breakup volcanic wedges, interpreted as SDRs in seismic data, at the other magma-rich rifted continental margins of the Atlantic (e.g. Eldholm & Grue, 1994; Barton & White, 1997; Talwani & Abreu, 2000; Franke et al., 2007, 2010; Koopmann et al., 2014). At the North Atlantic Margins offshore Norway and Greenland, the volcanic wedge emplaced during breakup is ~20-100 km wide and ~4-6 km thick (Eldholm & Grue, 1994; Barton & White, 1997). At the southern South Atlantic Margin offshore Argentina and Uruguay, the volcanic wedge emplaced during breakup is 60-120 km in width and up to ~6-7 km thick (Franke et al., 2007, 2010). At the central South Atlantic conjugate margins offshore Brazil and Namibia, the volcanic wedge emplaced during breakup is ~50-200 km wide and up to 15 km thick (Talwani & Abreu, 2000; Koopmann

et al., 2014). Our modeled volcanic wedge dimensions (~60-120 km wide; ~4-10 km thick) are similar to the dimensions observed at the other magma-rich Atlantic margins (Fig. 3.3), which suggests that the margin-scale magmatism at the ENAM is typical of the amount of magmatism at magma-rich margins to drive the breakup of Pangaea and the Atlantic opening.

The modeled volcanic wedge can be used to estimate the likely range of emplacement rates at the ENAM. There is considerable debate and uncertainty on the timing and duration of breakup magmatism at the ENAM due to the lack of direct age control and the uncertainty in the relationship between the onshore CAMP volcanism and the offshore volcanic wedge (Schlische et al., 2003; Withjack et al., 2012), along with the similarity in magnetic anomalies produced by a rapidly emplaced volcanic wedge with remanent magnetization (e.g. Talwani et al., 1995) and a slowly emplaced volcanic wedge with induced magnetization (e.g. Davis et al., 2018). Proposed ages for the breakup magmatism at the ENAM suggest that it could be coincident with the ~200 Ma CAMP volcanism (Hames et al., 2000; Schlische et al., 2003; Schettino & Turco, 2009; Witchjack et al., 2012), or up to 25 Myr after CAMP activity (Klitgord & Schouten, 1986; Benson, 2003; Labails et al., 2010). Estimated durations for the breakup magmatism include 6-31 Myr (Davis et al., 2018), ~15 Myr (Withjack et al., 2012), 2.3 Myr (Lizarralde & Holbrook, 1997), or as short as 0.6 Myr if the emplacement was coeval with the peak CAMP activity onshore (Withjack et al., 2012; Blackburn et al., 2013). The uncertainty in magmatic emplacement durations makes the estimation of a single volcanic emplacement rate difficult. The range of proposed magmatic

emplacement durations (0.6 to 31 Myr) coupled with our derived modeled volcanic volume (~373,000 km^3) suggests that volcanic emplacement rates at the ENAM driving breakup were 0.01 to 0.6 km^3/yr (Fig. 3.3).

The range of volcanic emplacement rates for the ENAM can be compared with other magmatic settings worldwide (Crisp, 1984; White et al., 2006). Volcanic emplacement rates for large igneous provinces and oceanic plateaus include 1.5 km^3/yr for the Deccan Traps (Richards et al., 1989), 0.78 km^3/yr for the Karoo Large Igneous Province (Svenson et al., 2012), 1.2-4.6 km^3/yr for Shatsky Rise (Sager, 2005), and 3 km^3/yr for Ontong Java Plateau (White et al., 2006). Modern volcanic emplacement at Iceland occurs at 0.02 km^3/yr (Crisp, 1984). Modern volcanic emplacement rates for a 1,650 km long section of the fast spreading East Pacific Rise and slow spreading Mid-Atlantic Ridge, equivalent to our along-margin model length, are 0.16 km^3/yr and 0.024 km^3/yr, respectively (White et al., 2006). Under the most rapid emplacement estimate coincident with the duration of onshore CAMP volcanism (e.g. Withjack et al., 2012; Blackburn et al., 2013), the magmatism at the ENAM (0.6 km^3/yr) approaches, but is still less than, that of large igneous provinces and oceanic plateaus. If the ENAM experienced a long duration of emplacement and slow rate of extension (e.g. Davis et al., 2018), the margin-scale magmatism (0.01 km^3/yr) may have been similar to what is experienced at the slow-spreading Mid-Atlantic Ridge, with vertical piling of layers at the margin causing a comparatively thicker volcanic section than what is observed at spreading centers. Our range of estimated volcanic emplacement rates indicates that the high emplacement rates documented within large igneous provinces are not necessary to

cause continental breakup. Additionally, the low-end of our estimated ENAM emplacement rates suggest that emplacement rates similar to slow-spreading mid-ocean ridges, like the modern Mid-Atlantic Ridge, were sufficient to drive the Atlantic opening if continental breakup occurred over a longer duration (e.g. Davies et al., 2018). This long-duration of breakup with a lower emplacement rate could have been aided by lithospheric weakening associated with the thermal effects of CAMP activity (Marzoli et al., 2018).

3.6.2. First-order magmatic segmentation during breakup at the ENAM

3.6.2.1. Rift transfer zone

Our modeling results show a first-order variation in the volcanic wedge width and thickness, separated into the Carolina and Mid-Atlantic Regions (Fig. 3.3). The modeled volcanic wedge changes from a widely distributed thinner volcanic wedge in the Carolina Region to a narrower but thicker volcanic wedge in the Mid-Atlantic Region (Fig. 3.3). This change indicates a first-order magmatic segmentation during breakup where each region experienced a different distribution and amount of magmatism (Fig. 3.5), suggesting that key parameters controlling melt production likewise varied along the margin (e.g. Withkjack et al., 2012; Shuck et al., 2019). One possible explanation for the change in character of the volcanic wedge is that a rift transfer zone exists just north of Cape Hatteras and separates two regions experiencing different modes of magma emplacement during breakup (e.g. Bellahsen et al., 2013).

Rift transfer zones are commonly observed in rifted continental margins (e.g. Franke et al., 2007; Bellahsen et al., 2013) and active rifts (e.g. Hayward & Ebinger, 1996) to divide a rift into distinct regions. Transfer zones accommodate differences in extension within a rift through a system of faults (Hayward & Ebinger, 1996; Bellahsen et al., 2013). Key diagnostic geological features of transfer zones include a lateral offset in the volcanic wedge and a change in volcanic wedge volume and distribution on either side of the transfer zone (Franke et al., 2007). Transfer zones are thought to be formed at preexisting zones of weakness, highlighting the persistence of structure between successive Wilson Cycles (Franke et al., 2007).

The change in the modeled volcanic wedge width and thickness near Cape Hatteras, and the lateral offset in both the ECMA and the modeled volcanic wedge, suggests that a rift transfer zone was present between the Carolina and Mid-Atlantic Regions during continental breakup, hereafter referred to as the Hatteras Transfer Zone (Fig. 3.3). The Hatteras Transfer Zone has formed at a suture zone separating an exotic Gondwanan terrane, which is thought to be present under the Chesapeake Bay, from Laurentian terranes, creating a preexisting weakness that is spatially correlated with the suggested location of this transfer zone (Fig. 3.2b) (Lefort & Max, 1991). This exotic Gondwanan terrane is inferred to represent a structural indenter of the Archean West African Craton during the Late Paleozoic Alleghanian collision, which was left behind during the subsequent continental breakup forming the ENAM (Lefort & Max, 1991). The presence of the BMA in the Carolina Region and absence in the Mid-Atlantic Region (Klitgord et al., 1988) provides additional support for the Hatteras Transfer

Zone. Suggested magnetic sources for the BMA imply rift activity (e.g. extension on a suture zone, rift basin formation, or rift-related mafic intrusions) in the Carolina Region that does not extend northward into the Mid-Atlantic Region (e.g. Hutchinson et al., 1983; Lizarralde et al., 1994; McBride & Nelson, 1988; Parker, 2014; Duff & Kellogg, 2019), and the boundary of this activity could be the Hatteras Transfer Zone.

The coincidence of the Hatteras transfer Zone, separating the first-order change in the modeled volcanic wedge geometry, with the inferred suture zone of the isolated piece of West African Craton under Chesapeake Bay (Lefort & Max, 1991) highlights the influence of preexisting structure on rifting, linking structural elements acquired during previous Wilson Cycles to the subsequent period of continental breakup. The Hatteras Transfer Zone also represents a key structural element of the rift that separates the first-order magmatic segmentation characterized by regions with distinct modes of magma emplacement during breakup. Parameters present during continental breakup, including the mantle temperature and the mode of crustal extension/thinning, can control the amount and distribution of magmatism (Fig. 3.5) (White & McKenzie, 1989; White et al., 2008; Keir et al., 2013; Koopmann et al., 2014). We propose that the Hatteras Transfer Zone most likely represents the boundary separating two distinct regions with combinations of these parameters.

3.6.2.2. Along-margin increase in mantle temperature

Mantle temperature plays a key role in magma production in rifts (White & McKenzie, 1989; White et al., 2008; Shuck et al., 2019). Understanding along-margin

changes in mantle temperature and the associated magma production identify where greater extension accommodation and thermal weakening was present to enable continental breakup at lower stress (Ebinger & Casey, 2001; Buck, 2004; Kendall et al., 2005; Bialas et al., 2010; Daniels et al., 2014). Based on the first-order magmatic segmentation at the ENAM indicated by the first-order variations in the thickness of our modeled volcanic wedge (Fig. 3.3), we suggest a south to north increase in mantle temperature was present during breakup at the ENAM across the Hatteras transfer zone, as warmer mantle temperatures can enhance melting to create greater magma production and a thicker volcanic package (White et al., 1987). The comparatively thicker modeled volcanic wedge emplaced over a narrower zone in the Mid-Atlantic Region could be caused by a higher amount of melt production related to a warmer mantle temperature beneath this region (Figs. 3.3, 3.5b, 3.5d). The comparatively wider but thinner modeled volcanic wedge in the Carolina Region could be caused by a lower amount of melt production related to a cooler mantle temperature beneath this region (Fig. 3.3, 3.5b-d). Shuck et al. (2019) use seismic velocities and petrological modeling of the MGL1408 seismic data to infer a ~2 km increase in the margin crustal thickness and ~10-25°C increase in mantle temperature from south to north across the zone we call the Hatteras Transfer Zone (Fig. 3.2a). The south to north increase in our modeled volcanic wedge thickness between the Carolina and Mid-Atlantic Regions is consistent with this mantle temperature and crustal thickness trend (Fig. 3.3) (Shuck et al., 2019).

Along-margin changes in mantle temperature can be related to the presence of a mantle plume (Ebinger & Sleep, 1998) or differences in the amount of thermal insulation

caused by preexisting crustal thickness (Shuck et al., 2019). Mantle temperatures, and therefore the scale of magmatism, decreases radially from the location of a mantle plume (Holbrook & Kelemen, 1993; Ebinger & Sleep, 1998). However, the relatively abrupt change, rather than systematic decrease, in our modeled volcanic wedge thickness suggest a similar abrupt change in mantle temperature that is not consistent with a mantle plume (Figs. 3.3, 3.4). Furthermore, while a mantle plume has been proposed to explain the CAMP volcanism and the (either coeval or later) breakup magmatism at the ENAM (White & McKenzie, 1989; Wilson, 1997), the existence of this plume has been debated (Marzoli et al., 2018). Available evidence, including magma geochemistry data, the timing and extent magmatism, the absence of a crustal thickness anomaly, and the lack of a Jurassic hotspot track, does not support the presence of a mantle plume (Holbrook & Kelemen, 1993; Kelemen & Holbrook, 1995; McHone, 2000; Marzoli et al., 2018).

A difference in the pre-breakup continental crustal thickness related to a difference in basement terranes could have been present prior to breakup at the ENAM, which would impact the amount of thermal insulation and the mantle temperature during breakup (Shuck et al., 2019). The Hatteras Transfer Zone is located just north of a suture zone from the Late Paleozoic Alleghanian orogeny (320-260 Ma) (Hatcher, 2002; Boote & Knapp, 2016) (Fig. 3.2b). This suture zone separates thicker crust (~38 km) of the pre-Alleghanian Laurentian terranes (and the thick crust of the isolated West African Craton beneath Chesapeake Bay; Lefort & Max, 1991), inboard of the Mid-Atlantic Region, from thinner crust (~32 km) of the Gondwana accreted terranes in the Carolina Region

(Marzen et al., 2019). The thicker Laurentian crust could provide more thermal insulation that would cause a comparatively higher mantle temperature in the Mid-Atlantic Region compared to the Carolina Region (Shuck et al., 2019). This difference in the thickness of the preexisting continental crust between the Carolina and Mid-Atlantic Regions could cause a south to north increase in mantle temperature (Marzen et al., 2019; Shuck et al., 2019), which we suggest is responsible for the south to north increase in melt production and the related increase in the thickness of our modeled volcanic wedge (Fig. 3.3).

3.6.2.3. Degree of crustal extension and thinning

Variations in the timing and amount of extension localization and crustal thinning can influence the duration, location, and amount of magma production during continental breakup (Franke et al., 2007; Keir et al., 2013; Koopmann et al., 2014). The first-order variations in the width and thickness of our modeled volcanic wedge (Fig. 3.3) is consistent with a variation in the timing and amount of extension localization and crustal thinning at the ENAM, and the associated amount and duration breakup magmatism, between the Carolina and Mid-Atlantic Regions (e.g. Withjack et al., 2012), with the Hatteras Transfer Zone accommodating the differences in extension between these two regions.

After a period of broadly distributed extension during the Late Triassic rifting at the ENAM (Fig. 3.5a), crustal extension and thinning became localized near the site of eventual continental breakup and was accommodated by magmatism and volcanic

wedge emplacement (Withjack et al., 1998). If the timing of extension localization was synchronous along the southern ENAM, both the Mid-Atlantic and Carolina Regions would have experienced a similar duration of breakup magmatism, and the first-order variations in the geometry of our modeled volcanic wedge would be the result of a different spatial distribution of magmatic emplacement (Fig. 3.3). In this scenario, the wider modeled volcanic wedge in the Carolina Region would be the result of a wider zone of magmatic emplacement compared to the narrower volcanic wedge in the Mid-Atlantic Region (Fig. 3.5b). However, the first-order variation in the geometry of our modeled volcanic wedge (Fig. 3.3) could instead be explained by a temporal difference in magmatic emplacement (Figs. 3.5c, 3.5d). Onshore rift basin activity and inferred timings of volcanic wedge emplacement suggest that the localization of crustal extension and initiation of volcanic wedge emplacement along the southern ENAM may have been diachronous, occurring earlier in the Carolina Trough and later in the Baltimore Canyon Trough (Schlische et al., 2003; Withjack et al., 2012). The wider zone of volcanic wedge emplacement in the Carolina Region suggested by our model is consistent with a prolonged period of breakup magmatism (Figs. 3.3, 3.5c), which would result from an earlier localization of extension (Withjack et al., 2012). This longer period of breakup magmatism would have also released heat, which could help additionally explain the inferred lower mantle temperature in the Carolina Region (Shuck et al., 2019). The narrower zone of modeled volcanic wedge emplacement in the Mid-Atlantic Region could be caused by a comparatively later localization of extension and a briefer duration of breakup magmatism, with the narrower lateral extent causing vertical piling of the

volcanic layers and the thicker modeled volcanic wedge in this region (Figs. 3.3, 3.5d). While this magmatic emplacement occurred in the Mid-Atlantic Region, magmatic emplacement would have continued to the south in the Carolina Region (Fig. 3.5d). Following volcanic wedge emplacement in both regions, seafloor spreading began producing oceanic (or proto-oceanic) crust outboard of the ECMA (Fig. 3.5e) (Klitgord & Schouten, 1986; Schettino & Turco, 2009; Labails et al., 2010; Shuck et al., 2019).

Withjack et al. (2012) suggest that the boundary between the diachronous localization of extension and volcanic wedge emplacement is located near Chesapeake Bay, occurring earlier to the south and later to the north. If the variations in the distribution and amount of breakup magmatism between the Carolina and Mid-Atlantic Regions are the result of a temporal difference in extension localization, we suggest that this boundary should instead be located slightly to the south, near Cape Hatteras (Fig. 3.3). This location coincides with Hatteras Transfer Zone, and also aligns with the inferred suture of the isolated piece of the West African Craton beneath Chesapeake Bay (Lefort & Max, 1991) (Fig. 3.2b). This location is also just north of an Alleghanian suture zone (Fig. 3.2b) between the pre-Alleghanian Laurentian Carolina terrane (to the north) and the Gondwanan Charleston/Suwannee terranes (to the south) (Higgins & Zietz, 1983; Boote & Knapp, 2016). Marzen et al. (2019) suggest that the rheology of the thinner Gondwanan terranes, which make up much of the Carolina Region, may have made the crust in this region easier to extend during the rifting of Pangaea compared to the thicker Laurentian terranes that predominantly make up the Mid-Atlantic Region (along with the thick piece of west African Craton beneath Chesapeake Bay; Lefort &

Max, 1991). The combination of a preexisting weakness with a regional difference in geologic terranes and crustal thickness could have influenced the timing of extension localization and the associated duration of breakup magmatism (e.g. Withjack et al., 2012), occurring first in the Carolina Region and later in the Mid-Atlantic Region (Figs. 3.5c-d).

3.6.3. Second-order magmatic segmentation during breakup at the ENAM

The remnants of previous Wilson Cycles produced the first-order magmatic segmentation at the ENAM (Lefort & Max, 1991; Withjack et al., 2012; Marzen et al., 2019; Shuck et al., 2019). The signature of the current Wilson Cycle is confined within second-order magmatic segmentation that developed during breakup at the ENAM. Amplitude variation (100-150 km wavelength) observed in the ECMA and margin isostatic gravity anomaly suggests that the ENAM is segmented along the margin (Behn & Lin, 2000). Magmatic segmentation at a similar scale is a feature in modern active rifts, such as the East African Rift, and indicates along-strike variations in the amount of magmatism available to accommodate the transition to mid-ocean ridge seafloor spreading (e.g. Ebinger & Casey, 2001; Kendall et al., 2005; Beutel et al., 2010; Keir et al., 2013). The along-margin variations in the width and thickness of our modeled volcanic wedge, which mimic the 100-150 km wavelength amplitude variation in the ECMA, suggest that analogous, second-order magmatic segmentation was present during breakup at the ENAM (Figs. 3.3, 3.4, 3.5). This second-order magmatic segmentation exists within the first-order magmatic segmentation (Figs. 3.3, 3.4, 3.5),

suggesting an independent cause for this segmentation. Second-order magmatic segmentation at the ENAM suggests that along-strike variations in melt production (e.g. Geoffroy, 2001; Hammond et al., 2013) and/or melt transport (e.g. Magde & Sparks, 1997; Shillington et al., 2009; Keir et al., 2015) were present during breakup. Following continental breakup, the segmentation of the ensuing Mid-Atlantic Ridge may have been inherited from the magmatic segmentation at the ENAM (Behn & Lin, 2000).

The cause of second-order magmatic segmentation in both active rifts and mid-ocean ridges is thought to be along-strike variations in either melt production or melt transport (e.g. Whitehead et al., 1984; Lin et al., 1990; Magde & Sparks, 1997; Geoffroy, 2001; Hammond et al., 2013; Keir et al., 2015). Variations in melt production can increase the amount of magma available at the center of each segment (e.g. Geoffroy, 2001). Variations in melt production have been explained by focused upwelling of warmer asthenospheric mantle associated with small-scale convection beneath the center of discrete segments (Whitehead et al., 1984; Schouten et al., 1985; Lin et al., 1990; Sempéré et al., 1993; Geoffroy, 2001). Alternatively, melt transport can occur at the base of the lithosphere to focus magma into the center of each segment (e.g. Magde & Sparks, 1997). Melt produced over a wide area rises vertically to the base of the lithosphere, and can be transported along this boundary (Magde & Sparks, 1997; Shillington et al., 2009; Keir et al., 2015). This transport process is facilitated by buoyancy driven flow and topography at the base of the lithosphere (Magde & Sparks, 1997; Ebinger & Sleep, 1998). Topography at the base of the lithosphere can be induced

by variations in the amount of extension and thinning, which produce locally shallower points beneath the segment centers where melt can focus (Shillington et al., 2009).

The second-order magmatic segmentation at the ENAM during breakup could be explained by along-margin variations in magma production, from focused upwelling in the asthenosphere (Geoffory, 2001), and/or magma transport at the base of the lithosphere (Keir et al., 2015). Focused upwelling is thought to produce modern magmatic segmentation in the Afar depression of the East African Rift (Hammond et al., 2013; Gallacher et al., 2016), the Gulf of California (Wang et al., 2009), and the Mid-Atlantic Ridge (Lin et al., 1990; Sempéré et al., 1993), and analogous upwelling could be responsible for the second-order magmatic segmentation at the ENAM. If sites of focused upwelling were present during breakup at the ENAM, the second-order volcanic wedge segments in our modeling identify where this upwelling occurred (Fig. 3.3), indicating the distribution of small-scale convection cells that developed in the underlying asthenosphere during breakup (Geoffroy, 2001).

The second-order magmatic segmentation at the ENAM could have alternatively, or additionally, been caused by melt transport at the base of the lithosphere (e.g. Keir et al., 2015). Melt transport at the base of the lithosphere has been proposed to cause magmatic segmentation in the East African Rift (Keir et al., 2015), eastern Black Sea (Shillington et al., 2009), and mid-ocean ridge segmentation (Magde & Sparks, 1997). Analogous melt transport at the base of the lithosphere could conceivably have occurred at the ENAM during breakup to create magmatic segmentation (Fig. 3.3). If the second-order magmatic segmentation at the ENAM was caused by melt transport at the base of

the lithosphere, the second-order volcanic wedge segments in our modeling identify where the melt was focused (Fig. 3.3), and may indicate locations that experienced greater extension and thinning during rifting (e.g. Shillington et al., 2009).

The length scales of the segmentation in mid-ocean ridges and the magmatic segmentation observed in rifts are equivalent, which indicates that the segmentation of the spreading centers may be inherited from the rifting and breakup process (e.g. Hayward & Ebinger, 1996; Behn & Lin, 2000; Beutel et al., 2010; Bellahsen et al., 2013). Mid-ocean ridge transform faults can originate from both rift transfer zones, related to preexisting structure that was acquired during previous Wilson Cycles, and from the magmatic segmentation present during breakup (Bellahsen et al., 2013). At the ENAM, both the Hatteras Transfer Zone, separating the first-order magmatic segmentation, and the second-order magmatic segmentation present during breakup likely influenced the segmentation and transform fault formation in the ensuing Mid-Atlantic Ridge.

At the ENAM, the Hatteras Transfer Zone may have facilitated the inheritance of a Mid-Atlantic Ridge transform fault from preexisting structure (e.g. Bellahsen et al., 2013). The landward extrapolation of the Northern Kane Fracture Zone (Kiltgord & Schouten, 1986) and offsets in the linear magnetic anomalies seaward of the ECMA (Greene et al., 2017) intersect the ENAM just north of Cape Hatteras, coincident with the Hatteras Transfer Zone (Figs. 3.1b, 3.3). The south end of the inferred suture from the isolated piece of the West African Craton beneath Chesapeake Bay is also present at this location (Fig. 3.2b), representing a preexisting structure formed during the

Alleghanian collision of the previous Wilson Cycle (Lefort & Max, 1991). The spatial relation of these features suggests that the Mid-Atlantic Ridge transform fault offset producing the Northern Kane Fracture Zone was inherited from preexisting structure from the previous Wilson Cycle through the Hatteras Transfer Zone during breakup (e.g. Bellahsen et al., 2013).

Numerous transform faults of the early and modern Mid-Atlantic Ridge may have formed from the second-order magmatic segmentation during breakup at the ENAM (Fig. 3.3) (e.g. Hayward & Ebinger, 1996; Beutel et al., 2010; Bellahsen et al., 2013). The second-order magmatic segmentation suggested by our modeling, and the ECMA amplitude variation, exists on a similar length scale to the Mid-Atlantic Ridge segmentation (Behn & Lin, 2000). The landward extrapolations of many Atlantic fracture zones also intersect the margin between, or close to, our modeled volcanic wedge segments and the Hatteras Transfer Zone (Figs. 3.1b, 3.3, 3.4). The combination of similar segmentation scales and coincident fracture zone locations suggests that the ensuing spreading center segmentation, which persists in the modern Mid-Atlantic Ridge, was inherited from the magmatic segmentation during breakup at the ENAM (Fig. 3.5e). This genetic relationship between breakup and seafloor spreading at the ENAM supports the hypothesis that mid-ocean ridge segmentation develops from the magmatic segmentation and transfer zones associated with continental breakup, linking the rifting and seafloor spreading stages of the Wilson Cycle (e.g. Hayward & Ebinger, 1996; Behn & Lin, 2000; Keranen et al., 2004; Beutel et al., 2010; Bellahsen et al., 2013; Hammond et al., 2013; Collier et al., 2017).

3.7. Conclusions

From this study we draw the following conclusions:

1. The margin-scale magmatism driving continental breakup at the ENAM, indicated by our modeled volcanic wedge, was similar in scale to the breakup magmatism observed at the other magma-rich rifted continental margins bounding the Atlantic Ocean.
2. Both first- and second-order magmatic segmentation, indicating along-margin variations in the distribution/amount of magmatism, were present during continental breakup at the ENAM, and can explain the observed along-margin variations in the amplitude and character of the ECMA.
3. Two regions representing the first-order magmatic segmentation were likely separated by a rift transfer zone (here called the Hatteras Transfer Zone) and could be related to differences in mantle temperature and/or the timing and amount of crustal extension/thinning, both of which are probably governed by preexisting structure acquired during the previous Wilson Cycle.
4. Second-order magmatic segmentation during breakup at the ENAM could be produced by along-margin variations in magma production and/or transport, and likely influenced the segmentation and transform fault spacing of the initial and modern Mid-Atlantic Ridge.

4. DEEP-OCEAN PALEO-SEAFLOOR EROSION IN THE NORTHWESTERN PACIFIC IDENTIFIED BY HIGH-RESOLUTION SEISMIC IMAGES

4.1. Overview

The deposition and diagenesis of pelagic marine sediments together play an important role in global geochemical cycles by returning elements, such as silica, from the hydrosphere to the geosphere and stably sequestering them within deep-ocean sedimentary sections around the world. Here, we present new seismic reflection data from the northwestern Pacific that we interpret to indicate a period of erosional activity that has returned silica to the hydrosphere and thus represents a departure from uniform sequestration of pelagic sediments. The interpreted erosional features are observed as a ~200- to 300-m-wide variation in reflector character within the ~20-m interval overlying the regional chert/porcellanite layer. This reflector character is not consistent with uniform pelagic sedimentation, and it has not previously been noted in the northwestern Pacific, where most seismic data are lower-resolution. Erosion of seafloor sediments could be caused by short-lived bottom-current activity, but the geometry of the observed features suggests that fluid-expulsion erosion from diagenesis of primarily siliceous sediment plays some role in driving this mass transfer. Regardless of the details of the process, erosion of deep-ocean seafloor sediments represents a return of silica and other chemicals from the sediment to the bottom water and, if pervasive in the oceans, these processes should be accounted for in models of global geochemical cycles.

4.2. Introduction

The deposition, burial, and diagenesis of pelagic marine sediments together create a major sink in global geochemical cycles, including the global silica cycle (DeMaster, 1981; Tréguer & De La Rocha, 2013; Renaudie, 2016). The silica cycle involves the transfer of silica from both the continent to the ocean, through continental chemical weathering and the dissolution of terrigenous sediment and dust, and from the mantle to the ocean, through the alteration of submarine basalt, all of which contributes dissolved silica to ocean water (Tréguer & De La Rocha, 2013). Dissolved silica in ocean water is converted to biogenic silica during primary production by marine organisms such as diatoms, radiolarians, and silicoflagellates (Nelson et al., 1995). Biogenic silica is then sequestered through the sedimentation, burial, and diagenesis of siliceous sediment composed of the skeletons of siliceous organisms (Hesse, 1988; DeMaster, 2001). Globally, ~3 Tmol per year of silica is transferred from the ocean into deep-ocean sediments (DeMaster, 2001). The chemical sequestration represented by the formation of marine sedimentary sections is thus an important component of the global silica cycle.

The global silica cycle is linked to other biogeochemical cycles, such as the carbon and nitrogen cycles, through the uptake of chemicals during the growth of siliceous marine organisms (Ragueneau et al., 2000; Tréguer & De La Rocha, 2013; Renaudie, 2016). Primary productivity of siliceous organisms extracts carbon from surface waters, and that carbon is then exported to the deep ocean through sedimentation (Ragueneau et al., 2000), impacting atmospheric carbon concentrations and global

temperature trends (Smetacek, 1999; Renaudie, 2016). Understanding each component of the silica cycle, including sequestration within sedimentary sections, thus provides insight into marine primary production through time and its relationship to atmospheric carbon (Ragueneau et al., 2000; Renaudie, 2016).

Siliceous pelagic marine sediments are present globally and typically dominate the biogenic component of sediments in deep-ocean settings below the calcium carbonate compensation depth (Hesse, 1988). Siliceous marine sediments are deposited on the seafloor as a silicicous ooze comprised of opal-A, the amorphous silica mineral (Hesse, 1988). Silica diagenesis converts pelagic siliceous ooze into dense, stable porcellanite and chert (Kastner et al., 1977). This pelagic sedimentation and diagenesis creates diagnostic flat-lying reflector packages that are observed in seismic images of deep-ocean sedimentary sections around the world (Ewing et al., 1968; Hüneke & Henrich, 2011). A widespread chert/porcellanite layer is inferred throughout the northwestern Pacific based on seismic observations of flat-lying reflectors that have been cored at discrete locations, implying that undisturbed pelagic sedimentation, burial, and diagenesis sequestered silica in this region (Heezen et al., 1973; Lancelot & Larson, 1975; Abrams et al., 1992; Moore, 2008).

In this study, we present new seismic reflection data that provide insight into the formation of the siliceous sedimentary section in the deep-ocean northwestern Pacific and suggest that the diagenetic processes acting on deposited sediments may lead to the reintroduction of silica back into the hydrosphere. We observe seismic reflector character that indicates a period of erosion that affected the paleo-seafloor and likely

returned chemicals to the bottom water. This seafloor erosion suggests that the entirety of material involved in pelagic sedimentation, burial, and diagenesis in the deep-ocean is not necessarily sequestered in the sedimentary section.

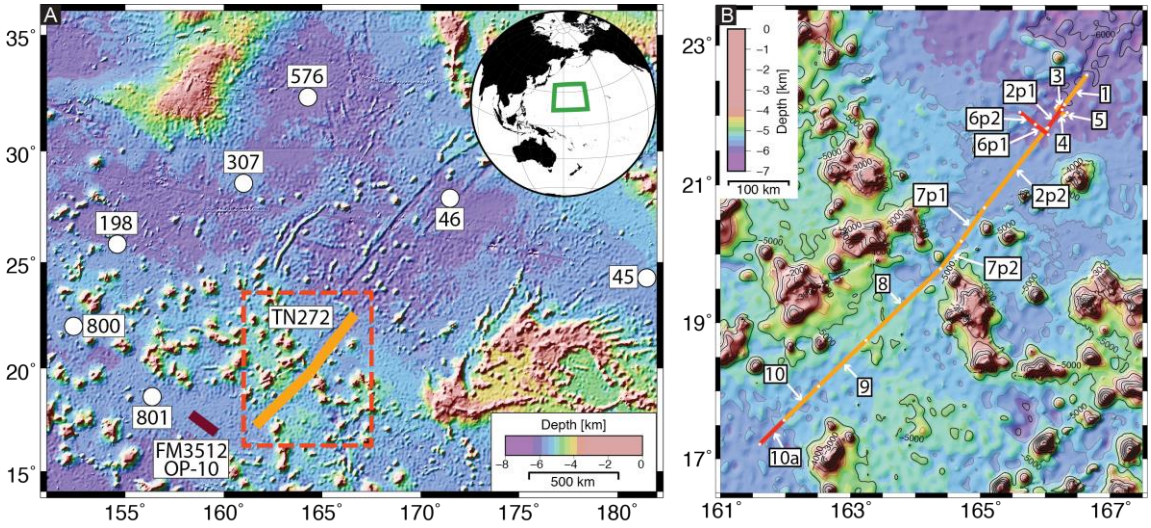

Figure 4.1 Northwestern Pacific and study area satellite-derived bathymetry data: (A) Northwestern Pacific satellite-derived bathymetry (ETOPO1; Amante and Eakins, 2009). Orange line denotes the main TN272 survey transect. White circles indicate DSDP/ODP drill sites. Dark red line indicates FM3512 Line OP-10 (Abrams et al., 1992). (B) Close up of TN272 survey (extent indicated by dashed red line in Fig. 4.1a). Individual survey segments labeled. Key seismic lines highlighted in red (Fig. 4.4-4.6).

4.3. Background

The Jurassic-age lithosphere in the northwestern Pacific (Fig. 4.1), the oldest in the Pacific Ocean, formed south of the equator before moving into the northern hemisphere (Lancelot & Larson, 1975). The Pacific plate has undergone pelagic sedimentation and diagenesis throughout its history, producing a sedimentary section predominantly made up of siliceous and clay sediments, with some volcanoclastic and

pelagic carbonate sediment found in the deeper section (Pimm et al., 1971; Heezen et al., 1973; Lancelot & Larson, 1975; Karl et al., 1992). The sedimentary section of the northwestern Pacific, formed through pelagic sedimentation, burial, and diagenesis of the siliceous sediment, represents a major sink for silica (Hesse, 1988; DeMaster, 2001).

Silica diagenesis occurs globally in deep-ocean siliceous sediment (Hesse, 1988), including in the northwestern Pacific (Karl et al., 1992; Moore, 2008). Silica diagenesis occurs in two phases to transform opal-A, the amorphous silica polymorph that is the dominant mineral in siliceous ooze, into opal-CT, the metastable silica polymorph mineral making up porcellanite, followed by microcrystalline quartz, the final, stable silica polymorph mineral in chert (Hesse, 1988). The silica diagenesis reaction occurs via a dissolution and reprecipitation pathway (Kastner et al., 1977). Substantial changes to sediment physical properties accompany silica diagenesis, including an increase in mineral density and rapid consolidation of the sediment, producing a decrease in porosity and overall sediment volume and an increase in bulk density and seismic velocity (Kastner et al., 1977; Isaacs, 1981; Guerin & Goldberg, 1996; Meadows & Davies, 2009; Wrona et al., 2017). Fluid expulsion accompanies this diagenesis due to both the decrease in porosity (10-35 porosity %) during each phase of the reaction (Issacs, 1981) and thermochemical dehydration releasing structurally bound water (1.5-15.3 weight %) (Jones & Renaut, 2004; Davies et al., 2008). The chert and porcellanite layer created by silica diagenesis is recognized in seismic data as a high-amplitude reflector package (e.g. Ewing et al., 1968; Davies & Cartwright, 2007) due to the high seismic-impedance contrast created when the bulk density and seismic velocity of

sediments increase as pore fluids are expelled and as opal-A is replaced by denser minerals (Guerin & Goldberg, 1996; Wrona et al., 2017).

As the Pacific plate transited under the high-biological-productivity equatorial zone (15°S to 5°N) during the Cretaceous (Late Cenomanian to Late Campanian; ~95 Ma to 75 Ma), pelagic siliceous ooze, primarily made up of radiolarian tests, was deposited at a rate of ~3 m/Myr and subsequently underwent silica diagenesis (Lancelot & Larson, 1975; Behl & Smith, 1992; Karl et al., 1992; Larson et al., 1992; Moore, 2008). Silica diagenesis converted this siliceous ooze (opal-A) into a chert/porcellanite (microcrystalline quartz/opal-CT) layer (Hesse, 1988; Behl & Smith, 1992; Karl et al., 1992). Since leaving the equatorial zone in the Late Cretaceous (Larson et al., 1992), the plate has been in a low biological productivity zone that is coincident with the present-day North Pacific Subtropical Gyre (NPSG) (~15°N to 35°N; Karl, 1999), where sediment deposition rates are ~0.5-1 m/Myr, and the sediment type is primarily pelagic clays (Karl et al., 1992).

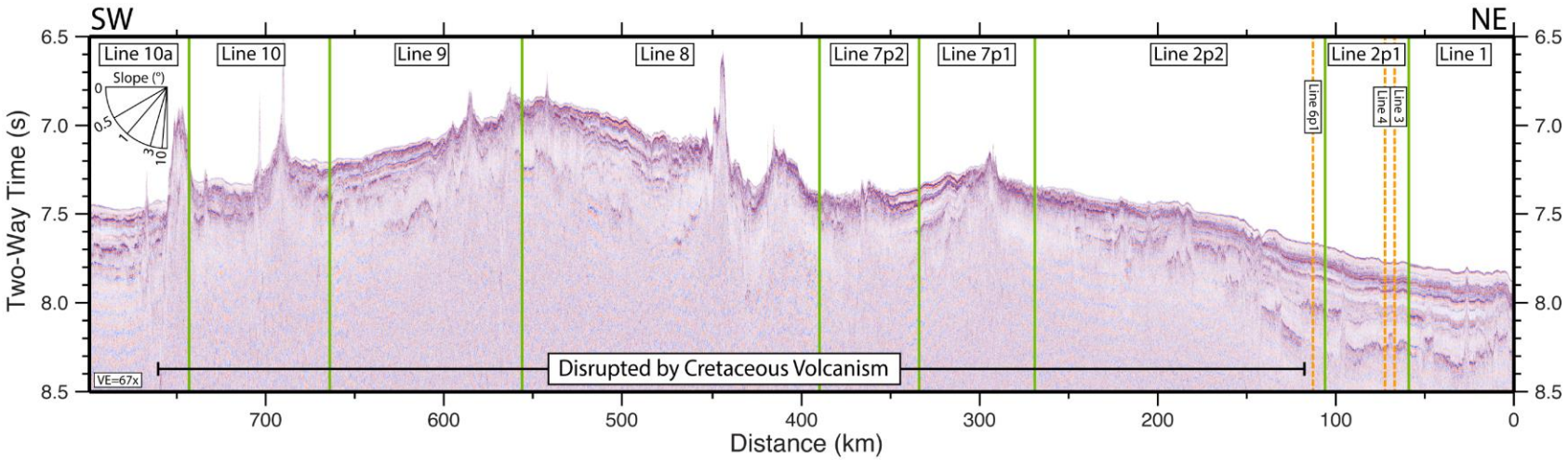

Figure 4.2 Multi-channel seismic profile from main TN272 survey transect (Fig. 4.1). Green lines separate individual segments (labeled). Orange dashed lines denote intersection of crosslines (labeled). Extent where sedimentary section is impacted by Cretaceous volcanism indicated.

Multi-channel seismic (MCS) data from the northwestern Pacific show four distinct, correlatable reflector packages with flat, horizontal reflectors that are laterally continuous throughout the region: (1) a low-amplitude “upper transparent” layer; (2) a high-amplitude “upper opaque” layer; (3) a low-amplitude “lower transparent” layer; and (4) the acoustic basement (Ewing et al., 1968). Drill-core samples of pelagic clays overlying chert/porcellanite recovered at sites throughout the northwestern Pacific, including Ocean Drilling Program (ODP) Sites 800 and 801 and Deep Sea Drilling Program (DSDP) Sites 45, 46, 198, and 307 (Fig. 4.1), correlate with the paired low-/high-amplitude reflection packages of the upper transparent and opaque layers observed in MCS data (Pimm et al., 1971; Heezen et al., 1973; Lancelot & Larson, 1975; Abrams et al., 1992). These pelagic-clay and chert/porcellanite layers are laterally continuous and observed throughout much of the northwestern Pacific in MCS data (Hesse, 1988; Karl et al., 1992).

4.4. Methods

High resolution MCS data were acquired during the R/V *Thomas G. Thompson* cruise TN272 to the Jurassic Quiet Zone (Figs. 4.1, 4.2) (Tominaga et al., 2012). The MCS data were acquired along an ~800-km-long, northeast/southwest transect using two 110-in^3 generator/injector air guns towed at 4 m depth with a 25-m shot spacing, and a 48-channel, 870-m-long streamer with a 12.5-m group spacing. Data processing of the MCS data involved: (1) application of a 50-200 Hz bandpass filter and manual removal of bad/noisy channels; (2) basic velocity analysis to apply a preliminary normal moveout

correction and stack; (3) construction of a velocity model based on concurrently collected sonobuoy refraction data (Feng et al., 2015); (4) reapplication of the normal moveout correction and stack; (5) post-stack Kirchhoff time migration; and (6) predictive gap deconvolution. The TN272 MCS data have a higher frequency (20-200 Hz) than previous seismic data available in the northwestern Pacific (Fig. 4.3) (Abrams et al., 1992). These new, higher-resolution data allow for an unprecedented examination of the processes forming the deep-sea sedimentary section of the northwestern Pacific.

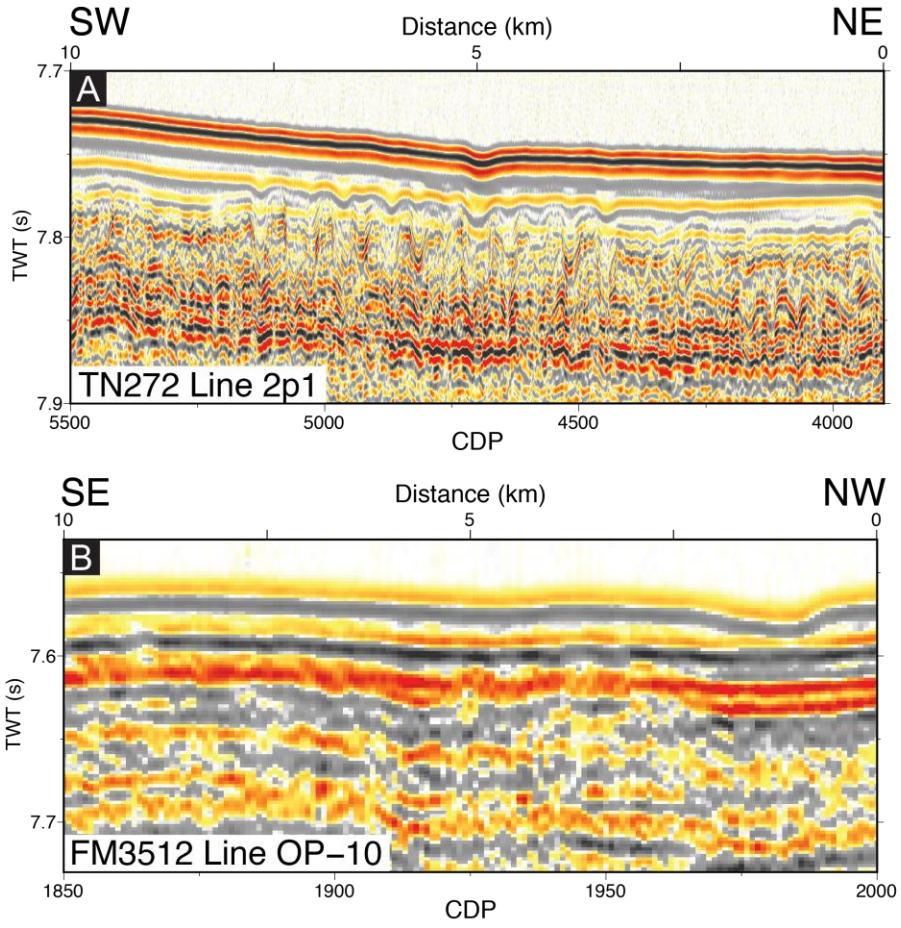

Figure 4.3 Comparison between new and legacy seismic data for the northwestern Pacific (Fig. 4.1A). (A) New MCS data from TN272 Line 2p1, with a 6.25 m CDP (common depth point) spacing. (B) Legacy MCS data from FM3512 Line OP-10 (Abrams et al., 1992), with a 66.66 m CDP spacing.

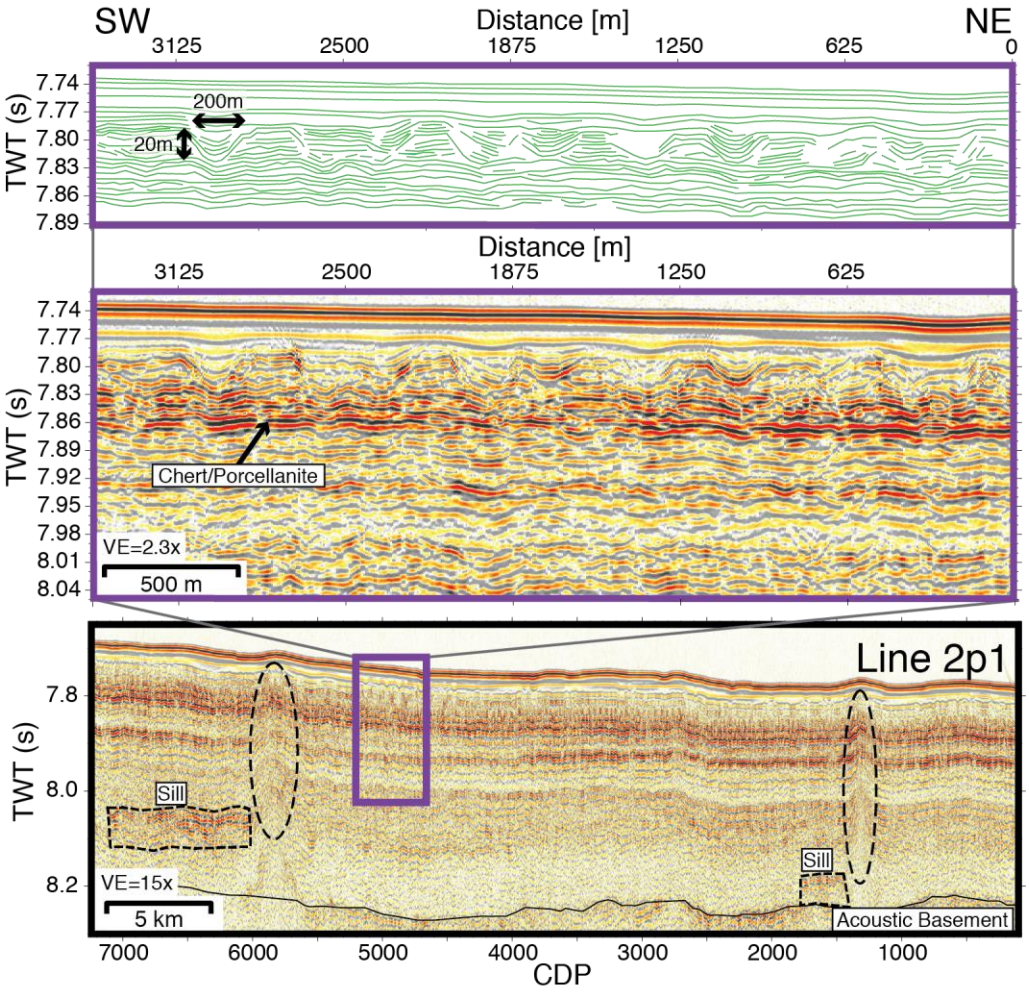

Figure 4.4 Multi-channel seismic profile 2p1. Shows variation in reflector character above the chert/porcellanite on the northeastern end of the TN272 survey (Fig. 4.1). Bottom panel shows full seismic section. Purple box in bottom panel is expanded laterally in the middle and top panels. Middle panel shows seismic section zoomed in to show reflector character above the chert/porcellanite layer. Top panel shows reflector traces from the shallow time interval in the middle panel. Dashed ovals indicate areas of disrupted reflectors that could represent fluid expulsion from sills (labeled).

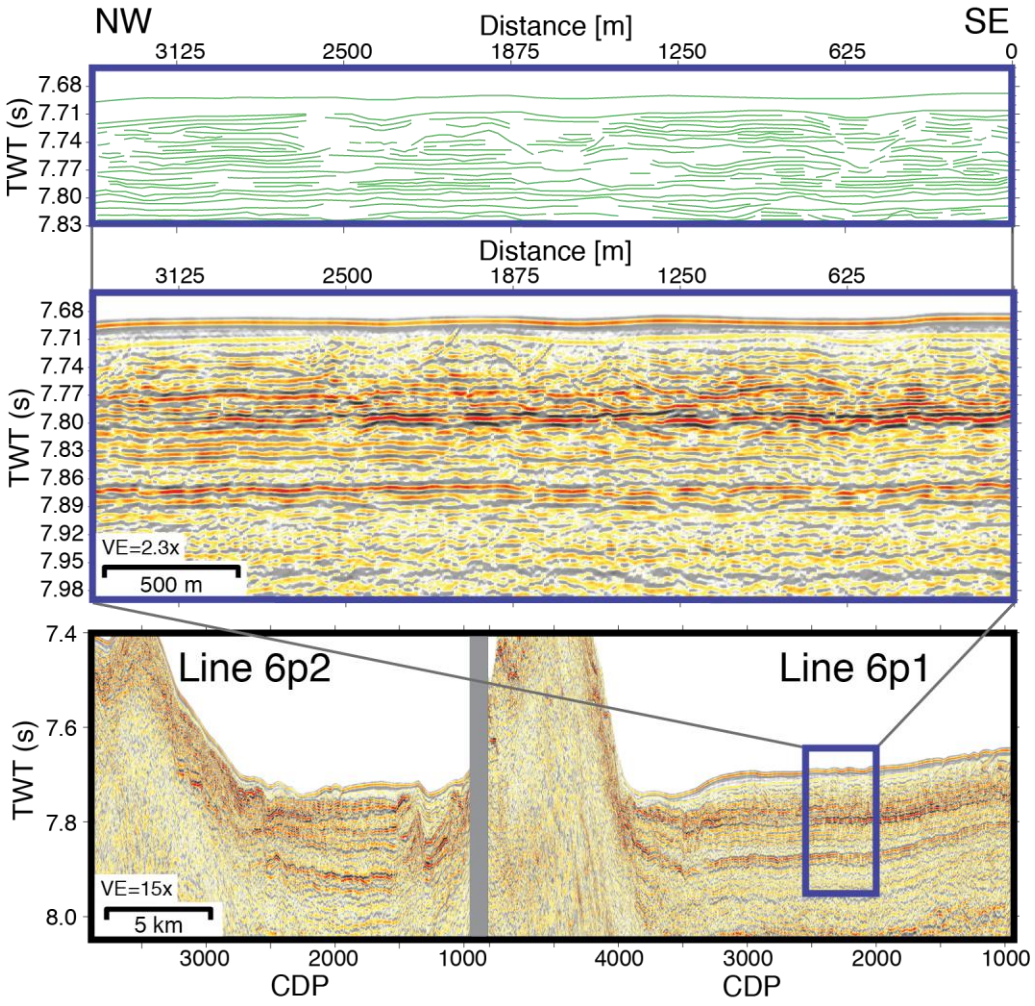

Figure 4.5 Multi-channel seismic profile 6p1/6p2. Shows variation in reflector character above the chert/porcellanite on the northeastern end of the TN272 survey Crosslines 6p1 and 6p2 (Fig. 4.1). Bottom panel shows full seismic section. Blue box in bottom panel is expanded laterally in the middle and top panels. Middle panel shows seismic section zoomed in to show reflector character above the chert/porcellanite layer. Top panel shows reflector traces from the shallow time interval in the middle panel.

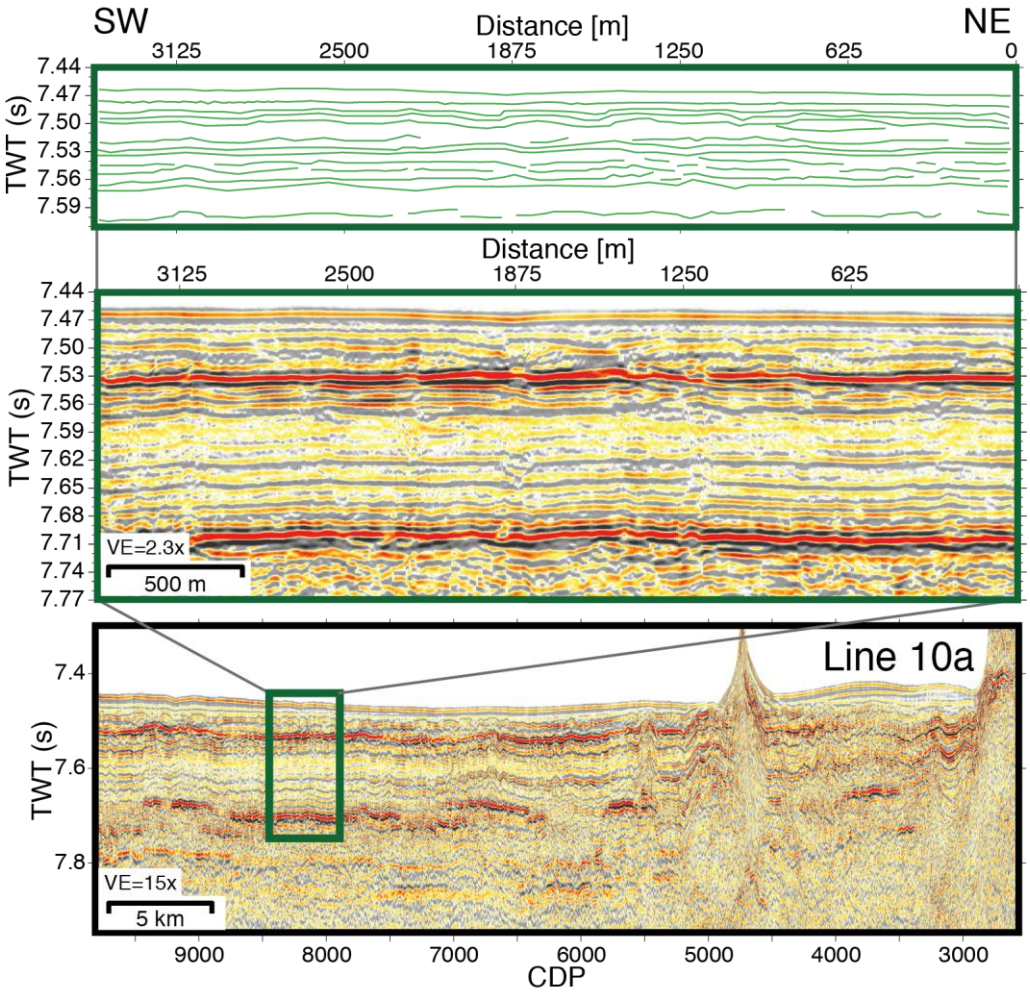

Figure 4.6 Multi-channel seismic profile 10a. Shows flat-lying reflector character above the chert/porcellanite on the southwestern end of the TN272 survey (Fig. 4.1). Bottom panel shows full seismic section. Green box in bottom panel is expanded laterally in the middle and top panels. Middle panel shows seismic section zoomed in to show reflector character above the chert/porcellanite layer. Top panel shows reflector traces from the shallow time interval in the middle panel.

4.5. Results

The high-resolution TN272 MCS data from the northeastern section of the survey image the paired low-/high-amplitude reflection packages interpreted throughout the northwestern Pacific as pelagic clay overlying Cretaceous-age chert/porcellanite (Fig.

4.2) (Ewing et al., 1968; Hesse, 1988). However, the new higher resolution MCS data reveal a repeated ~200- to 300-m horizontal variation in reflector character in the ~20 m interval overlying the high-amplitude chert/porcellanite package over the northeastern 100 km of the TN272 MCS profile (Fig. 4.4). This variation is manifested as a series of discrete zones of horizontal, parallel reflectors that terminate against intervening arcuate, concave upward reflectors (Fig. 4.4). The reflectors below this interval are high-amplitude and generally flat-lying, consistent with what is expected for the regional chert/porcellanite layer (Ewing et al., 1968), and the reflectors overlying this interval are generally flat-lying, but are depressed downward directly above the arcuate reflectors. This reflector variation is observed both along the primary northeast/southwest transect and, at the same scale, on crosslines perpendicular to the main survey transect (Figs. 4.2, 4.4, 4.5), suggesting that these features may exhibit a polygonal planform. This reflector variation could also extend beyond the survey area to the northeast. However, similar variation does not persist for the southwestern 700 km of the TN272 profile (Figs. 4.2, 4.6). The southwestern 50 km of the TN272 profile exhibits flat-lying, horizontal reflectors (Figs. 4.2, 4.6), while the middle 650 km of the TN272 MCS profile is structurally disrupted by the Cretaceous volcanism that affected much of the northwestern Pacific (Wessel & Lyons, 1997; Stadler & Tominaga, 2015) (Fig. 4.2). Reflector variation with the spatial scale seen on the northeastern section of the survey would likely not be easily resolved in lower-frequency MCS data (Fig. 4.3) and be misinterpreted in subbottom profiler data, which have ping spacings typically too large to enable migration.

4.6. Discussion

4.6.1. Causes of deep-ocean reflector character variation

The repeated, ~200- to 300-m horizontal reflector character variation observed in the TN272 MCS data (Figs. 4.4, 4.5) represents a departure from the seafloor-parallel reflectors representative of undisturbed pelagic sedimentation, burial, and diagenesis observed in seismic data throughout the northwestern Pacific (Ewing et al., 1968; Pimm et al., 1971; Heezen et al., 1973; Lancelot & Larson, 1975; Abrams et al., 1992). This reflector character suggests that additional processes beyond pelagic sedimentation, burial, and diagenesis affected the formation of the sedimentary section in the northwestern Pacific.

It is difficult to explain the observed repetitive reflector variation as deformation from faulting or folding, or as a product, such as turbidites or seafloor bedforms, of depositional processes. While faulting does occur in abyssal plain sediments (e.g. Williams, 1987), there are no clear reflector offsets present in the seismic data indicative of faulting, and faulting could not explain the arcuate nature of the intervening reflectors. Folding also seems unlikely given the lack of structures that could plausibly be interpreted as folding in this interval and the generally flat-lying nature of the reflectors above and below this interval, which should be similarly disrupted if folding affected the sedimentary section. Additionally, deep-ocean turbidites (Orwig, 1981; Karl et al., 1992) are not likely the cause of the observed reflector variation, particularly given that this variation is restricted to the northeastern section of the MCS profile, far away from the more prevalent and larger seamounts bounding the central and southwestern portions of

the MCS profile (Fig. 4.1). Finally, while seafloor bedforms created by bottom-current activity, including mudwaves, are observed at a range of scales, these features are typically elongate and their internal reflector geometry is sinuous (Flood & Shor, 1988), rather than the truncated, horizontal reflectors observed in the MCS data.

The spacing and vertical relief of the reflector-character variation observed on the northeastern 100 km of the TN272 MCS profile are of a similar scale to the features produced by the differential advancement of a silica diagenetic front, where the transformation of opal-A to opal-CT occurs at a shallower depth in some locations along the diagenetic front (Davis & Cartwight, 2007). For differential advancement to be occurring, silica diagenesis would have to be active in the Northwestern Pacific, with unconverted siliceous ooze present to sustain the reaction. Presently available unconverted siliceous ooze in the northwest Pacific would require that either siliceous ooze was deposited while the plate was still within the equatorial zone during the Cretaceous (Karl et al., 1992) and has not yet undergone diagenesis, which would necessitate slow silica diagenesis at a shallow depth over a long period of time (e.g. Riech, 1981), or siliceous ooze was deposited in more recent time within the otherwise oligotrophic NPSG (Karl, 1999; Benitez-Nelson et al., 2007). Mesoscale eddies within the NPSG have been found to significantly stimulate locally enhanced primary production and the export of silica from surface waters (e.g. Karl, 1999; Benitez-Nelson et al., 2007). However, to create significant accumulations of siliceous ooze to sustain active diagenesis, numerous eddies would have to repeatedly be active over the northeastern 100 km of the TN272 MCS profile and the silica produced would need to

be buried and preserved at the seafloor to prevent dissolution into the bottom water (DeMaster, 2001). Therefore, it seems unlikely that the observed reflector character is the product of an active silica-diagenesis front undergoing differential advancement unless substantial local enhancement of siliceous ooze accumulation occurs within the Northwestern Pacific, and there are no existing observations to support this. Additionally, the relief of the reflectors overlying this interval is difficult to reconcile with differential advancement (Fig. 4.4), as a characteristic feature of this activity are reflectors that are depressed downward directly above the areas that have undergone differential advancement due to greater compaction associated with the more substantial diagenesis (Davis & Cartwight, 2007).

The observed repeated ~200- to 300-m horizontal variation in reflector character on the northeastern 100 km of the TN272 MCS profile could be interpreted to indicate a period of erosional activity acting on the sedimentary section (e.g. Davies et al., 2008; Hernández-Molina et al., 2008; Sun et al., 2011; 2016). The reflector terminations bounding the zones of horizontal, parallel reflectors could represent erosional truncation from erosion into the flat-lying pelagic sediment at the paleo-seafloor (Figs. 4.4, 4.5). The arcuate, concave upward reflectors that the zones of horizontal reflectors terminate against could represent deformed sediment and/or infill drape onlapping the erosional surfaces and filling the void produced by erosional activity (Figs. 4.4, 4.5).

4.6.2. Mechanisms and implications of seafloor erosion

Erosional features, such as those inferred on the northeastern 100 km of the TN272 MCS profile, are unexpected in the abyssal northwestern Pacific, and have implications for our understanding of the formation of deep-sea sedimentary sections and the budgets of global geochemical cycles. The observed reflector character and inferred erosional features in the TN272 MCS data suggest that other processes beyond pelagic sedimentation, burial, and diagenesis impacted the formation of the sedimentary section and could reintroduce silica and other chemicals to the hydrosphere for further participation in biogeochemical cycling. Two possible mechanisms that could cause seafloor erosion in this setting are bottom current activity (e.g. Hernández-Molina et al., 2008; Sun et al., 2016) or, perhaps more likely, fluid-expulsion erosion associated with silica diagenesis (e.g. Davies et al., 2008; Sun et al., 2011).

Bottom current activity has been documented to induce seafloor erosion, cutting erosional troughs that are later infilled with sediment (Fig. 4.7) (Flood & Hollister, 1974; Hollister et al., 1974; Hernández-Molina et al., 2008; Sun et al., 2016). Erosional troughs can exhibit a similar spatial scale and reflector character to what is observed in the TN272 MCS data (Figs. 4.4, 4.5). Erosional troughs observed in the South China Sea (Shao et al., 2007; Sun et al., 2016) have dimensions of 50-1500 m in width and vertical relief of 10-90 m, with horizontal reflectors truncating against arcuate, concave upward reflectors (e.g. Sun et al., 2016, their figure 10).

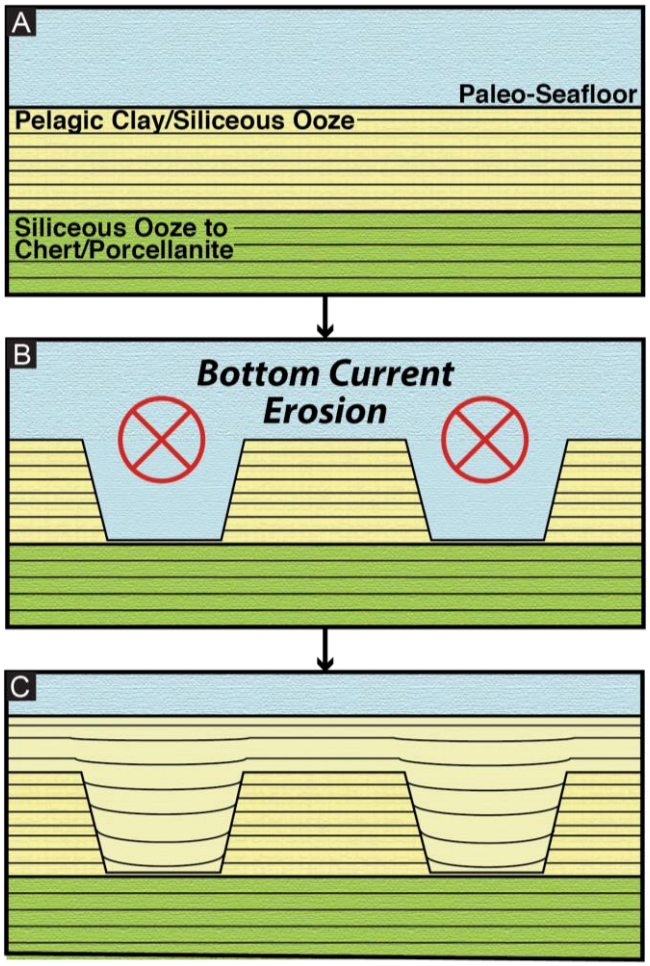

Figure 4.7 Schematic showing bottom current paleo-seafloor erosion mechanism: (A) Initial condition prior to erosion, with pelagic clay and/or siliceous ooze overlying a layer of siliceous ooze undergoing diagenesis to form chert/porcellanite. (B) Erosion from bottom current activity. Bottom currents oriented in/out of the page erode sediment from the paleo-seafloor. (C) Infill of erosional features by continued sedimentation following the termination of bottom current activity.

It is difficult to identify an obvious mechanism in the northwestern Pacific for past bottom current activity to create erosion on the paleo-seafloor in only a discrete interval of the sedimentary section. Present day oceanographic measurements of near-bottom particulate matter concentrations, related to erosion and resuspension of seafloor

sediment, suggest that the northwestern Pacific is presently an area of relatively weak bottom current activity (Gardner et al., 2018), and there are no clear explanations to support a past departure from this quiescence. Plate reconstructions do not include any major land mass reconfigurations near the western Pacific soon after the late Cretaceous age of the underlying chert/porcellanite that might induce major, but relatively short-lived, changes to oceanographic current circulation to cause erosion (Müller et al., 2016).

Some factors, such as seafloor topography or oceanographic activity, can locally increase bottom current strength and erosional activity. Topographic obstacles to flow or restricted gateways can accelerate the velocities and erosive ability of bottom currents (Hernández-Molina et al., 2008; Sun et al., 2016). However, the reflectors underlying the inferred erosional features have a generally horizontal geometry (Figs. 4.4, 4.5) and there are no seamounts visible in the bathymetry adjacent to the northeastern portion of the MCS line (Fig. 4.1), making it unlikely that prominent paleo-topographic highs were present to influence bottom current flow and increase erosion. The intensification of bottom current activity has also been associated with eddies and benthic storms (Hernández-Molina et al., 2008; Gardner et al., 2017). Mesoscale eddies in the northwestern Pacific have been observed in satellite data to occur in our study area approximately once every 1 to 4 years, averaging 16 weeks in duration (Cheng et al., 2014), and such eddies could have occurred in the past. However, global studies do not show high concentrations of near-bottom particulate matter indicative of resuspension by bottom currents in the vicinity of our study area, as have been observed in areas with

high eddy kinetic energy (Gardner et al., 2018). Additionally, eddy-induced bottom-current activity would require repeated occurrence of eddies that only locally influenced the northeastern 100 km of the MCS profile and did not affect the remainder of the transect.

Fluid expulsion driven by silica diagenesis could plausibly explain the inferred erosional features on the northeastern 100 km of the TN272 profile, forming pockmarks on the paleo-seafloor (Fig. 4.8). Pockmarks have been documented worldwide (Hovland and Judd, 1988; Pilcher & Argent, 2007; Davies et al., 2008; Sun et al., 2011), including on the modern seafloor of the northwestern Pacific near ODP Site 801 (Fig. C.1). Globally, pockmarks occur at a range of sizes (Hovland & Judd, 1988; Pilcher & Argent, 2007; Sun et al., 2011), including the ~200- to 300-m-wide, ~20-m-tall dimensions of the inferred fluid-expulsion erosional features in this study. Pockmarks also commonly occur in fields with numerous, relatively regularly spaced pockmarks (Pilcher & Argent, 2007), similar to the fairly regular spacing of the inferred fluid-expulsion erosional features on the main and cross lines of the TN272 MCS data. The reflector geometry expected from fluid expulsion is likewise consistent with our observations, with truncated reflectors from the diagenetic shrinking and removal of sediment at the location of fluid expulsion, which are then infilled with sediment creating onlapping, arcuate, concave upward reflectors (Pilcher & Argent, 2007; Davies et al., 2008) (Fig. 4.8).

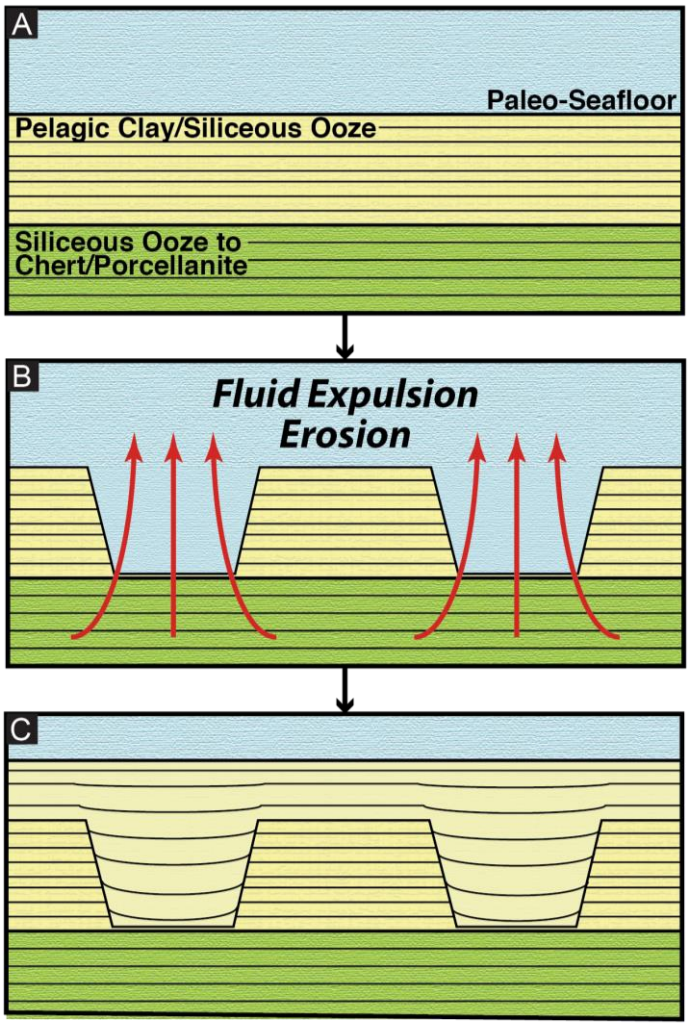

Figure 4.8 Schematic showing fluid expulsion paleo-seafloor erosion mechanism: (A) Initial condition prior to erosion, with pelagic clay and/or siliceous ooze overlying a layer of siliceous ooze undergoing diagenesis to form chert/porcellanite. (B) Erosion from fluid expulsion. Fluid expelled from the underlying silica diagenesis removes sediment and creates pockmarks on the paleo-seafloor. (C) Infill of erosional features by continued sedimentation following the termination of fluid expulsion.

Pockmark formation requires a source for the fluid expelled at the paleo-seafloor. Igneous sills have been documented to serve as a fluid source for pockmark formation (e.g. Jamtveit et al., 2004; Gay et al., 2015), and sills are present in our study area (Figs.

4.2, 4.4) that are likely associated with the mid-Cretaceous volcanism of the western Pacific (Wessel and Lyons, 1997; Stadler & Tominaga, 2015). A few vertical columns of disrupted reflectors suggestive of fluid-migration pathways are spatially correlated with sills interpreted in the MCS data (Fig. 4.4), suggesting that the emplacement of these sills may have driven fluid expulsion to cause localized sediment deformation. However, the inferred pockmarks do not have an associated column of disrupted reflectors beneath them extending down to the typical sill emplacement depth, nor are there obvious sills directly beneath these features that could serve as a source of fluid (Figs. 4.4, 4.5), making it difficult to attribute the inferred erosional features to sill-induced fluid expulsion unless there was lateral migration of the fluid within the shallower sedimentary section.

Fluid expulsion to create pockmarks could be sourced from the silica diagenesis reaction that formed the chert/porcellanite layer situated directly beneath these inferred erosional features (e.g. Davies et al., 2008). Fluid expulsion occurs during silica diagenesis due to both the decrease in porosity and the mineral dehydration associated with this thermochemical dehydration reaction (Isaacs, 1981; Hesse, 1988; Wrona et al., 2017). Fluid expulsion from silica diagenesis has been observed around the world (e.g. Hesse, 1988; Volpi et al., 2003; Davies and Cartwright, 2007; Davies et al., 2008; Behl, 2011). Pockmark formation driven by fluid expulsion does not necessarily require a catastrophic release of overpressured fluids; rather, it can occur through vertical fluid flow and entrainment of sediment grains (Hovland & Judd, 1988). In the northwestern Pacific, it is plausible that fluid from the diagenesis of siliceous ooze to form

chert/porcellanite could have been expelled in discrete locations to create pockmark features on the paleo-seafloor, which have now been buried after continued sedimentation and are manifested as the observed ~200- to 300-m variation in reflector character with a polygonal planform in the TN272 MCS data (Figs. 4.4, 4.5).

The volume of water expelled from silica diagenesis that could contribute to pockmark formation on the paleo-seafloor, and the associated amount of sediment eroded, can be estimated for our study area. The volume of water expelled can be estimated based on the amount of chert/porcellanite sediment present and measurements from analogous sites of silica diagenesis (Davies et al., 2008). For an average chert/porcellanite layer thickness of ~50 m, similar to what is observed at ODP Sites 800 and 801 (Karl et al., 1992), the original layer of opal-A sediment prior to diagenesis would be ~125 m thick, assuming sediment porosities of 0.8 and 0.5 for the sediment before and following diagenesis (Meadows & Davies, 2009). The inferred pockmarks are present on the northeastern 100 km of the TN272 survey (Fig. 4.2), and a 100 km by 100 km area would contain ~1,250 km^3 of opal-A sediment present prior to silica diagenesis. Davies et al. (2008) calculated that the volume of water expelled during silica diagenesis is 39% of the volume of opal-A-bearing sediment in the Faeroe-Shetland Basin. Using this as an analogue for the northwestern Pacific, we estimate that ~488 km^3 of water was expelled from silica diagenesis over a 100 km by 100 km area covering the northeastern end of the TN272 survey. The calculated expulsion percentage by Davies et al. (2008) is only for the opal-A to opal-CT stage of silica diagenesis, and the presence of chert in the northwestern Pacific indicates that diagenesis also proceeded

through the subsequent opal-CT to microcrystalline quartz stage, which would further release fluid (Isaacs, 1981; Hesse, 1988; Wrona et al., 2017). Therefore, the total volume of water expelled from silica diagenesis that was available in this area to create pockmarks on the paleo-seafloor could be even greater than what we estimate here. The corresponding volume of sediment eroded in our study area during pockmark formation on the paleo-seafloor can be estimated assuming 250-m diameter, circular pockmarks spaced every 250 m over a 100 km by 100 km area covering the northeastern end of the TN272 survey (Figs. 2, 4, 5). Using these assumptions, we estimate that ~40 km^3 of sediment was removed during the inferred fluid-expulsion erosion in our study area.

Regardless of the causative mechanism, the inferred erosional features do not extend upward to the present-day seafloor, suggesting that the erosional mechanism responsible is not presently active and was instead only operating during a discrete time interval after the deposition of siliceous ooze that formed the top of the underlying chert/porcellanite layer (Karl et al., 1992) (Figs. 4.7, 4.8). If the erosion was from bottom-current activity (e.g. Sun et al., 2016), the top of the inferred erosional features indicates when bottom current strength decreased. Alternatively, and perhaps more likely, if the erosion is driven by fluid expulsion from the underlying silica diagenesis (e.g. Davis et al., 2008), the end of pockmark formation could coincide with the waning of diagenesis where there was no longer sufficient fluid production to sustain pockmark formation. The timing and duration of fluid-expulsion erosion is directly related to the timing and duration of silica diagenesis, which is dominantly controlled by the temperature conditions governed by burial depth, bottom water temperature, and local

heat flow (Kastner et al., 1977; Hesse, 1988; Moore, 2008), and also affected by the host-rock lithology and pore-water chemistry (Kastner et al., 1977). The factors that control the timing of silica transformation are dependent on local conditions and thus may also explain the localized observation of these erosional features.

An approximate timeframe for the end of the erosional activity can be estimated based on the height of the erosional features in relation to the top of the chert/porcellanite layer, which has a known age based on regional drilling results. The top of the chert/porcellanite layer at ODP Sites 800 and 801, which presumably left the equatorial zone at a similar time as the TN272 MCS profile given their similar latitudes (~20° N) (Fig. 4.1), has a Late Campanian age (~75 Ma) (Karl et al., 1992; Larson et al., 1992). The truncated reflectors extend ~20 m above the top of the chert/porcellanite layer (Fig. 4.4), representing the paleo-seafloor at the termination of erosional activity. Given the ~0.5-1 m/Myr sedimentation rate for the sediment above the chert/porcellanite layer recorded at ODP Sites 800 and 801 (Karl et al., 1992), the height of these features suggests that erosional activity ended ~20-40 Myr after the Late Campanian, between approximately 35 and 55 Ma. If the erosion is from fluid expulsion, silica diagenesis could have continued after this time. Since the rates of silica diagenesis are influenced by temperature and time (Kastner et al., 1977; Hesse, 1988; Moore, 2008), the shallow burial depths and lower temperature during diagenesis in the northwestern Pacific would create a longer conversion time (Behl & Smith, 1992) compared to more rapid conversion that occurs elsewhere under deeper burial depth and higher temperature conditions (e.g. continental margins) (e.g. Davies & Cartwright, 2007). However, the

flux of fluid released by the reaction would presumably not have been sufficient to create pockmarks beyond this time.

Deep-ocean sedimentation and burial serves as a major sink in global geochemical cycles (DeMaster, 1981; Renaudie, 2016). However, sediment erosion, and fluid expulsion, could impact the budgets of these geochemical cycles by facilitating sediment dissolution and the release of chemical-rich fluid to the bottom water, returning chemicals to the hydrosphere that would otherwise have been sequestered in the geosphere. If these inferred erosional features formed (fully or partially) in siliceous ooze that had not yet undergone diagenesis, the erosional activity would have re-suspended unconsolidated siliceous ooze particles into the water column, and the erosion itself would have created a greater surface area of siliceous ooze exposed to the bottom water (Figs. 4.7, 4.8). Both of these factors would facilitate greater silica dissolution at the sediment/water interface to reintroduce silica to the bottom water, as oceanic bottom waters are typically highly undersaturated with respect to silica (DeMaster, 2001; Tréguer & De La Rocha, 2013). If this erosion was from fluid expulsion, the pore water would contain dissolved silica, as silica diagenesis is a dissolution/reprecipitation reaction (Kastner et al., 1977). Other chemicals are also released during silica diagenesis, including magnesium- and hydroxyl-rich fluids produced during the opal-CT to microcrystalline quartz conversion (Davies & Cartwright, 2007). During fluid-expulsion erosion, the dissolved silica and associated chemicals from diagenesis would undergo advective transport and be reintroduced into the bottom water (Fig. 4.8). The timing and duration of this chemical return to the bottom water via both fluid expulsion

and erosion is controlled by the timing and duration of the silica diagenesis in the underlying sediment (Kastner et al., 1977; Hesse, 1988; Moore, 2008). If similar fluid-expulsion erosion is present throughout the abyssal ocean, the effects of this previously unaccounted seafloor erosion, and the associated fluid expulsion, returning chemicals to the hydrosphere should be assessed and accounted for in models of global geochemical cycles.

4.7. Conclusions

Seismic images of repeated ~200- to 300-m horizontal variation in reflector character on the northeastern 100 km of the TN272 MCS survey may indicate that erosional activity took place during the formation of the northwestern Pacific sedimentary section. Erosional activity implies that a causative mechanism, present for a discrete period of time, acted on the sedimentary section to create erosional features restricted to a ~20 m interval above the regional chert/porcellanite layer in the MCS data. Paleo-seafloor erosion could have been facilitated by bottom current activity or fluid expulsion, but the geometry and setting of the observed features favors fluid-expulsion erosion stemming from the underlying silica diagenesis reaction that formed the regional chert/porcellanite layer. Observation of these interpreted fluid-expulsion erosional features were enabled by high-resolution MCS data. Similar fluid-expulsion erosional activity may be present elsewhere throughout the northwestern Pacific and in other deep-ocean settings around the world, and could return chemicals from seafloor sediments back into the ocean bottom water. Our results show that additional processes

beyond pelagic sedimentation and diagenesis, such as seafloor erosion, can occur during the formation of deep-ocean sedimentary sections. If seafloor erosion, possibly driven by diagenesis, is a pervasive process in the oceans, then the impact of this process on global geochemical cycles should be assessed and accounted for in global biogeochemical models.

5. CONCLUSIONS

The oceanic lithosphere formation and early seafloor spreading history of the North Atlantic Ocean was investigated by analyzing magnetic anomaly data from the Eastern North American Margin (ENAM). Magnetic anomaly correlations were refined throughout the ENAM and early Atlantic, and five new coherent, correlatable magnetic anomalies were identified that may document the earliest seafloor spreading of the Atlantic Ocean. Calculated seafloor spreading rates for the early Atlantic opening were slower in the north compared to the south, and a 15° counterclockwise reorientation of the spreading axis was found that could be caused by asymmetric spreading and/or westward ridge jumps. This seafloor spreading activity accommodated a straightening of the ridge from the prominent bend in the East Coast Magnetic Anomaly (ECMA) to the more linear strike of magnetic anomaly M25 and the modern Mid-Atlantic Ridge (Section II).

Magnetic modeling was used to identify the amount and distribution of magmatic activity that drove continental breakup at the ENAM. Modeling results indicated that the margin-scale magmatism at the ENAM was similar in scale to the breakup magmatism observed at the other magma-rich rifted continental margins bounding the Atlantic Ocean. Both first- and second-order magmatic segmentation were identified at the ENAM. The first-order magmatic segmentation could be related to parameters governed by preexisting structure acquired during the previous Wilson Cycle. The second-order

magmatic segmentation during breakup likely influenced the segmentation and transform fault spacing of the initial, and modern, Mid-Atlantic Ridge (Section III).

Seismic reflection data from the northwestern Pacific Ocean was used to investigate the formation of the sedimentary section and its role as a sink in global geochemical cycles. An unexpected variation in seismic reflector character was interpreted to indicate that a discrete period of seafloor erosion was present, impacting a ~20 m interval in the sedimentary section and terminating between 35 and 55 Ma. Paleo-seafloor erosion could have been caused by bottom current erosion or fluid expulsion from the underlying silica diagenesis reaction, but evidence favors fluid-expulsion erosion stemming from silica diagenesis. Similar processes may be present elsewhere throughout the ocean. If seafloor erosion is a pervasive process in the oceans, then the impact of this process should be assessed and accounted for in global biogeochemical models (Section IV).

REFERENCES

Abrams, L.J., Larson, R.L., Shipley, T.H., & Lancelot, Y. (1992). The seismic stratigraphy and sedimentary history of the East Mariana and Pigafetta Basins of the western Pacific. In R.L. Larson, Y. Lancelot, et al. (Eds.), *Proceeding of the Ocean Drilling Program, Science Results, 129* (pp. 551-561). College Station, TX: Ocean Drilling Program.

Ajay, K., Chaubey, A., Krishna, K., Rao, D. G., & Sar, D. (2010). Seaward dipping reflectors along the SW continental margin of India: Evidence for volcanic passive margin. *Journal of Earth System Science, 119*(6), 803. https://doi.org/10.1007/s12040-010-0061-2

Almalki, K. A., Betts, P. G., & Ailleres, L. (2015). The Red Sea–50 years of geological and geophysical research. *Earth-Science Reviews, 147*, 109-140. https://doi.org/10.1016/j.earscirev.2015.05.002

Amante, C., & Eakins, B.W. (2009). *ETOPO1 1 Arc-Minute Global Relief Model: Procedures, Data Sources and Analysis. NOAA Technical Memorandum NESDIS NGDC-24* (pp. 1-19). Boulder, CO: National Geophysical Data Center, Marine Geology and Geophysics Division. doi:10.7289/V5C8276M

Andrews, B. D., Chaytor, J. D., ten Brink, U. S., Brothers, D. S., Gardner, J. V., Lobecker, E. A., & Calder, B. R. (2016). Bathymetric terrain model of the Atlantic margin for marine geological investigations (ver. 2.0, May 2016): *U.S.*

Geological Survey open-file report 2012–1266, 19 p., 1 pl. https://doi.org/10.3133/ofr20121266

Arsenault, M. A., Miller, N. C., Hutchinson, D. G., Baldwin, W. E., Moore, E. M., Foster, D. F., ... Fortin, W. F. (2017). Geophysical data collected along the Atlantic continental slope and rise 2014, U.S. Geological Survey Field Activity 2014-011-FA, cruise MGL1407: U.S. Geological Survey data release. https://doi.org/10.5066/F7V69HHS

Austin Jr, J. A., Stoffa, P. L., Phillips, J. D., Oh, J., Sawyer, D. S., Purdy, G. M., . . . Makris, J. (1990). Crustal structure of the Southeast Georgia embayment-Carolina trough: Preliminary results of a composite seismic image of a continental suture (?) and a volcanic passive margin. *Geology, 18*(10), 1023-1027. http://10.0.4.106/0091-7613(1990)018%3C1023:CSOTSG%3E2.3.CO;2

Bankey, V., Cuevas, A., Daniels, D., Finn, C. A., Hernandez, I., Hill, P., ... Ravat, D. (2002). Digital data grids for the magnetic anomaly map of North America. *U.S. Geological Survey Open-File Report 02-414.*

Barrett, D. L., & Keen, C. E. (1976). Mesozoic magnetic lineations, the magnetic quiet zone, and sea floor spreading in the northwest Atlantic. *Journal of Geophysical Research, 81*(26), 4875–4884. https://doi.org/10.1029/JB081i026p04875

Barton, A., & White, R. (1997). Volcanism on the Rockall continental margin. *Journal of the Geological Society, 154*(3), 531-536. https://doi.org/10.1144/gsjgs.154.3.0531

Bastow, I. D., & Keir, D. (2011). The protracted development of the continent–ocean transition in Afar. *Nature Geoscience, 4*(4), 248-250. https://doi.org/10.1038/ngeo1095

Bauer, K., Neben, S., Schreckenberger, B., Emmermann, R., Hinz, K., Fechner, N., . . . Weber, K. (2000). Deep structure of the Namibia continental margin as derived from integrated geophysical studies. *Journal of Geophysical Research: Solid Earth, 105*(B11), 25829-25853. https://doi.org/10.1029/2000jb900227

Bazin, S., Harding, A., Kent, G., Orcutt, J., Tong, C., Pye, J., ... White, R. (2001). Three-dimensional shallow crustal emplacement at the 9°03°N over-lapping spreading center on the East Pacific Rise: Correlations between magnetization and tomographic images. *Journal of Geophysical Research, 106*(B8), 16,101–16,117. https://doi.org/10.1029/2001JB000371

Bécel, A. (2016). *Constraints on the Final Stages of Breakup and Early Spreading history of the Eastern North American Margin from New Multichannel Seismic Data of the Community Seismic Experiment*. Paper presented at the AGU Fall Meeting Abstracts. https://ui.adsabs.harvard.edu/abs/2016AGUFM.T51G2999B

Behl, R.J., & Smith, B.M. (1992). Silicification of deep-sea sediments and the oxygen isotope compositions of diagenetic siliceous rocks from the western Pacific Pigafetta and East Mariana Basins, Leg 129. In R.L. Larson, Y. Lancelot, et al. (Eds.), *Proceeding of the Ocean Drilling Program, Science Results, 129* (pp. 81-117). College Station, TX: Ocean Drilling Program.

Behn, M. D., & Lin, J. (2000). Segmentation in gravity and magnetic anomalies along the US East Coast passive margin: Implications for incipient structure of the oceanic lithosphere. *Journal of Geophysical Research: Solid Earth, 105*(B11), 25769-25790. https://doi.org/10.1029/2000JB900292

Bellahsen, N., Leroy, S., Autin, J., Razin, P., d'Acremont, E., Sloan, H., . . . Khanbari, K. (2013). Pre-existing oblique transfer zones and transfer/transform relationships in continental margins: new insights from the southeastern Gulf of Aden, Socotra Island, Yemen. *Tectonophysics, 607*, 32-50. https://doi.org/10.1016/j.tecto.2013.07.036

Benitez-Nelson, C.R., Buesseler, K.O., Karl, D.M., & Andrews, J. (2007). Mesoscale eddies drive increased silica export in the subtropical Pacific Ocean. *Science, 316*, 1017-1021. doi:10.1126/science.1136221

Benson, R. N. (2003). Age estimates of the seaward-dipping volcanic wedge, earliest oceanic crust, and earliest drift-stage sediments along the North American Atlantic continental margin. *Geophysical Monograph Series, 136*, 61–75. https://doi.org/10.1029/136GM04

Berndt, C., Planke, S., Alvestad, E., Tsikalas, F., & Rasmussen, T. (2001). Seismic volcanostratigraphy of the Norwegian Margin: constraints on tectonomagmatic break-up processes. *Journal of the Geological Society, 158*(3), 413-426.

Beutel, E., van Wijk, J., Ebinger, C., Keir, D., & Agostini, A. (2010). Formation and stability of magmatic segments in the Main Ethiopian and Afar rifts. *Earth and*

Planetary Science Letters, 293(3-4), 225-235. https://doi.org/10.1016/j.epsl.2010.02.006

Bialas, R. W., Buck, W. R., & Qin, R. (2010). How much magma is required to rift a continent? *Earth and Planetary Science Letters, 292*(1-2), 68-78. https://doi.org/10.1016/j.epsl.2010.01.021

Biari, Y., Klingelhoefer, F., Sahabi, M., Funck, T., Benabdellouahed, M., Schnabel, M., ... Austin, J. A. (2017). Opening of the central Atlantic Ocean: Implications for geometric rifting and asymmetric initial seafloor spreading after continental breakup. *Tectonics, 36*(6), 1129–1150. https://doi.org/10.1002/2017TC004596

Bird, D. E., Hall, S. A., Burke, K., Casey, J. F., & Sawyer, D. S. (2007). Early Central Atlantic Ocean seafloor spreading history. *Geosphere, 3*(5), 282–298. https://doi.org/10.1130/GES00047.1

Blackburn, T. J., Olsen, P. E., Bowring, S. A., McLean, N. M., Kent, D. V., Puffer, J., . . . Et-Touhami, M. (2013). Zircon U-Pb geochronology links the end-Triassic extinction with the Central Atlantic Magmatic Province. *Science, 340*(6135), 941-945. doi:10.1126/science.1234204

Blakely, R. J. (1996). *Potential theory in gravity and magnetic applications*. Cambridge, UK: Cambridge university press.

Boote, S. K., & Knapp, J. H. (2016). Offshore extent of Gondwanan Paleozoic strata in the southeastern United States: The Suwannee suture zone revisited. *Gondwana Research, 40*, 199-210. doi:10.1016/j.gr.2016.08.011

Bortolotti, V., & Principi, G. (2005). Tethyan ophiolites and Pangea break‐up. *Island Arc, 14*(4), 442-470.

Boschman, L. M., & van Hinsbergen, D. J. (2016). On the enigmatic birth of the Pacific Plate within the Panthalassa Ocean. *Science Advances, 2*(7), e1600022.

Boyden, J. A., Müller, R. D., Gurnis, M., Torsvik, T. H., Clark, J. A., Turner, M., ... Cannon, J. S. (2011). Next-generation plate-tectonic reconstructions using GPlates. In G. R. Keller & C. Baru (Eds.), *Geoinformatics: Cyberinfrastructure for the Solid Earth Sciences* (pp. 95–114). Cambridge, UK: Cambridge University Press. https://doi.org/10.1017/CBO9780511976308.008

Bradley, D. C. (2008). Passive margins through earth history. *Earth-Science Reviews, 91*(1-4), 1-26.

Bridges, D. L., Mickus, K., Gao, S. S., Abdelsalam, M. G., & Alemu, A. (2012). Magnetic stripes of a transitional continental rift in afar. *Geology, 40*(3), 203–206. https://doi.org/10.1130/G32697.1

Bronner, A., Sauter, D., Manatschal, G., Péron-Pinvidic, G., & Munschy, M. (2011). Magmatic breakup as an explanation for magmatic anomalies at magma-poor rifted margins. *Nature Geoscience, 4*(8), 549–553. https://doi.org/10.1038/NGEO1201

Brune, S., Williams, S. E., Butterworth, N. P., & Muller, R. D. (2016). Abrupt plate accelerations shape rifted continental margins. *Nature, 536*(7615), 201-204. doi:10.1038/nature18319

Buck, W. R. (2004). Consequences of asthenospheric variability on continental rifting. In G. D. Karner, Taylor, B., Driscoll, N.W., Kohlstedt, D.L. (Ed.), *Rheology and deformation of the lithosphere at continental margins* (pp. 1-31): Columbia University Press.

Buck, W. R. (2017). The role of magmatic loads and rift jumps in generating seaward dipping reflectors on volcanic rifted margins. *Earth and Planetary Science Letters, 466*, 62-69. https://doi.org/10.1016/j.epsl.2017.02.041

Buiter, S. J., & Torsvik, T. H. (2014). A review of Wilson Cycle plate margins: A role for mantle plumes in continental break-up along sutures? *Gondwana Research, 26*(2), 627-653.

Butman, B., Twichell, D. C., Rona, P. A., Tucholke, B. E., Middleton, T. J., & Robb, J. M. (2006). Seafloor topography and backscatter intensity of the Hudson Canyon Region Offshore of New York and New Jersey. *U.S. Geological Survey Open-File Report 2004–1411*.

Chapman, M. C., & Beale, J. N. (2010). On the geologic structure at the epicenter of the 1886 Charleston, South Carolina, earthquake. *Bulletin of the Seismological Society of America, 100*(3), 1010–1030. https://doi.org/10.1785/0120090231

Chaytor, J. D., Twichell, D. C., ten Brink, U. S., Buczkowski, B. J., & Andrews, B. D. (2007). Revisiting submarine mass movements along the U.S. Atlantic continental margin: Implications for tsunami hazards. In V. Lykousis, D. Sakellariou, & J. Locat (Eds.), *Submarine mass movements and their*

consequences (pp. 395–403). Switzerland: Springer. https://doi.org/10.1007/978-1-4020-6512-5_41

Chaytor, J. D., Uri, S., Solow, A. R., & Andrews, B. D. (2009). Size distribution of submarine landslides along the US Atlantic margin. *Marine Geology, 264*(1-2), 16-27.

Cheng, Y-H., Ho, C-R., Sheng, Q., & Kuo, N-J. (2014). Statistical characteristics of mesoscale eddies in the North Pacific derived from satellite altimetry. *Remote Sensing, 6,* 5164-5183. doi:10.3390/rs6065164

Collier, J. S., McDermott, C., Warner, G., Gyori, N., Schnabel, M., McDermott, K., & Horn, B. W. (2017). New constraints on the age and style of continental breakup in the South Atlantic from magnetic anomaly data. *Earth and Planetary Science Letters, 477,* 27-40. https://doi.org/10.1016/j.epsl.2017.08.007

Corner, B., Cartwright, J., & Swart, R. (2002). Volcanic passive margin of Namibia: A potential fields perspective. In M. A. Menzies, S. L. Klemperer, C. J. Ebinger, & J. Baker (Eds.), *Volcanic Rifted Margins* (pp. 203-220). Boulder, CO: Geological Society of America Special Paper 362.

Crisp, J. A. (1984). Rates of magma emplacement and volcanic output. *Journal of Volcanology and Geothermal Research, 20*(3-4), 177-211.

Daniels, K. A., Bastow, I., Keir, D., Sparks, R., & Menand, T. (2014). Thermal models of dyke intrusion during development of continent–ocean transition. *Earth and Planetary Science Letters, 385,* 145-153.

Davies, R.J., & Cartwright, J.A. (2007). Kilometer-scale chemical reaction boundary patterns and deformation in sedimentary rocks. *Earth and Planetary Science Letters, 262*(1), 125-137. https://doi.org/10.1016/j.epsl.2007.07.042

Davies, R.J., Goulty, N.R., & Meadows, D. (2008). Fluid flow due to the advance of basin-scale silica reaction zones. *GSA Bulletin, 120*(1/2), 195-206. doi:10.1130/B26099.1

Davis, J., Bécel, A., & Buck, W. (2018). Estimating emplacement rates for seaward-dipping reflectors associated with the US East Coast Magnetic Anomaly. *Geophysical Journal International, 215*(3), 1594-1603. https://doi.org/10.1093/gji/ggy360

de Boer, J. Z., McHone, G., Puffer, J. H., Ragland, P. C., & Whillington, D. (1988). Mesozoic and Cenozoic magmatism. In R. E. Sheridan & J. A. Grow (Eds.), *The Geology of North America, I-2, the Atlantic continental margin, U.S.* (pp. 217–241). Boulder, CO: Geological Society of America.

DeMaster, D.J. (1981). The supply and accumulation of silica in the marine environment. *Geochimica et Cosmochimica Acta, 45*, 1715-1732. https://doi.org/10.1016/0016-7037(81)90006-5

DeMaster, D.J. (2001). Marine Silica Cycle. In J.H. Steele, S.A. Thorpe & K.K. Turekian (Eds.), *Encyclopedia of ocean sciences* (pp. 678-685). San Diego, CA: Academic Press. doi:10.1006/rwos.2001.0278

Dillon, W. P., Manheim, F. T., Jansa, L. F., Pálmason, G., Tucholke, B. E., & Landrum, R. S. (1986). Resource potential of the western North Atlantic Basin. In P. R.

Vogt & B. E. Tucholke (Eds.), *The geology of North America, Vol. M, the Western North Atlantic Region,* (pp. 661–676). Boulder, CO: Geological Society of America.

Donnadieu, Y., Goddéris, Y., Pierrehumbert, R., Dromart, G., Fluteau, F., & Jacob, R. (2006). A GEOCLIM simulation of climatic and biogeochemical consequences of Pangea breakup. *Geochemistry, Geophysics, Geosystems, 7*(11), 1-21.

Duff, P. D., & Kellogg, J. N. (2017). Reinterpretation of adcoh and cocorp seismic reflection data with constraints from detailed forward modeling of potential field data—Implications for Laurentia-Peri-Gondwana suture. *Tectonophysics, 712*, 426-437. http://dx.doi.org/10.1016/j.tecto.2017.06.002

Dunbar, J. A., & Sawyer, D. S. (1989). How preexisting weaknesses control the style of continental breakup. *Journal of Geophysical Research, 94*(B6), 7278. https://doi.org/10.1029/JB094iB06p07278

Duncan, R. A. (1984). Age progressive volcanism in the New England seamounts and the opening of the central Atlantic Ocean. *Journal of Geophysical Research, 89*(B12), 9980–9990. https://doi.org/10.1029/JB089iB12p09980

Ebinger, C. (2005). Continental break-up: the East African perspective. *Astronomy & Geophysics, 46*(2), 2.16-12.21.

Ebinger, C. J., & Sleep, N. (1998). Cenozoic magmatism throughout east Africa resulting from impact of a single plume. *Nature, 395*(6704), 788-791.

Ebinger, C., & Casey, M. (2001). Continental breakup in magmatic provinces: An Ethiopian example. *Geology, 29*(6), 527-530.

Elderfield, H., Wheat, C., Mottl, M., Monnin, C., & Spiro, B. (1999). Fluid and geochemical transport through oceanic crust: a transect across the eastern flank of the Juan de Fuca Ridge. *Earth and Planetary Science Letters, 172*(1-2), 151-165.

Eldholm, O., & Grue, K. (1994). North Atlantic volcanic margins: dimensions and production rates. *Journal of Geophysical Research: Solid Earth, 99*(B2), 2955-2968. https://doi.org/10.1029/93jb02879

Eldholm, O., Gladczenko, T., Skogseid, J., & Planke, S. (2000). Atlantic volcanic margins: a comparative study. In A. Nøttvedt (Ed.), *Dynamics of the Norwegian Margin* (Vol. 167, pp. 411-428): Geological Society, London, Special Publications.

Eldholm, O., Skogseid, J., Planke, S., & Gladczenko, T. P. (1995). Volcanic margin concepts. In E. Banda, Torné, M, Talwani, M (Ed.), *Rifted ocean-continent boundaries* (pp. 1-16). Dordrecht, The Neatherlands: Springer.

Eldholm, O., Thiede, J., & Taylor, E. (1989). The Norwegian continental margin: tectonic, volcanic, and paleoenvironmental framework. In O. Eldholm, J. Thiede, & E. Taylor et al. (Eds.), *Proceedings of the Ocean Drilling Program: Scientific Results* (Vol. 104, pp. 5-25). College Station, TX: Ocean Drilling Program.

Embley, R. M., & Jacobi, R. (1986). Mass wasting in the western North Atlantic. In P. R. Vogt & B. E. Tucholke (Eds.), *The geology of North America, Vol. M, the Western North Atlantic Region* (pp. 479–490). Boulder, CO: Geological Society of America.

Ewing, J., Ewing, M., Aitken, T., & Ludwig, W. J. (1968). North Pacific sediment layers measured by seismic profiling. In L. Knopoff, C.L. Drake, & P.J. Hart (Eds.), *The crust and upper mantle of the Pacific Area* (pp. 147-173). Washington, D. C.: American Geophysical Union. doi:10.1029/GM012p0147

Feng, H., Lizarralde, D., Tominaga, M., Hart, L., Tivey, M., & Swift, S.A. (2015). *Extent and impact of Cretaceous magmatism on the formation and evolution of Jurassic oceanic crust in the western Pacific*. Paper presented at AGU Fall Meeting, San Francisco, CA., V21A-3016.

Finlay, C. C., Maus, S., Beggan, C. D., Bondar, T. N., Chambodut, A., Chernova, T. A., ... Zvereva, T. I. (2010). International geomagnetic reference field: The eleventh generation. *Geophysical Journal International, 183*(3), 1216–1230.

Flood, R.D., & Hollister, C.D. (1974). Current-controlled topography on the continental margin off the eastern United States. In C.A. Burk & C.L. Drake (Eds.), *The Geology of Continental Margins* (pp. 197-205). New York, NY: Springer-Verlag.

Flood, R.D., & Shor, A.N. (1998). Mud waves in the Argentine Basin and their relationship to regional bottom current circulation patters. *Deep-Sea Research, 35*(6), 943-971. https://doi.org/10.1016/0198-0149(88)90070-2

Folger, D. W. (1988). Geologic hazards of the Atlantic continental margin. In R. E. Sheridan & J. A. Grow (Eds.), *The geology of North America, Vol. I-2, the Atlantic Continental Margin: U.S.* (pp. 529–548). Boulder, CO: Geological Society of America.

Franke, D. (2013). Rifting, lithosphere breakup and volcanism: Comparison of magma-poor and volcanic rifted margins. *Marine and Petroleum Geology, 43*, 63-87.

Franke, D., Klitzke, P., Barckhausen, U., Berglar, K., Berndt, C., Damm, V., . . . Funck, T. (2019). Polyphase magmatism during the formation of the northern East Greenland continental margin. *Tectonics, 38*(8), 2961-2982. https://doi.org/10.1029/2019tc005552

Franke, D., Ladage, S., Schnabel, M., Schreckenberger, B., Reichert, C., Hinz, K., . . . Siciliano, M. (2010). Birth of a volcanic margin off Argentina, South Atlantic. *Geochemistry, Geophysics, Geosystems, 11*(2), 1-20.

Franke, D., Neben, S., Ladage, S., Schreckenberger, B., & Hinz, K. (2007). Margin segmentation and volcano-tectonic architecture along the volcanic margin off Argentina/Uruguay, South Atlantic. *Marine Geology, 244*(1-4), 46-67.

Funck, T., Jackson, H. R., & Shimeld, J. (2011). The crustal structure of the Alpha Ridge at the transition to the Canadian Polar Margin: Results from a seismic refraction experiment. *Journal of Geophysical Research: Solid Earth, 116*(B12). https://doi.org/10.1029/2011JB008411

Gallacher, R. J., Keir, D., Harmon, N., Stuart, G., Leroy, S., Hammond, J. O., . . . Ahmed, A. (2016). The initiation of segmented buoyancy-driven melting during continental breakup. *Nature Communications, 7*(1), 1-9. doi:10.1038/ncomms13110

Gardner, W. D. (1989). Baltimore canyon as a modern conduit of sediment to the deep sea. *Deep Sea Research Part A: Oceanographic Research Papers, 36*(3), 323–358. https://doi.org/10.1016/0198-0149(89)90041-1

Gardner, W.D., Tucholke, B.E., Richardson, M.J., & Biscaye, P.E. (2017). Benthic storms, nepheloid layers, and linkage with upper ocean dynamics in the Western North Atlantic. *Marine Geology, 385*, 304-327.

Gay, A., Mourgues, R., Berndt, C., Bureau, D., Planke, S., Laurent, D., Gautier, S., Lauer, L., & Loggia, D. (2012). Anatomy of a fluid pipe in the Norway Basin: Initiation, propagation and 3D shape. *Marine Geology, 332-334*, 75-88. doi:10.1016/j.margeo.2012.08.010

Geoffroy, L. (2001). The structure of volcanic margins: some problematics from the North-Atlantic/Labrador-Baffin system. *Marine and Petroleum Geology, 18*(4), 463-469.

Geoffroy, L., Burov, E., & Werner, P. (2015). Volcanic passive margins: another way to break up continents. *Scientific Reports, 5*(1), 1-12. https://doi.org/10.1038/srep14828

Grauch, V. J. S., Hudson, M. R., Minor, S. A., & Caine, J. S. (2006). Sources of along-strike variation in magnetic anomalies related to intrasedimentary faults: A case study from the Rio Grande Rift, USA. *Exploration Geophysics, 37*(4), 372–378. https://doi.org/10.1071/EG06372

Greene, J. A., Tominaga, M., Miller, N. C., Hutchinson, D. R., & Karl, M. R. (2017). Refining the formation and early evolution of the Eastern North American

Margin: New insights from multiscale magnetic anomaly analyses. *Journal of Geophysical Research: Solid Earth, 122*(11), 8724-8748. https://doi.org/10.1002/2017jb014308

Grow, J. A., Klitgord, K. D., & Schlee, J. S. (1988). Structure and evolution of Baltimore Canyon Trough. In R. E. Sheridan & J. A. Grow (Eds.), *The geology of North America, Vol. I-2, the Atlantic Continental Margin: U.S.* (pp. 269–290). Boulder, CO: Geological Society of America.

Gudmundsson, A. (1993). On the structure and formation of fracture-zones. *Terra Nova, 5*(3), 215–224. https://doi.org/10.1111/ j.1365-3121.1993.tb00252.x

Guerin, G., & Goldberg, D. (1996). Acoustic and elastic properties of calcareous sediments across a siliceous diagenetic front on the eastern U.S. continental slope. *Geophysical Research Letters, 23*(19), 2697-2700. https://doi.org/10.1029/96GL02188

Gunn, P. J. (1997). Regional magnetic and gravity responses of extensional sedimentary basins. *Journal of Australian Geology and Geophysics, 17*(2), 115–131.

Gupta, S., Kanna, N., & Akilan, A. (2017). Volcanic passive continental margin beneath Maitri station in central DML, East Antarctica: constraints from crustal shear velocity through receiver function modelling. *Polar Research, 36*(1), 1332947. 10.1080/17518369.2017.1332947

Hames, W. E., Renne, P. R., & Ruppel, C. (2000). New evidence for geologically instantaneous emplacement of earliest Jurassic Central Atlantic magmatic

province basalts on the North American margin. *Geology, 28*(9), 859-862. 10.1130/0091-7613(2000)28<859:Nefgie>2.0.Co;2

Hammond, J. O., Kendall, J.-M., Stuart, G., Ebinger, C., Bastow, I., Keir, D., . . . Ogubazghi, G. (2013). Mantle upwelling and initiation of rift segmentation beneath the Afar Depression. *Geology, 41*(6), 635-638.

Hatcher Jr., R. D. (2002). Alleghanian (Appalachian) orogeny, a product of zipper tectonics: Rotational transpressive continent-continent collision and closing of ancient oceans along irregular margins. In J. R. Martfnez Catalan, R. D. Hatcher Jr., R. Arenas, & E. Díaz Garda (Eds.), *Variscan-Appalachian dynamics: The building of the late Paleozoic basement* (pp. 199-208). Boulder, CO: Geological Society of America Special Paper 364.

Hatcher, R. D. (1989). Tectonic synthesis of the U.S. Appalachians. In R. D. Hatcher, W. A. Thomas, & G. W. Viele (Eds.), *The Geology of North America, Vol. F-2, the Appalachian-Ouachita Orogen in the United States* (pp. 511–535). Boulder, CO: Geological Society of America.

Hatcher, R. D. (2010). The Appalachian orogen: A brief summary. *Geological Society of America Memoirs, 206*(1), 1–19. https://doi.org/10.1130/ 2010.1206(01)

Hayward, N., & Ebinger, C. (1996). Variations in the along‐axis segmentation of the Afar Rift system. *Tectonics, 15*(2), 244-257. https://doi.org/10.1029/95tc02292

Heezen, B.C., MacGregor, I.D., Foreman, H.P., Forristal, G., Hekel, H., Hesse,R., Hoskin, R.H., Jones, E.J.W., Kaneps, A., Krasheninnikov, V.A., Okada, H., & Ruef, M.H. (1973). Diachronous deposits: A kinematic interpretation of the post

Jurassic sedimentary sequence of the Pacific Plate. *Nature, 241*, 25-32. https://doi.org/10.1038/241025a0

Hernández-Molina, F.J., Maldonado, A., & Stow, D.A.V. (2008). Abyssal plain contourites. In M. Rebesco, & A. Camerlenghi (Eds.), *Contourites, Developments in Sedimentology, 60* (pp. 347-378). Amsterdam, The Netherlands: Elsevier Science. doi:10.1016/S0070-4571(08)00218-5

Hesse, R., (1988), Diagenesis #13. Origin of chert: Diagenesis of biogenic siliceous sediments. *Geoscience Canada, 3*, 171-192.

Hey, R. N. (1977). A new class of "pseudofaults" and their bearing on plate tectonics: A propagating rift model. *Earth and Planetary Science Letters, 37*(2), 321–325. https://doi.org/10.1016/0012-821X(77)90177-7

Hey, R. N., & Wilson, D. S. (1982). Propagating rift explanation for the tectonic evolution of the northeast Pacific the pseudomovie. *Earth and Planetary Science Letters, 58*(2), 167–184. https://doi.org/10.1016/0012-821X(82)90192-3

Hey, R. N., Duennebier, F. K., & Morgan, W. J. (1980). Propagating rifts on mid-ocean ridges. *Journal of Geophysical Research, 85*(B7), 3647–3658. https://doi.org/10.1029/JB085iB07p03647

Hey, R. N., Kleinrock, M. C., Miller, S. P., Atwater, T. M., & Searle, R. C. (1986). Sea Beam/Deep-Tow Investigation of an Active Oceanic Propagating Rift System, Galapagos 95.5°W. *Journal of Geophysical Research, 91*(B3), 3369–3393.

Hey, R. N., Menard, H. W., Atwater, T. M., & Caress, D. W. (1988). Changes in direction of seafloor spreading revisited. *Journal of Geophysical Research, 93*(B4), 2803–2811. https://doi.org/10.1029/JB093iB04p02803

Higgins, M. W., & Zietz, I. (1983). Geological interpretation of geophysical maps of the pre-Cretaceous "basement" beneath the coastal plain of the southeastern United States. *Geological Society of America Memoirs, 158*, 125–130. https://doi.org/10.1130/MEM158-p125

Hinz, K. (1981). A hypothesis on terrestrial catastrophies Wedges of very thick oceanward dipping layers beneath passive continental margins. Their origin and paleoenvironmental significance. *Geologisches Jahrbuch. Reihe E, Geophysik* (22), 3-28.

Holbrook, W. S., Purdy, G., Collins, J., Sheridan, R., Musser, D., Glover III, L., . . . Smithson, S. (1992). Deep velocity structure of rifted continental crust, US Mid‐Atlantic Margin, from wide‐angle reflection/refraction data. *Geophysical Research Letters, 19*(16), 1699-1702. https://doi.org/10.1029/92gl01799

Holbrook, W. S., Reiter, E., Purdy, G., Sawyer, D., Stoffa, P., Austin Jr, J., . . . Makris, J. (1994). Deep structure of the US Atlantic continental margin, offshore South Carolina, from coincident ocean bottom and multichannel seismic data. *Journal of Geophysical Research: Solid Earth, 99*(B5), 9155-9178. https://doi.org/10.1029/93jb01821

Holbrook, W., & Kelemen, P. (1993). Large igneous province on the US Atlantic margin and implications for magmatism during continental breakup. *Nature, 364*(6436), 433-436.

Hollister, C. D., Ewing, J. I., Habib, D., Hathaway, J. C., Lancelot, Y., Luterbacher, H., ... Worstell, P. (1972). *Initial reports of the Deep Sea Drilling Project* (Vol. 11, pp. 313–349). Washington, DC: U.S. Government Printing Office.

Hollister, C.D., Flood, R.D., Johnson, D.A., Lonsdale, P., & Southard, J.B. (1974). Abyssal furrows and hyperbolic echo traces on the Bahama outer ridge, *Geology, 2(8)*, 395-400.

Hopper, J. R., Mutter, J. C., Larson, R. L., & Mutter, C. Z. (1992). Magmatism and rift margin evolution: Evidence from northwest Australia. *Geology*, *20*(9), 853-857. https://doi.org/10.1130/0091-7613(1992)020<0853:marmee>2.3.co;2

Horen, H., & Fleutelot, C. (1998). Highly magnetized and differentiated basalts at the 18–19° S propagating spreading center in the North Fiji Basin. *Marine Geophysical Researches, 20*(2), 129–137. https://doi.org/10.1023/A:1004457812905

Horton, J. W. Jr., Drake, A. A. Jr., & Rankin, D. R. (1989). Tectonostratigraphic terranes and their Paleozoic boundaries in the central and southern Appalachians. *Geological Society Special Papers, 230*, 213–246. https://doi.org/10.1130/SPE230-p213

Hovland, M., & Judd, A.G. (1988). *Seabed pockmarks and seepages: Impacts on geology, biology, and the marine environment*. London, UK: Graham & Trotman. doi:10.13140/RG.2.1.1414.1286

Hüneke, H., & Henrich, R. (2011). Pelagic Sedimentation in Modern and Ancient Oceans. In H. Hüneke, & T. Mulder (Eds.), *Deep-sea sediments, Developments in sedimentology, 63* (pp. 215-351). Amsterdam, The Netherlands: Elsevier Science. doi:10.1016/B978-0-444-53000-4.00004-4

Hutchinson, D. R., Grow, J. A., Klitgord, K. D., & Swift, B. A. (1982). Deep Structure and Evolution of the Carolina Trough. In J. S. Watkins & C. L. Drake (Eds.), *Studies in Continental Margin Geology* (Vol. 34, pp. 129-152). Tulsa, OK: American Association of Petroleum Geologists.

Hutchinson, D. R., Poag, C. W., & Popenoe, P. (1995). Geophysical database of the east coast of the United States; southern Atlantic margin, stratigraphy and velocity from multichannel seismic profiles. *U.S. Geological Survey Open-File Report 95-27*.

Isaacs, C.M. (1981). Porosity reduction during diagenesis of the Monterey Formation, Santa Barbara Coastal Area, California. In R.E. Garrison & R.G. Douglas (Eds.), *The Monterey Formation and related siliceous rocks of California* (pp. 257–271). Los Angeles, CA: Society of Economic Paleontologists and Mineralogists, Pacific Section.

Jamtveit, B., Svensen, H., Podladchikov, Y.Y., & Planke, S. (2004). Hydrothermal vent complexes associated with sill intrusions in sedimentary basins. *Geological*

Society London Special Publications, 234, 233-241. doi:10.1144/GSL.SP.2004.234.01.15

Johnson, P., & Pariso, J. E. (1993). Do layer 3 rocks make a significant contribution to marine magnetic anomalies? In situ magnetization of gabbros at Ocean Drilling Program hole 735B. *Journal of Geophysical Research, 98*(B1), 435–445. https://doi.org/10.1029/93JB01097

Jones, B., & Renaut, R.W. (2004). Water content of opal-A: implications for the origin of laminae in geyserite and sinter. *Journal of Sedimentary Research, 74*(1), 117-128. https://doi.org/10.1306/052403740117

Karl, D.M. (1999). A sea of change: Biogeochemical variability in the North Pacific Subtropical Gyre. *Ecosystems, 2*, 181-214. https://doi.org/10.1007/s100219900068

Karl. S.M., Wandless, G.A., & Karpoff, A.M. (1992). Sedimentological and geochemical characteristics of Leg 129 siliceous deposits. In R.L. Larson, Y. Lancelot, et al. (Eds.), *Proceeding of the Ocean Drilling Program, Science Results, 129* (pp. 31-79). College Station, TX: Ocean Drilling Program.

Kastner, M., Keene, J.B., & Gieske, J.M. (1977). Diagenesis of siliceous oozes-Chemical controls on the rate of opal-A to opal-CT transformation- an experimental study. *Geochimica et Cosmochimica Acta*, *41*(8), 1041-1059. https://doi.org/10.1016/0016-7037(77)90099-0

Keen, C. E., & Potter, D. P. (1995a). The transition from a volcanic to a nonvolcanic rifted margin off eastern Canada. *Tectonics, 14*(2), 359–371. https://doi.org/10.1029/94TC03090

Keen, C. E., & Potter, D. P. (1995b). Formation and evolution of the Nova Scotian rifted margin: Evidence from deep seismic reflection data. *Tectonics, 14*(4), 918–932. https://doi.org/10.1029/95TC00838

Keir, D., Bastow, I. D., Corti, G., Mazzarini, F., & Rooney, T. O. (2015). The origin of along‐rift variations in faulting and magmatism in the Ethiopian Rift. *Tectonics, 34*(3), 464-477. https://doi.org/10.1002/2014tc003698

Keir, D., Bastow, I. D., Pagli, C., & Chambers, E. L. (2013). The development of extension and magmatism in the Red Sea rift of Afar. *Tectonophysics, 607*, 98-114. https://doi.org/10.1016/j.tecto.2012.10.015

Kelemen, P. B., & Holbrook, W. S. (1995). Origin of thick, high‐velocity igneous crust along the US East Coast Margin. *Journal of Geophysical Research: Solid Earth, 100*(B6), 10077-10094. https://doi.org/10.1029/95jb00924

Keller, F. Jr., Meuschke, J. L., & Alldredge, L. R. (1954). Aeromagnetic surveys in the Aleutian, Marshall, and Bermuda Islands. *Eos, Transactions American Geophysical Union, 35*(4), 558–572. https://doi.org/10.1029/TR035i004p00558

Kendall, J. M., Stuart, G. W., Ebinger, C. J., Bastow, I. D., & Keir, D. (2005). Magma-assisted rifting in Ethiopia. *Nature, 433*(7022), 146-148. doi:10.1038/nature03161

Kendall, J.-M., & Lithgow-Bertelloni, C. (2016). Why is Africa rifting? In T. J. Wright, A. Ayele, D. J. Ferguson, T. Kidane, & C. Vye-Brown (Eds.), *Magmatic Rifting and Active Volcanism* (Vol. 420, pp. 11-30): Geological Society, London, Special Publications.

Keranen, K., Klemperer, S., Gloaguen, R., & Group, E. W. (2004). Three-dimensional seismic imaging of a protoridge axis in the Main Ethiopian rift. *Geology, 32*(11), 949-952.

Klitgord, K. D., & Behrendt, J. C. (1977). Aeromagnetic map of the United States Atlantic continental margin: U.S. Geological Survey Miscellaneous Field Studies Map MF-913, 2 sheets, scale 1:1,000,000.

Klitgord, K. D., & Grow, J. A. (1980). Jurassic seismic stratigraphy and basement structure of western Atlantic magnetic quiet zone. *AAPG Bulletin, 64*(10), 1658–1680.

Klitgord, K. D., & Schouten, H. (1986). Plate kinematics of the central Atlantic. In P. R. Vogt & B. E. Tucholke (Eds.), *The Geology of North America, Vol. M, the Western North Atlantic Region* (pp. 351–378). Boulder, CO: Geological Society of America.

Klitgord, K. D., Hutchinson, D. R., & Schouten, H. (1988). U.S. Atlantic continental margin; structural and tectonic framework. In R. E. Sheridan & J. A. Grow (Eds.), *The Geology of North America, I-2, the Atlantic Continental Margin, U.S.* (pp. 19–56). Boulder, CO: Geological Society of America.

Klitgord, K. D., Poag, C., Schneider, C., & North, L. (1994). Geophysical database of the East Coast of the United States northern Atlantic margin--cross sections and gridded database (Georges Bank Basin, Long Island Platform, and Baltimore Canyon Trough). *U.S. Geological Survey Open-File Report 94-637*.

Kneller, E. A., Johnson, C. A., Karner, G. D., Einhorn, J., & Queffelec, T. A. (2012). Inverse methods for modeling non-rigid plate kinematics: Application to mesozoic plate reconstructions of the Central Atlantic. *Computers & Geosciences, 49*, 217–230. https://doi.org/10.1016/ j.cageo.2012.06.019

Koopmann, H., Franke, D., Schreckenberger, B., Schulz, H., Hartwig, A., Stollhofen, H., & di Primio, R. (2014). Segmentation and volcano-tectonic characteristics along the SW African continental margin, South Atlantic, as derived from multichannel seismic and potential field data. *Marine and Petroleum Geology, 50*, 22-39.

Kusky, T., Windley, B., Safonova, I., Wakita, K., Wakabayashi, J., Polat, A., & Santosh, M. (2013). Recognition of ocean plate stratigraphy in accretionary orogens through Earth history: A record of 3.8 billion years of sea floor spreading, subduction, and accretion. *Gondwana Research, 24*(2), 501-547.

Labails, C., Olivet, J. L., Aslanian, D., & Roest, W. R. (2010). An alternative early opening scenario for the Central Atlantic Ocean. *Earth and Planetary Science Letters*, 297(3-4), 355–368. https://doi.org/10.1016/j.epsl.2010.06.024

Lancelot, Y., & Larson, R.L. (1975). Sedimentary and tectonic evolution of the northwestern Pacific. In R.L. Larson, R. Moberly, et al. (Eds.), *Initial Reports of*

the Deep Sea Drilling Program, 32 (pp. 925-939). Washington D.C.: U.S. Government Printing Office.

Larson, R. L., & Chase, C. G. (1972). Late Mesozoic evolution of the western Pacific Ocean. *Geological Society of America Bulletin, 83*(12), 3627-3644.

Larson, R. L., & Pitman, W. C. (1972). World-wide correlation of Mesozoic magnetic anomalies and its implications. *Geological Society of America Bulletin, 83*(12), 3645–3662. https://doi.org/10.0.4.106/0016-7606(1972)83[3645:WCOMMA]2.0.CO;2

Larson, R., Steiner, M., Erba, E., & Lancelot, Y. (1992). Paleolatitudes and tectonic reconstructions of the oldest portion of the Pacific plate: A comparative study. In R.L. Larson, Y. Lancelot, et al. (Eds.), *Proceeding of the Ocean Drilling Program, Science Results, 129* (pp. 615-631). College Station, TX: Ocean Drilling Program.

Lase Study Group (1986). Deep structure of the US East Coast passive margin from large aperture seismic experiments (LASE). *Marine and Petroleum Geology, 3*(3), 234-242. https://doi.org/10.1016/0264-8172(86)90047-4

Lefort, J., & Max, M. (1991). is there an Archean Crust beneath Chesapeake Bay? *Tectonics, 10*(1), 213-226. https://doi.org/10.1029/90TC00911

Li, C. F., Lu, Y., & Wang, J. (2017). A global reference model of Curie-point depths based on EMAG2. *Scientific Reports, 7*, 1-9. doi:10.1038/srep45129

Lin, J., Purdy, G., Schouten, H., Sempere, J.-C., & Zervas, C. (1990). Evidence from gravity data for focused magmatic accretion along the Mid-Atlantic Ridge. *Nature, 344*(6267), 627-632. https://doi.org/10.1038/344627a0

Lizarralde, D., & Holbrook, W. S. (1997). US mid−Atlantic margin structure and early thermal evolution. *Journal of Geophysical Research: Solid Earth, 102*(B10), 22855-22875. https://doi.org/10.1029/96jb03805

Lizarralde, D., Holbrook, W. S., & Oh, J. (1994). Crustal structure across the Brunswick magnetic anomaly, offshore Georgia, from coincident ocean bottom and multi-channel seismic data. *Journal of Geophysical Research: Solid Earth, 99*(B11), 21741-21757. https://doi.org/10.1029/94JB01550

Lizarralde, D., Axen, G. J., Brown, H. E., Fletcher, J. M., Gonzalez-Fernandez, A., Harding, A. J., . . . Umhoefer, P. J. (2007). Variation in styles of rifting in the Gulf of California. *Nature, 448*(7152), 466-469. doi:10.1038/nature06035

Lowrie, A. Jr., & Heezen, B. C. (1967). Knoll and sediment drift near Hudson Canyon. *Science, 157,* 1152–1153.

Lowrie, W. (2007). *Fundamentals of Geophysics*. New York, USA: Cambridge University Press.

Lynner, C., JA Van Avendonk, H., Bécel, A., Christeson, G. L., Dugan, B., Gaherty, J. B., . . . Long, M. D. (2020). The Eastern North American Margin Community Seismic Experiment: An Amphibious Active‐and Passive‐Source Dataset. *Seismological Research Letters, 91*(1), 533-540. https://doi.org/10.1785/0220190142

Magde, L. S., & Sparks, D. W. (1997). Three‐dimensional mantle upwelling, melt generation, and melt migration beneath segment slow spreading ridges. *Journal of Geophysical Research: Solid Earth, 102*(B9), 20571-20583. https://doi.org/10.1029/97jb01278

Makris, J., & Ginzburg, A. (1987). The Afar Depression: transition between continental rifting and sea-floor spreading. *Tectonophysics, 141*(1-3), 199-214.

Mann, P., Gahagan, L., & Gordon, M. B. (2003). Tectonic setting of the world's giant oil and gas fields. In M.T. Halbouty (Ed.), *Giant oil and gas fields of the decade 1990–1999* (Vol. 34, pp. 15-105). Tulsa, OK: American Association of Petroleum Geologists.

Manspeizer, W. (1988). Triassic-Jurassic rifting and the opening of the Atlantic: An overview. In W. Manspeizer (Ed.), *Triassic-Jurassic Rifting* (pp. 41–79). Amsterdam: Elsevier.

Manspeizer, W., & Cousminer, H. L. (1988). Late Triassic-Early Jurassic synrift basins of the US Atlantic margin. In R. E. Sheridan & J. A. Grow (Eds.), *The Geology of North America, I-2, the Atlantic Continental Margin, U.S* (pp. 197-216). Boulder, CO: Geological Society of America.

Marzen, R. E., Shillington, D. J., Lizarralde, D., & Harder, S. H. (2019). Constraints on Appalachian Orogenesis and Continental Rifting in the Southeastern United States From Wide‐Angle Seismic Data. *Journal of Geophysical Research: Solid Earth, 124*(7), 6625-6652. https://doi.org/10.1029/2019jb017611

Marzoli, A., Callegaro, S., Dal Corso, J., Davies, J. H., Chiaradia, M., Youbi, N., . . . Jourdan, F. (2018). The Central Atlantic magmatic province (CAMP): a review. In L. Tanner (Ed.), *The Late Triassic World* (pp. 91-125). Basel, Switzerland: Springer.

Marzoli, A., Renne, P. R., Piccirillo, E. M. E. M., Ernesto, M., Bellieni, G., & De Min, A. (1999). Extensive 200-million-year-old continental flood basalts of the Central Atlantic Magmatic Province. *Science, 284*(5414), 616–618. https://doi.org/10.1126/science.284.5414.616

Mattick, R. E., & Libby-French, J. (1986). Petroleum geology of the United States Atlantic continental margin. In P. R. Vogt & B. E. Tucholke (Eds.), *The geology of North America, Vol. M, the Western North Atlantic Region* (pp. 445–462). Boulder, CO: Geological Society of America.

McBride, J. H., & Nelson, K. D. (1988). Integration of COCORP-deep reflection and magnetic anomaly analysis in the southeastern United States: Implications for origin of the Brunswick and East Coast magnetic anomalies. *Geological Society of America Bulletin, 100*(3), 436–445. https://doi.org/10.0.4.106/0016-7606(1988)100%3C0436:IOCDRA%3E2.3.CO;2

Mchone, J. G. (2000). Non-plume magmatism and rifting during the opening of the central Atlantic Ocean. *Tectonophysics, 316*(3-4), 287–296. https://doi.org/10.1016/S0040-1951(99)00260-7

Meadows, D., & Davies, R.J. (2009). Predicting porosity reduction due to silica diagenesis using seismic reflection data. *Marine and Petroleum Geology, 26*, 1543-1553. doi:10.1016/j.marpetgeo.2008.09.006

Menard, H. W., & Atwater, T. (1968). Changes in direction of sea floor spreading. *Nature, 219*(5153), 463–467. https://doi.org/10.1038/ 219463a0

Menzies, M. A., Klemperer, S. L., Ebinger, C. J., & Baker, J. (2002). Characteristics of volcanic rifted margins. In M. A. Menzies, S. L. Klemperer, C. J. Ebinger, & J. Baker (Eds.), *Volcanic Rifted Margins* (pp. 1-14). Boulder, CO: Geological Society of America Special Paper 362.

Meyer, B., Saltus, R., & Chulliat, A. (2016). EMAG2: Earth magnetic anomaly grid (2-arc-minute resolution) version 3. National Centers for Environmental Information, NOAA. Model. https://doi.org/10.7289/V5H70CVX

Miller, S. P., & Hey, R. N. (1986). Three-dimensional magnetic modeling of a propagating rift, Galapagos 95°30°W. *Journal of Geophysical Research, 91*(B3), 3395–3406. https://doi.org/10.1029/JB091iB03p03395

Mjelde, R., Kvarven, T., Faleide, J. I., & Thybo, H. (2016). Lower crustal high-velocity bodies along North Atlantic passive margins, and their link to Caledonian suture zone eclogites and Early Cenozoic magmatism. *Tectonophysics, 670*, 16-29. https://doi.org/10.1016/j.tecto.2015.11.021

Monteleone, V., Minshull, T. A., & Marin‐Moreno, H. (2019). Spatial and temporal evolution of rifting and continental breakup in the Eastern Black Sea Basin

revealed by long‐offset seismic reflection data. *Tectonics, 38*(8), 2646-2667. https://doi.org/10.1029/2019tc005523

Moore, T.C. (2008). Chert in the Pacific: Biogenic silica and hydrothermal circulation. *Palaeogeography Palaeoclimatology Palaeoecology, 261*(1-2), 87-99. https://doi.org/10.1016/j.palaeo.2008.01.009

Morgan, R., & Watts, A. (2018). Seismic and gravity constraints on flexural models for the origin of seaward dipping reflectors. *Geophysical Journal International, 214*(3), 2073-2083. https://doi.org/10.1093/gji/ggy243

Müller, R. D., & Roest, W. R. (1992). Fracture zones in the North Atlantic from combined Geosat and Seasat data. *Journal of Geophysical Research, 97*(B3), 3337–3350. https://doi.org/10.1029/91JB02605

Müller, R. D., Roest, W. R., Royer, J. Y., & Sclater, J. G. (1997). Digital isochrons of the world's ocean floor. *Journal of Geophysical Research, 102*(B2), 3211–3214. https://doi.org/10.1029/96JB01781

Müller, R. D., Sdrolias, M., Gaina, C., & Roest, W. R. (2008). Age, spreading rates, and spreading asymmetry of the world's ocean crust. *Geochemisty, Geophysics, Geosystems, 9*(4), 1–19. https://doi.org/10.1029/2007GC001743

Müller, R.D., Seton, M., Zahirovic, S., Williams, S.E., Matthews, K.J., Wright, N.M., … Cannon, J. (2016). Ocean basin evolution and global-scale plate reorganization events since Pangea breakup. *Annual Review of Earth and Planetary Sciences, 44*, 107-138. https://doi.org/10.1146/annurev-earth-060115-012211

Mutter, J. C. (1985). Seaward dipping reflectors and the continent-ocean boundary at passive continental margins. *Tectonophysics, 114*(1-4), 117-131.

Mutter, J. C., Talwani, M., & Stoffa, P. L. (1982). Origin of seaward-dipping reflectors in oceanic crust off the Norwegian margin by "subaerial sea-floor spreading". *Geology, 10*(7), 353-357. https://doi.org/10.1130/0091-7613(1982)10<353:oosrio>2.0.co;2

Nelson, D. M., Tréguer, P., Brzezinski, M. A., Leynaert, A., & Quéguiner, B. (1995). Production and dissolution of biogenic silica in the ocean: revised global estimates, comparison with regional data and relationship to biogenic sedimentation. *Global Biogeochemical Cycles, 9*(3), 359-372.

Nelson, R., Patton, T., & Morley, C. (1992). Rift-segment interaction and its relation to hydrocarbon exploration in continental rift systems (1). *AAPG Bulletin, 76*(8), 1153-1169.

Nomade, S., Knight, K. B., Beutel, E., Renne, P. R., Verati, C., & Féraud, G. (2007). Chronology of the Central Atlantic Magmatic Province: Implications for the Central Atlantic rifting processes and the Triassic – Jurassic biotic crisis. *Palaeogeography Palaeoclimatology Palaeoecology, 244*(1-4), 326–344. https://doi.org/10.1016/j.palaeo.2006.06.034

Ogg, J. G. (2012). Geomagnetic polarity time scale. In F. M. Gradstein et al. (Eds.), *The geologic time scale* (pp. 85–113). Amsterdam: Elsevier. https://doi.org/10.1016/B978-0-444-59425-9.00005-6

Oh, J., Austin, J. A., Phillips, J. D., Coffin, M. F., & Stoffa, P. L. (1995). Seaward-dipping reflectors offshore the southeastern United States: Seismic evidence for extensive volcanism accompanying sequential formation of the Carolina Trough and Blake Plateau Basin. *Geology, 23*(1), 9–12. https://doi.org/10.0.4.106/0091-7613(1995)023%3C0009:SDROTS%3E2.3.CO;2

Olsen, P. E., Kent, D. V., Et-Touhami, M., & Puffer, J. H. (2003). Cyclo-, magneto-, and bio-stratigraphy constraints on the duration of the CAMP event and its relationship to the Triassic-Jurassic boundary. In *The Central Atlantic Magmatic Province: Insights from Fragments of Pangea, Geophysical Monograph Series* (Vol. 136, pp. 7–32). https://doi.org/10.1029/136GM02

Orwig, T.L. (1981). Channeled turbidites in the eastern Central Pacific Basin, *Marine Geology, 39,* 33-57. https://doi.org/10.1016/0025-3227(81)90027-X

Oufi, O., & Cannat, M. (2002). Magnetic properties of variably serpentinized abyssal peridotites. *Journal of Geophysical Research, 107*(B5), 2095. https://doi.org/10.1029/2001JB000549

Pariso, J. E., & Johnson, H. P. (1991). Alteration processes at deep sea drilling project/ocean drilling program hole 504B at the Costa Rica rift: Implications for magnetization of oceanic crust. *Journal of Geophysical Research: Solid Earth, 96*(B7), 11703-11722. https://doi.org/10.1029/91jb00872

Parker, R. L. (1973). The rapid calculation of potential anomalies. *Geophysical Journal International, 31*(4), 447–455. https://doi.org/10.1111/ j.1365-246X.1973.tb06513.x

Parker, R., & Huestis, S. (1974). The inversion of magnetic anomalies in the presence of topography. *Journal of Geophysical Research, 79*(11), 1587-1593. https://doi.org/10.1029/jb079i011p01587

Parker Jr, E. (2014). Crustal magnetism, tectonic inheritance, and continental rifting in the southeastern United States. *GSA Today, 24*(4), 4-9.

Peace, A. L., Phethean, J., Franke, D., Foulger, G., Schiffer, C., Welford, J., . . . Doré, A. (2019). A review of Pangaea dispersal and Large Igneous Provinces–In search of a causative mechanism. *Earth-Science Reviews,* 102902. https://doi.org/10.1016/j.earscirev.2019.102902

Pilcher, R., & Argent, J. (2007). Mega-pockmarks and linear pockmark trains on the West African continental margin. *Marine Geology, 244*, 15-32. doi:10.1016/j.margeo.2007.05.002

Pilkey, O. H., & Cleary, W. J. (1986). Turbidite sedimentation in the northwestern Atlantic Ocean basin. In P. R. Vogt & B. E. Tucholke (Eds.), *The Geology of North America, Vol. M, the Western North Atlantic Region* (pp. 437–450). Boulder, CO: Geological Society of America.

Pimm, A.C., Garrison, R.E., & Boyce, R.E. (1971). Sedimentology synthesis: Lithology, chemistry and physical properties of sediments in the northwestern Pacific Ocean, In A.G. Fischer, et al. (Eds.), *Initial Reports of the Deep Sea Drilling Program, 6* (pp. 1131-1252). Washington, D.C.: U.S. Government Printing Office. doi:10.2973/dsdp.proc.6.138.1971

Poag, C. W., & Sevon, W. D. (1989). A record of Appalachian denundation in postrift Mesozoic and Cenozoic sedimentary deposits of the U.S. Middle Atlantic Continental Margin. *Geomorphology*, *2*(1-3), 119–157. https://doi.org/10.1016/0169-555X(89)90009-3

Poag, C. W., & Ward, L. W. (1993). Allostratigraphy of the U.S. middle Atlantic continental margin- characteristics, distribution, and depositional history of principle unconformity-bounded upper Cretaceous and Cenozoic sedimentary units, Geological Survey professional paper 1542, U.S. Geological Survey, Washington D.C.

Pollack, H. N., Hurter, S. J., & Johnson, J. R. (1993). Heat flow from the Earth's interior: analysis of the global data set. *Reviews of Geophysics, 31*(3), 267-280.

QGIS Development Team (2015). QGIS geographic information system, Open Source Geospatial Foundation Project.

Ragueneau, O, Tréguer, P., Leynaert, A., Anderson, R.F., Brzezinski, M.A., DeMaster, D.J., … Quéquiner, B. (2000). A review of the Si cycle in the modern ocean: recent progress and missing gaps in the application of biogenic opal as a paleoproductivity proxy. *Global and Planetary Change*, *26*, 317-365. https://doi.org/10.1016/S0921-8181(00)00052-7

Rajaram, M. (2007). Depth To Curie Temperature. In D. Gubbins & E. Herrero-Bervera (Eds.), *Encyclopedia of Geomagnetism and Paleomagnetism*. Dordrecht, The Neatherlands: Springer.

Ramberg, I. B., Gray, D. F., & Raynolds, R. G. H. (1977). Tectonic evolution of the FAMOUS area of the Mid-Atlantic Ridge, lat 35°50° to 37°20°N. *Geological Society of America Bulletin, 88*(5), 609–620. https://doi.org/10.0.4.106/0016-7606(1977)88%3C609:TEOTFA%3E2.0.CO;2

Rankin, D. W. (1994). Continental margin of the eastern United States: Past and present. In R. C. Speed (Ed.), *Phanerozoic evolution of North America continent–ocean transitions* (pp. 129-218). Boulder, CO: Geological Society of America.

Renaudie, J. (2016). Quantifying the Cenozoic marine diatom deposition history: links to the C and Si cycles. *Biogeosciences, 13*(21), 6003-6014. 10.5194/bg-13-6003-2016

Richards, M. A., Duncan, R. A., & Courtillot, V. E. (1989). Flood basalts and hot-spot tracks: plume heads and tails. *Science, 246*(4926), 103-107. doi:10.1126/science.246.4926.103

Riech, V. (1981). Siliceous sediments from the Nauru Basin: Diagenetic alteration of biogenic opal and authigenesis of silica and silicates. In R.L. Larson, S.O. Schlanger, et al. (Eds.), *Initial Reports of the Deep Sea Drilling Program, 61* (pp. 523-531). Washington, D.C.: U.S. Government Printing Office, doi:10.2973/dsdp.proc.61.109.1981

Riggs, S. R., & Manheim, F. T. (1988). Mineral resources of the U.S. Atlantic margin. In R. E. Sheridan & J. A. Grow (Eds.), *The geology of North America, I-2, the Atlantic Continental Margin, U.S*. (pp. 501–520). Boulder, CO: Geological Society of America.

Robertson, E. C. (1988). Thermal properties of rocks. *U.S. Geological Survey Open-File Report 88-441*.

Roeser, H. A., Steiner, C., Schreckenberger, B., & Block, M. (2002). Structural development of the Jurassic Magnetic Quiet Zone off Morocco and identification of Middle Jurassic magnetic lineations. *Journal of Geophysical Research, 107*(B10), 2207. https://doi.org/10.1029/2000JB000094

Roest, W. R., Danobeitia, J. J., Verhoef, J., & Collette, B. J. (1992). Magnetic-anomalies in the canary basin and the Mesozoic evolution of the central North-Atlantic. *Marine Geophysical Researches, 14*(1), 1–24. https://doi.org/10.1007/Bf01674063

Rona, P. A., & Gray, D. F. (1980). Structural behavior of fracture zones symmetric and asymmetric about a spreading axis: Mid-Atlantic Ridge (latitude 23°N to 27°N). *Geological Society of America Bulletin, 91*(8), 485–494. https://doi.org/10.0.4.106/0016-7606(1980)91%3C485:SBOFZS%3E2.0.CO;2

Rona, P. A., Brakl, J., & Heirtzler, J. R. (1970). Magnetic anomalies in the northeast Atlantic between the canary and Cape Verde Islands. *Journal of Geophysical Research, 75*(35), 7412–7420. https://doi.org/10.1029/JB075i035p07412

Russell, S. M., & Whitmarsh, R. B. (2003). Magmatism at the west Iberia non-volcanic rifted continental margin: Evidence from analyses of magnetic anomalies. *Geophysical Journal International, 154*(3), 706–730. https://doi.org/10.1046/j.1365-246X.2003.01999.x

Sager, W. W. (2005). What built Shatsky Rise, a mantle plume or ridge tectonics? In G. R. Foulger, J. H. Natland, D. C. Presnall, & D. L. Anderson (Eds.), *Plates, plumes, and paradigms* (Vol. 388, pp. 721-733). Boulder, CO: Geological Society of America Special Paper 388.

Sahabi, M., Aslanian, D., & Olivet, J. L. (2004). A new starting point for the central Atlantic. *Comptes Rendus Geoscience*, *336*(12), 1041–1052. https://doi.org/10.1016/j.crte.2004.03.017

Sandwell, D. T., Müller, R. D., Smith, W. H. F., Garcia, E., & Francis, R. (2014). New global marine gravity model from CryoSat-2 and Jason-1 reveals buried tectonic structure. *Science, 346*(6205), 65–67. https://doi.org/10.1016/j.crte.2004.03.017

Sawyer, D. S. (1985). Total tectonic subsidence: A parameter for distinguishing crust type at the U.S. Atlantic Continental Margin. *Journal of Geophysical Research, 90*(B9), 7751–7769. https://doi.org/10.1029/JB090iB09p07751

Schettino, A. (2014). Quantitative plate tectonics. New York, NY: Springer.

Schettino, A., & Scotese, C. R. (2005). Apparent polar wander paths for the major continents (200 Ma to the present day): A paleomagnetic reference frame for global plate tectonic reconstructions. *Geophysical Journal International, 163*(2), 727–759. https://doi.org/10.1111/j.1365-246X.2005.02638.x

Schettino, A., & Turco, E. (2009). Breakup of Pangaea and plate kinematics of the central Atlantic and Atlas regions. *Geophysical Journal International, 178*(2), 1078-1097. https://doi.org/10.1111/j.1365-246X.2009.04186.x

Schlische, R. W. (1993). Anatomy and evolution of the Triassic‐Jurassic continental rift system, eastern North America. *Tectonics, 12*(4), 1026-1042. https://doi.org/10.1029/93tc01062

Schlische, R. W., Withjack, M. O., & Olsen, P. E. (2003). Relative timing of CAMP, rifting, continental breakup, and basin inversion: Tectonic significance. In W. E. Hames, J. G. Mchone, P. Renne, & C. Ruppel (Eds.), *The Central Atlantic Magmatic Province: Insights from Fragments of Pangea, Geophysical Monograph Series* (Vol. 136, pp. 33-59). Washington, DC: American Geophysical Union.

Schouten, H., & Klitgord, K. D. (1977). Map showing Mesozoic magnetic anomalies: Western North Atlantic, U. S. Geol. Surv. Misc. Field Stud. Map, MF-195.

Schouten, H., & White, R. S. (1980). Zero-offset fracture zones. *Geology, 8*, 175–179.

Schouten, H., Klitgord, K. D., & Whitehead, J. A. (1985). Segmentation of mid-ocean ridges. *Nature, 317*(6034), 225-229. https://doi.org/10.1038/317225a0

Sempéré, J.-C., Lin, J., Brown, H. S., Schouten, H., & Purdy, G. (1993). Segmentation and morphotectonic variations along a slow-spreading center: The Mid-Atlantic Ridge (24 00′ N‐30 40′ N). *Marine Geophysical Researches, 15*(3), 153-200.

Shao, L., Li, X., Geng, J., Pang, X., Lei, Y., Qiao, P., Wang, L., & Wang, H. (2007). Deep water bottom current deposition in the Northern South China Sea. *Science in China Series D, 50*, 1060-1066. doi:10.1007/s11430-007-0015-y

Sheridan, R. E. (1987). The passive margin of the U.S.A. *Episodes, 10*(4), 254–258.

Sheridan, R. E. (1989). The Atlantic passive margin. In A. W. Bally & A. R. Palmer (Eds.), *The geology of North America: An overview, U.S.* (pp. 81–96). Boulder, CO: Geological Society of America. https://doi.org/10.1130/DNAG-GNA-A.81

Sheridan, R. E., Musser, D. L., Glover III, L., Talwani, M., Ewing, J. I., Holbrook, W. S., . . . Smithson, S. (1993). Deep seismic reflection data of EDGE US mid-Atlantic continental-margin experiment: Implications for Appalachian sutures and Mesozoic rifting and magmatic underplating. *Geology, 21*(6), 563-567. doi:10.1130/0091-7613(1993)021<0563:DSRDOE>2.3.CO;2

Shillington, D. J., Holbrook, W. S., Van Avendonk, H. J., Tucholke, B. E., Hopper, J. R., Louden, K. E., . . . Nunes, G. T. (2006). Evidence for asymmetric nonvolcanic rifting and slow incipient oceanic accretion from seismic reflection data on the Newfoundland margin. *Journal of Geophysical Research: Solid Earth, 111*(B9). https://doi.org/10.1029/2005jb003981

Shillington, D. J., Scott, C. L., Minshull, T. A., Edwards, R. A., Brown, P. J., & White, N. (2009). Abrupt transition from magma-starved to magma-rich rifting in the eastern Black Sea. *Geology, 37*(1), 7-10. https://doi.org/10.1130/g25302a.1

Shuck, B. D., Van Avendonk, H. J., & Bécel, A. (2019). The role of mantle melts in the transition from rifting to seafloor spreading offshore eastern North America. *Earth and Planetary Science Letters, 525*, 115756. https://doi.org/10.1016/j.epsl.2019.115756

Simms, M. J., & Ruffell, A. H. (1989). Synchroneity of climatic change and extinctions in the Late Triassic. *Geology, 17*(3), 265-268.

Sinton, J. M., Wilson, D. S., Christie, D. M., Hey, R. L., & Delaney, J. R. (1983). Petrologic consequences of rift propagation on oceanic spreading ridges. *Earth and Planetary Science Letters, 62*(2), 193–207. https://doi.org/10.1016/0012-821X(83)90083-3

Sleep, N. H., & Fujita, K. (1997). *Principles of geophysics*. Malden, Massachusetts: Blackwell Science.

Smetacek, V. (1999). Diatoms and the ocean carbon cycle. *Protist, 150,* 25-32. https://doi.org/10.1016/S1434-4610(99)70006-4

Stadler, T. J., & Tominaga, M. (2015). Intraplate volcanism of the western Pacific: New insights from geological and geophysical observations in the Pigafetta Basin. *Geochemistry Geophysics Geosystems, 16*(9), 3015-3033. https://doi.org/10.1002/2015GC005873

Stein, S., Stein, C. A., Elling, R., Kley, J., Keller, G. R., Wysession, M., . . . Moucha, R. (2018). Insights from North America's failed Midcontinent Rift into the evolution of continental rifts and passive continental margins. *Tectonophysics, 744*, 403-421. https://doi.org/10.1016/j.tecto.2018.07.021

Sun, Q., Cartwright, J., Wu, S., Zhong, G., Wang, S., & Shang, H. (2016). Submarine erosional troughs in the northern South China Sea: evidence for Early Miocene deepwater circulation and paleoceanographic change. *Marine and Petroleum Geology*, *77*, 75-91. http://dx.doi.org/10.1016/j.marpetgeo.2016.06.005

Sun, Q., Wu, S., Hovland, M., Luo, P., Lu, Y., & Qu, T. (2011). The morphologies and genesis of mega-pockmarks near the Xisha Uplift, South China Sea. *Marine and Petroleum Geology*, *28*, 1146-1156. doi:10.1016/j.marpetgeo.2011.03.003

Sundvik, M. T., & Larson, R. L. (1988). Seafloor spreading history of the western North Atlantic Basin derived from the Keathley sequence and computer graphics. *Tectonophysics, 155*(1–4), 49–71. https://doi.org/10.1016/0040-1951(88)90260-0

Svensen, H., Corfu, F., Polteau, S., Hammer, Ø., & Planke, S. (2012). Rapid magma emplacement in the Karoo large igneous province. *Earth and Planetary Science Letters, 325*, 1-9. https://doi.org/10.1016/j.epsl.2012.01.015

Sweeney, E. M., Gardner, J. V., Johnson, J. E., & Mayer, L. A. (2012). Geological interpretation of a low-backscatter anomaly found on the New Jersey continental margin. *Marine Geology, 326–328*, 46–54. https://doi.org/10.1016/j.margeo.2012.08.007

Talwani, M., & Abreu, V. (2000). Inferences regarding initiation of oceanic crust formation from the U.S. East Coast Margin and Conjugate South Atlantic Margins. *Geophysical Monograph Series, 115,* 211–233.

Talwani, M., & Heirtzler, J. R. (1964). Computation of magnetic anomalies caused by two dimensional structures of arbitrary shape. In G. A. Parks (Ed.), *Computers in the mineral industry* (pp. 464–480). Stanford: Stanford University Press.

Talwani, M., Ewing, J., Sheridan, R. E., Holbrook, W. S., & Glover, L. III (1995). The EDGE experiment and the US East Coast magnetic anomaly. In E. Banda, M. Torné, & M. Talwani (Eds.), *Rifted ocean-continent boundaries* (pp. 155–181).

Dordrecht, The Netherlands: Kluwer Academic. https://doi.org/10.1007/978-94-011-0043-4_9

Taylor, P. T., Zietz, I., & Dennis, L. S. (1968). Geologic implications of aeromagnetic data for the eastern continental margin of the United States. *Geophysics, 33*(5), 775–780.

Thomas, W. A. (2019). Tectonic inheritance at multiple scales during more than two complete Wilson cycles recorded in eastern North America. In R. W. Wilson, G. A. Houseman, K. J. W. McCaffrey, D. A.G., & S. J. H. Butter (Eds.), *Fifty Years of the Wilson Cycle Concept in Plate Tectonics* (Vol. 470, pp. 337-352): Geological Society, London, Special Publications.

Tivey, M. A., Sager, W. W., Lee, S.-M., & Tominaga, M. (2006). Origin of the Pacific Jurassic quiet zone. *Geology, 34*(9), 789-792.

Tominaga, M., & Sager, W. W. (2010a). Origin of the smooth zone in early cretaceous North Atlantic magnetic anomalies. *Geophysical Research Letters, 37*, L01304. https://doi.org/10.1029/2009GL040984

Tominaga, M., & Sager, W. W. (2010b). Revised Pacific M-anomaly geomagnetic polarity timescale. *Geophysical Journal International, 182*, 203–232. https://doi.org/10.1111/j.1365-246X.2010.04619.x

Tominaga, M., Tivey, M. A., MacLeod, C. J., Lissenberg, C. J., Morris, A., Shillington, D. J., & Ferrini, V. (2016). Characterization of the in situ magnetic architecture of oceanic crust (Hess Deep) using near-source vector magnetic data. *Journal of*

Geophysical Research: Solid Earth, 121, 4130–4146. https://doi.org/10.1002/2015JB012783

Tominaga, M., Tivey, M., Lizarralde, D., Oakley, A., & Sager, S. (2012), Multi-channel seismic field data in the Hawaiian Lineation Jurassic Magnetic Quiet Zone, North Pacific Ocean, acquired by the R/V Thomas G. Thompson in 2011 (TN272). Academic Seismic Portal at UTIG, Marine Geoscience Data System. http://dx.doi.org/10.1594/IEDA/500209

Tréguer, P.J., & De La Rocha, C.L. (2013). The world ocean silica cycle. *Annual Review of Marine Sciences, 5*(1), 477–501. doi:10.1146/annurev-marine-121211-172346

Tréhu, A. M., Ballard, A., Dorman, L., Gettrust, J., Klitgord, K. D., & Schreiner, A. (1989). Structure of the lower crust beneath the Carolina Trough, US Atlantic continental margin. *Journal of Geophysical Research: Solid Earth, 94*(B8), 10585-10600. doi:10.1029/JB094iB08p10585

Tucholke, B. E. (1986). Structure of the basement and distribution of sediments in the western North Atlantic Ocean. In P. R. Vogt & B. E. Tucholke (Eds.), *The geology of North America, Vol. M, the Western North Atlantic Region* (pp. 331–340). Boulder, CO: Geological Society of America.

Tucholke, B. E., & Schouten, H. (1988). Kane Fracture Zone. *Marine Geophysical Researches, 10*(1-2), 1–39. https://doi.org/10.1007/BF02424659

Tugend, J., Gillard, M., Manatschal, G., Nirrengarten, M., Harkin, C., Epin, M.-E., . . . Mcdermott, K. (2018). Reappraisal of the magma-rich versus magma-poor rifted margin archetypes. In K. R. McClay & J. A. Hammerstein (Eds.), *Passive*

Margins: Tectonics, Sedimentation and Magmatism (Vol. 476): Geological Society, London, Special Publications.

Van Avendonk, H. J. A., Christeson, G. L., Norton, I. O., & Eddy, D. R. (2015). Continental rifting and sediment infill in the northwestern Gulf of Mexico. *Geology, 43*(7), 631–634. https://doi.org/10.1130/G36798.1

Van Avendonk, H. J., Holbrook, W. S., Nunes, G. T., Shillington, D. J., Tucholke, B. E., Louden, K. E., . . . Hopper, J. R. (2006). Seismic velocity structure of the rifted margin of the eastern Grand Banks of Newfoundland, Canada. *Journal of Geophysical Research: Solid Earth, 111*(B11). doi:10.1029/2005JB004156

Vandamme, D., & Ali, J. R. (1998). 21. Paleomagnetic results from basement rocks from Site 917 (East Greenland Margin). In A. D. Saunders, H. C. Larsen, & S. W. Wise Jr. (Eds.), *Proceedings of the Ocean Drilling Program: Scientific Results* (Vol. 152, pp. 259). College Station, TX: Ocean Drilling Program.

Verhoef, J., Collette, B. J., Dañobeitia, J. J., Roeser, H. A., & Roest, W. R. (1990). Magnetic anomalies off West-Africa (20–38°N). *Marine Geophysical Researches, 13*, 81–103.

Vogt, P. (1973). Early events in the opening of the North Atlantic. In D. H. Taling & S. K. Runcorn (Eds.), *Implications of continental rift to the Earth Sciences* (Vol. 2, pp. 693-712). New York: Academic Press.

Vogt, P. R. (1973). Early events in the opening of the North Atlantic. In D. H. Taling & S. K. Runcorn (Eds.), *Implications of continental rift to the Earth Sciences* (pp. 693–712). New York: Academic Press.

Vogt, P. R. (1986). Magnetic anomalies and crustal magnetization. In P. R. Vogt & B. E. Tucholke (Eds.), *The geology of North America, Vol. M, the Western North Atlantic Region* (pp. 229–256). Boulder, CO: Geological Society of America.

Vogt, P. R., Anderson, C. N., & Bracey, D. R. (1971). Mesozoic magnetic anomalies, sea-floor spreading, and geomagnetic reversals in the southwestern North Atlantic. *Journal of Geophysical Research, 76*(20), 4796–4823. https://doi.org/10.1029/JB076i020p04796

Vogt, P. R., Anderson, C. N., Bracey, D. R., & Schneider, E. D. (1970). North Atlantic magnetic smooth zones. *Journal of Geophysical Research, 75*(20), 3955–3968. https://doi.org/10.1029/JB075i020p03955

Volpi, V., Camerlenghi, A., Hillenbrand, C.-D., Rebescon, M., & Ivaldiz, R. (2003). Effects of biogenic silica on sediment compaction and slope stability on the Pacific margin of the Antarctic Peninsula. *Basin Research, 15*, 339–363. https://doi.org/10.1046/j.1365-2117.2003.00210.x

Wang, Y., Forsyth, D. W., & Savage, B. (2009). Convective upwelling in the mantle beneath the Gulf of California. *Nature, 462*(7272), 499-501. doi:10.1038/nature08552

Wanless, V. D., Perfit, M. R., Klein, E. M., White, S., & Ridley, W. I. (2012). Reconciling geochemical and geophysical observations of magma supply and melt distribution at the 9°N overlapping spreading center, East Pacific Rise. *Geochemistry, Geophysics, Geosystems, 13*(11), 1–22, Q11005.

Weiwei, D., Schnabel, M., Franke, D., Aiguo, R., & Zhenli, W. (2012). Crustal structure across the Northwestern margin of South China Sea: evidence for magma‐poor rifting from a wide‐angle seismic profile. *Acta Geologica Sinica‐English Edition, 86*(4), 854-866.

Wessel, P., & Lyons, S. (1997). Distribution of large Pacific seamounts from Geosat/ERS-1: Implications for the history of intraplate volcanism. *Journal of Geophysical Research Solid Earth, 102*(B10), 22459-22475. doi:10.1029/97JB01588

White, R. S., Smith, L. K., Roberts, A. W., Christie, P. A., Kusznir, N. J., i, S. T., . . . Tymms, V. J. (2008). Lower-crustal intrusion on the North Atlantic continental margin. *Nature, 452*(7186), 460-464. doi:10.1038/nature06687

White, R. S., Spence, G. D., Fowler, S. R., McKenzie, D. P., Westbrook, G. K., & Bowen, A. N. (1987). Magmatism at rifted continental margins. *Nature, 330*(6147), 439-444.

White, R., & McKenzie, D. (1989). Magmatism at rift zones: the generation of volcanic continental margins and flood basalts. *Journal of Geophysical Research: Solid Earth, 94*(B6), 7685-7729. https://doi.org/10.1029/jb094ib06p07685

White, S. M., Crisp, J. A., & Spera, F. J. (2006). Long‐term volumetric eruption rates and magma budgets. *Geochemistry, Geophysics, Geosystems, 7*(3), 1-20.

Whitehead, J. A., Dick, H. J., & Schouten, H. (1984). A mechanism for magmatic accretion under spreading centres. *Nature, 312*(5990), 146-148. https://doi.org/10.1038/312146a0

Whitmarsh, R. B., Manatschal, G., & Minshull, T. A. (2001). Evolution of magma-poor continental margins from rifting to seafloor spreading. *Nature, 413*(6852), 150-154. doi:10.1038/35093085

Williams, H., & Hatcher, R. D. (1982). Suspect terranes and accretionary history of the Appalachian orogen. *Geology, 10*(10), 530–536. https://doi.org/10.0.4.106/0091-7613(1982)10%3C530:STAAHO%3E2.0.CO;2

Williams, S.R.J. (1987). Faulting in abyssal-plain sediments, Great Meteor East, Madeira Abyssal Plain. *Geological Society London Special Publications, 31*, 87-104. https://doi.org/10.1144/GSL.SP.1987.031.01.08

Wilson, D. S., & Hey, R. N. (1995). History of rift propagation and magnetization for the Cocos-Nazca spreading center. *Journal of Geophysical Research, 100*(B6), 10,041–10,056. https://doi.org/10.1029/95JB00762

Wilson, D. S., Hey, R. N., & Nishimura, C. (1984). Propagation as a mechanism of reorientation of the Juan de Fuca Ridge. *Journal of Geophysical Research, 89*(B11), 9215–9225. https://doi.org/10.1029/JB089iB11p09215

Wilson, J. T. (1966). Did the Atlantic close and then re-open? *Nature, 211*(5050), 676–681. https://doi.org/10.1038/211676a0

Wilson, M. (1997). Thermal evolution of the Central Atlantic passive margins: continental break-up above a Mesozoic super-plume. *Journal of the Geological Society, 154*(3), 491-495.

Withjack, M. O., Schlische, R. W., & Olsen, P. E. (1998). Diachronous rifting, drifting, and inversion on the passive margin of central eastern North America: An analog for other passive margins. *AAPG Bulletin, 82*(5A), 817–835.

Withjack, M. O., Schlische, R. W., & Olsen, P. E. (2012). Development of the passive margin of eastern North America: Mesozoic rifting, igneous activity, and breakup. In D. G. Roberts & A. W. Bally (Eds.), *Regional Geology and Tectonics: Phanerozoic Rift Systems and Sedimentary Basins* (Vol. 1, pp. 301-335). Amsterdam, The Neatherlands: Elsevier.

Wrona, T., Taylor, K.G., Jackson, C.A.-L., Huuse, M., Najorka, J., & Pan, I. (2017). Impact of silica diagenesis on the porosity of fine-grained strata. An analysis of Cenozoic mudstones from the North Sea. *Geochemistry Geophysics Geosystems, 18,* 1537-1549. doi:10.1002/ 2016GC006482

Wyer, P., & Watts, A. B. (2006). Gravity anomalies and segmentation at the East Coast, USA continental margin. *Geophysical Journal International, 166*(3), 1015–1038. https://doi.org/10.1111/j.1365-246X.2006.03066.x

Zietz, I. (1982). Composite magnetic anomaly map of the United States; Part A, Conterminous United States: U.S. Geological Survey Investigations Map GP-954-A, 59 pp., 2 sheets, scale 1:2,500,000.

APPENDIX A

SUPPLEMENTARY MATERIAL FOR SECTION 2

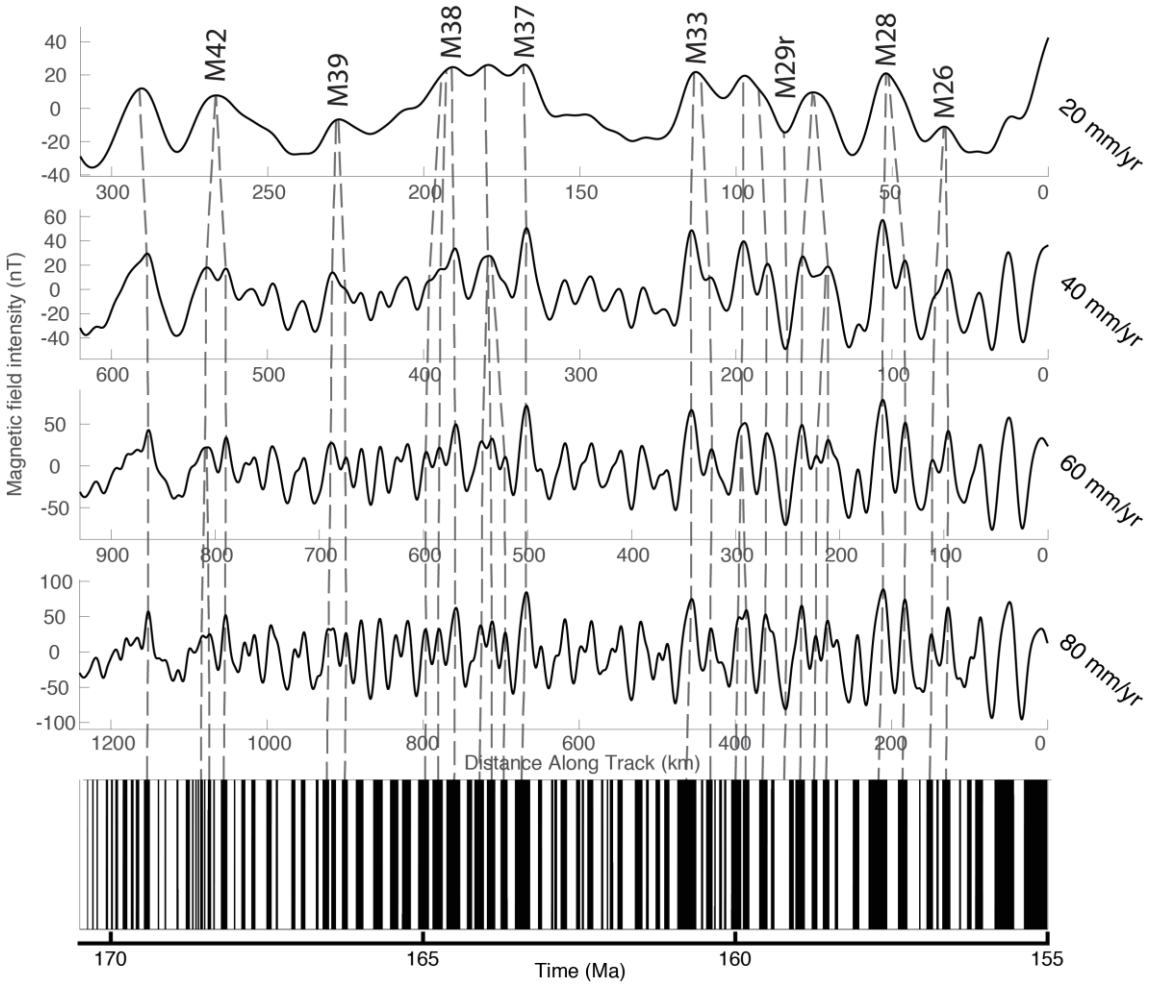

Figure A.1 Shows magnetic anomaly superposition from slower spreading during a period of rapid polarity reversals in the Atlantic JQZ. Synthetic magnetic anomaly profiles were created for a variety of half seafloor spreading rates. More rapid spreading rates better display the magnetic anomaly signal from individual chrons, which could then be used to determine chrons creating the peaks and troughs for the comparatively slower spreading rates in the OMQZ.

APPENDIX B

SUPPLEMENTARY MATERIAL FOR SECTION 3

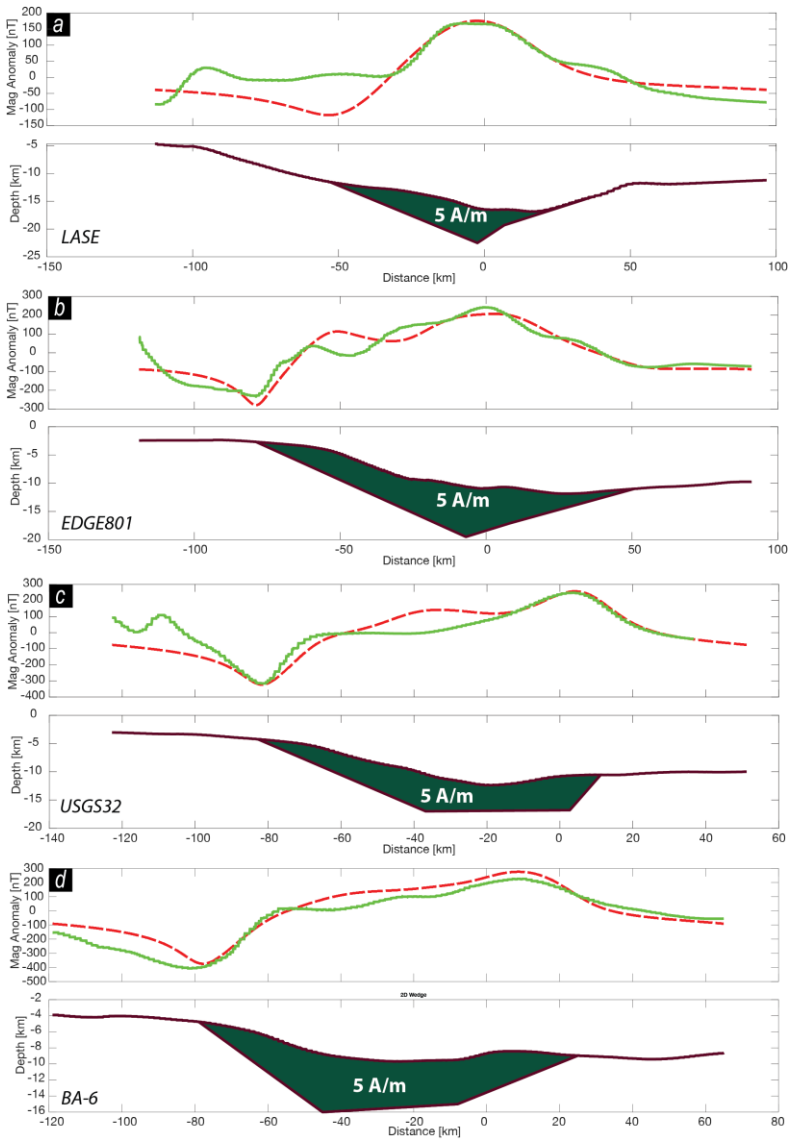

Figure B.1 2D magnetic forward models of the ECMA along ENAM seismic lines. (a) LASE, (b) EDGE Line 801, (c) USGS Line 32, and (d) BA-6. Red dashed line is calculated magnetic anomaly; green line is observed magnetic anomaly (Fig. 3.1). Constraints provided by previous SDR interpretations (Fig. 3.2b). Remanent magnetization of 5 A/m used, with an inclination of 45° and a declination of -2° based on the estimates of the Jurassic geomagnetic pole (Austin et al., 1990; Talwani et al., 1995). Model results are consistent with previous 2D magnetic models at the ENAM (e.g. Talwani et al., 1995).

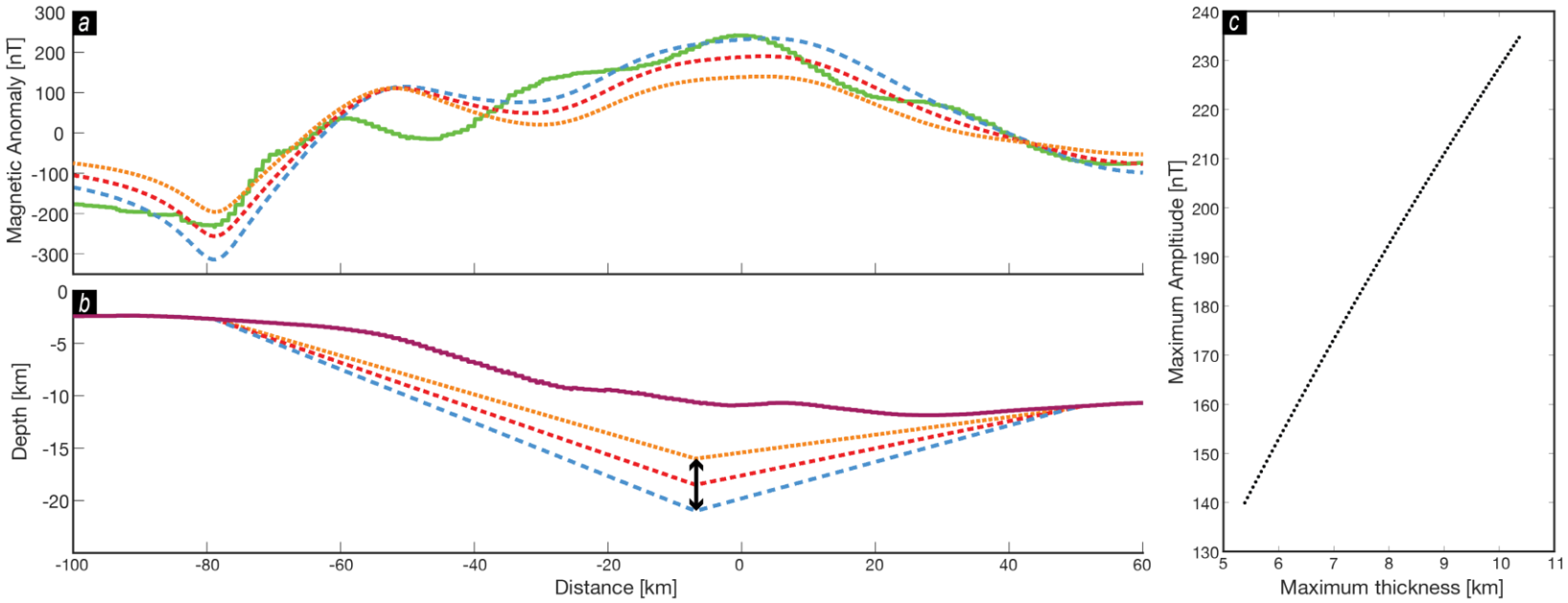

Figure B.2 Magnetic forward modeling sensitivity to source body thickness changes. (a) Calculated (dashed lines) and observed (green line) (Fig. 3.1) magnetic anomaly. (b) Model source volcanic wedge geometry. Color of wedge base line matches corresponding anomaly in panel a. Red dashed line corresponds to the geometry in the EDGE Line 801 2D forward model (Fig. B.1b). (c) Plot of maximum source wedge thickness vs maximum amplitude of resulting magnetic anomaly. Analysis suggests that every 500 m change in the maximum thickness of volcanic wedge produces a ~10 nT change in the maximum magnetic anomaly amplitude.

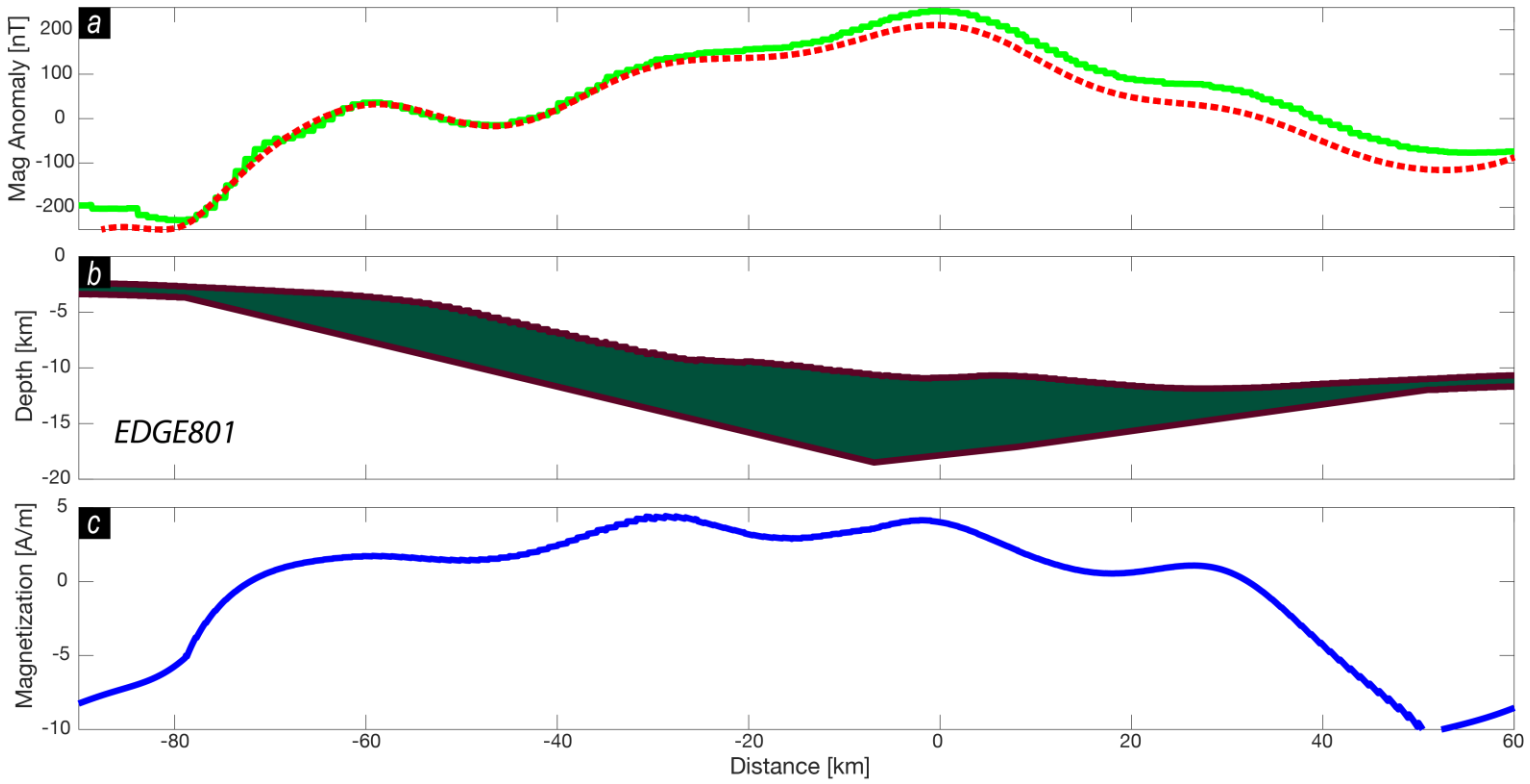

Figure B.3 2D inversion for volcanic wedge magnetization (Parker and Huestis, 1974). (a) Magnetic anomaly. Red dashed line is calculated magnetic anomaly using inverted magnetization distribution; green line is observed magnetic anomaly (Fig. 3.1). (b) Model volcanic wedge geometry. Model constrained by seismic interpretations of SDR wedge at EDGE Line 801 (Sheridan et al., 1993; Talwani et al., 1995). Thickness at edges of wedge is 1 km to avoid instability that occurs in inversion as source body thickness approaches 0 km. (c) Inverted magnetization distribution along profile. Inversion assumes remanent magnetization with an inclination of 45° and a declination of -2° based on the estimates of the Jurassic geomagnetic pole (Austin et al., 1990; Talwani et al., 1995). Inversion shows that ECMA can be explained by a magnetic volcanic wedge, with a magnetization in the vicinity of 5 A/m.

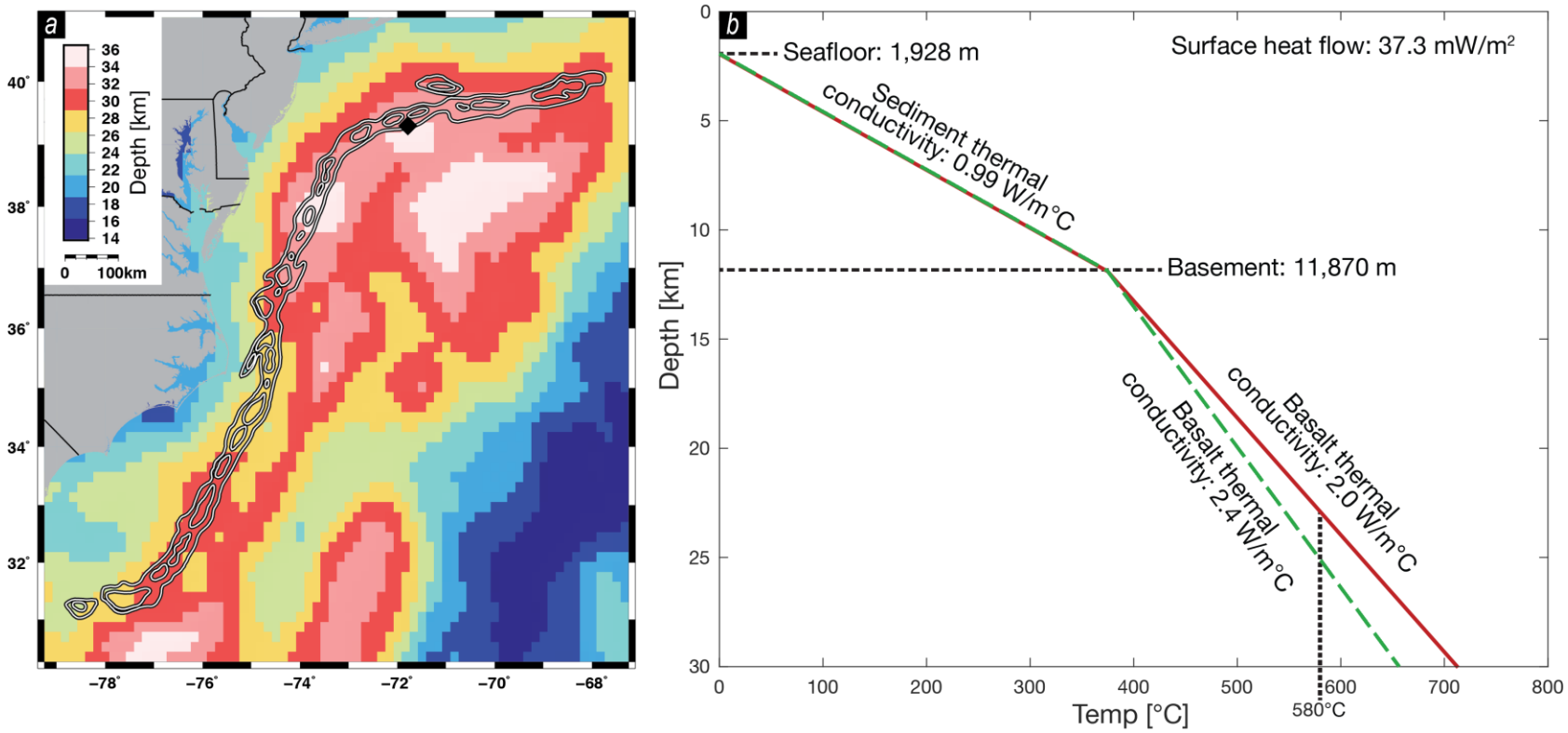

Figure B.4 Curie point depth at the ENAM. (a) Plot of global estimated Curie depth grid derived from magnetic anomaly inversion (Li et al., 2017). ECMA extent indicated by black/white contours (Fig. 3.1a) (Klitgord et al., 1988). Black diamond indicates location of heat flow Site V20-232. (b) Estimate of the Curie depth based on heat flow data collected at Site V20-232 (Pollack et al., 1993). Site data retrieved from GeoMapApp (http://www.geomapapp.org). Surface heat flow, seafloor depth, and sediment thermal conductivity measured at Site V20-232. Basement depth from seismically-derived basement depth grid (Klitgord et al., 1994) (Fig. 3.2b). Range of basalt thermal conductivities from Robertson (1988). Magnetite Curie point of 580°C assumed (Rajam, 2007). Calculation done following Sleep and Fujita (1997).

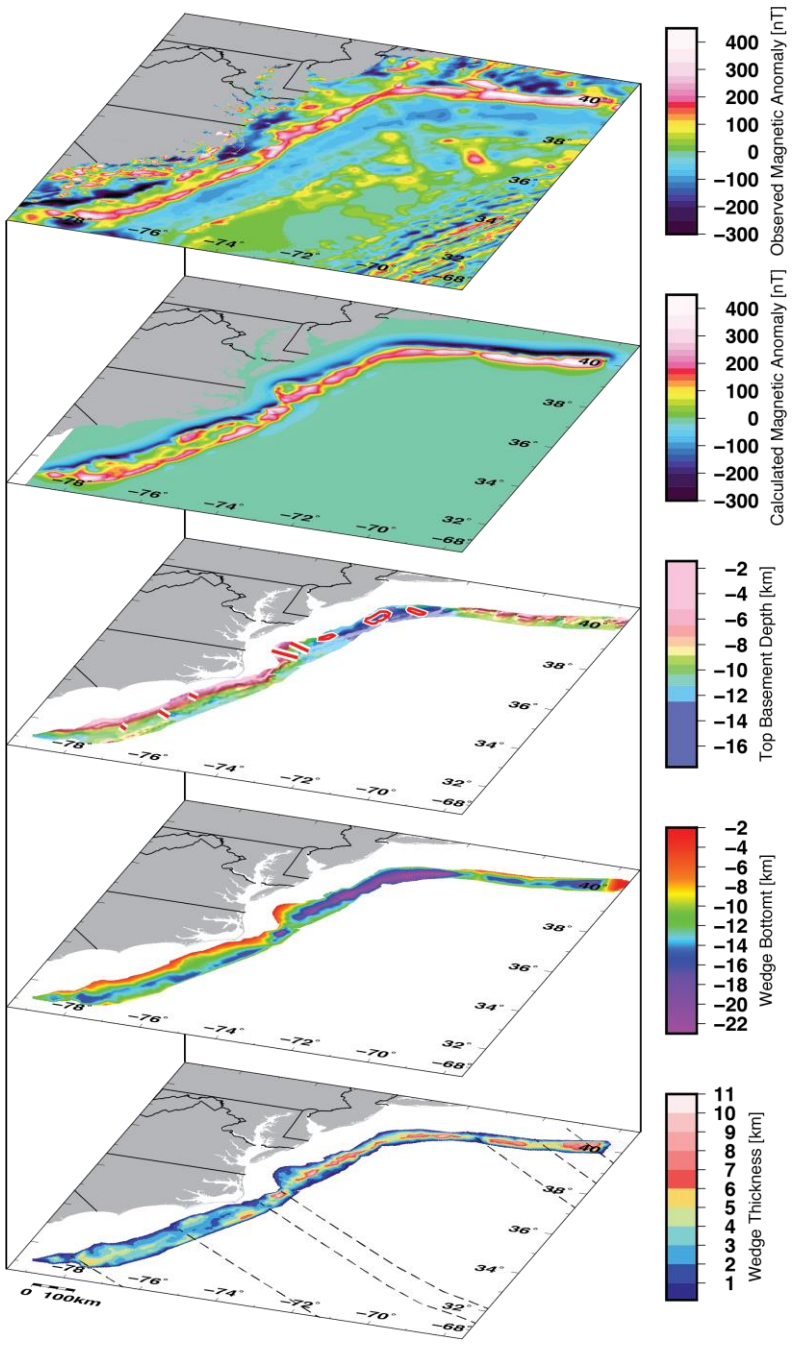

Figure B.5 Results of 3D magnetic forward modeling, including base of modeled volcanic wedge. From top to bottom: Observed magnetic anomaly (Bankey et al., 2002), model calculated magnetic anomaly, top of modeled volcanic wedge from basement depth grid (Fig. 3.2b), base of modeled volcanic wedge, and modeled volcanic wedge thickness. Locations of SDR interpretations from previous studies indicated by red/white lines (Fig. 3.2b). Grey dashed lines show landward extrapolations of major Atlantic fracture zones (Fig. 3.1b).

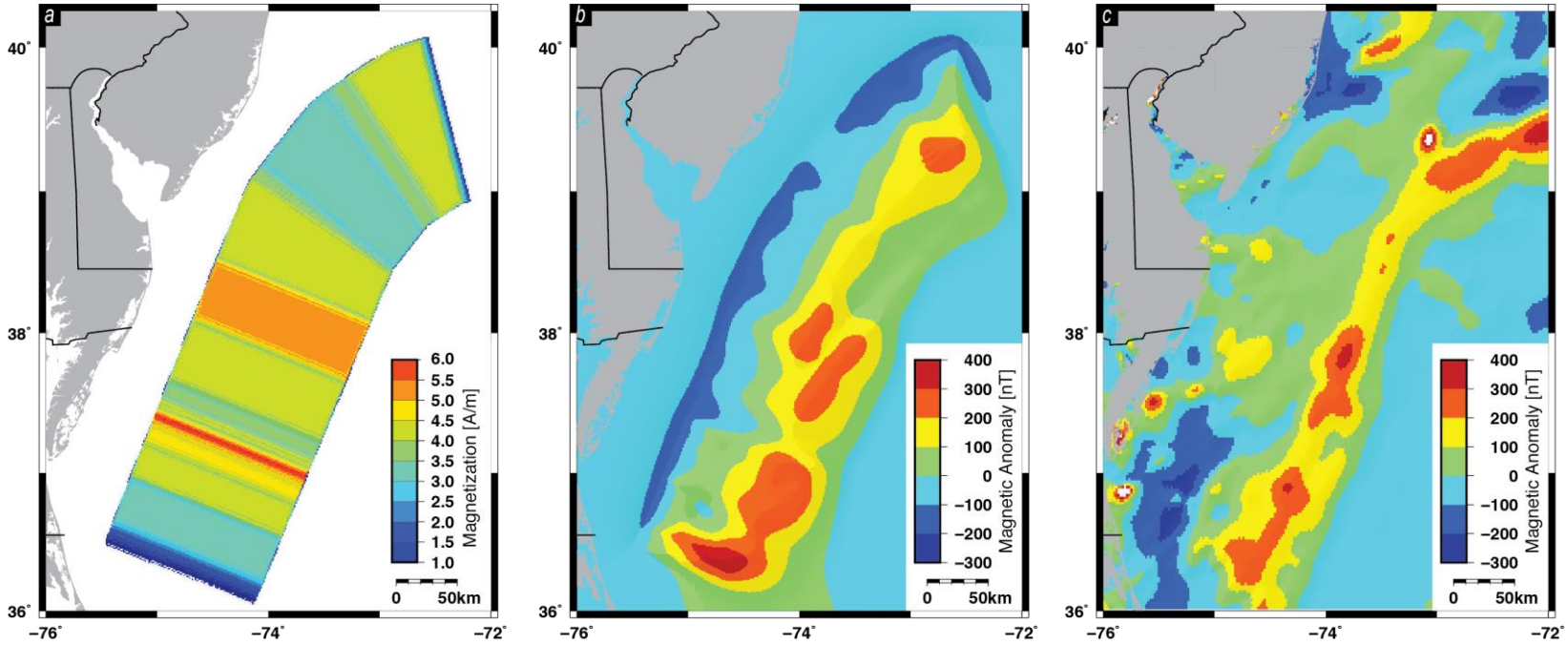

Figure B.6 3D forward model of the Baltimore Canyon Trough using a variable along-strike magnetization. (a) Magnetization distribution. (b) Calculated magnetic anomaly. (c) Observed magnetic anomaly (Fig. 3.1). Volcanic wedge in model uses geometry derived from EDGE Line 801 2D forward model (Fig. B.1b), extended along-strike.

APPENDIX C

SUPPLEMENTARY MATERIAL FOR SECTION 4

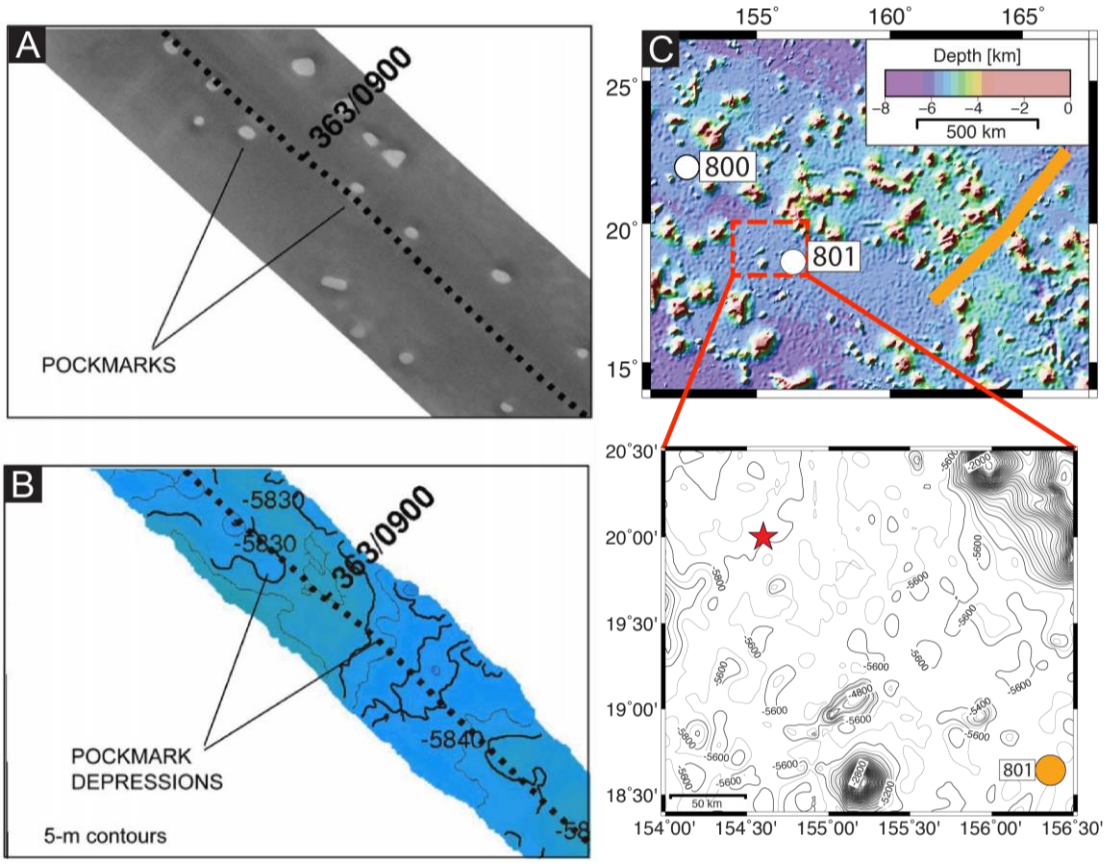

Figure C.1 Supplementary Figure 1. DSL-120A (A) sidescan and (B) phase bathymetry showing pockmark terrain on the modern seafloor of the northwestern Pacific near ODP Site 801. Pockmarks are ~100 m in diameter and ~5 m deep. High backscatter in sidescan is dark grey; low backscatter is light gray. (C) Map showing location of DSL-120A data shown (red star) in relation to ODP Site 801 (orange circle) and TN272 MCS profile (orange line). Data collected during the R/V Thomas G. Thompson cruise TN152.